Aus dem Alfred-Wegener-Institut
für Polar- und Meeresforschung Bremerhaven

Photosynthesis in Antarctic sea-ice diatoms

Dissertation zur Erlangung des Grades eines Doktors der Naturwissenschafften
-Dr. rer. nat.-

Aus dem Fachbereich 2 (Biologie/Chemie) der Universität Bremen

Vorgelegt von
Thomas Mock

Bremerhaven 2003

1. Gutachter:

   Prof. Dr. V. Smetacek
   (Alfred-Wegener-Institut für Polar- und Meeresforschung, Bremerhaven)

2. Gutachter:

   Prof. Dr. G.O. Kirst
   (Universität Bremen)

Tag des öffentlichen Kolloquiums: _____09.05.2003_____

Eidesstattliche Erklärung

Gem. § 6(5) Nr. 1 – 3 PromoO

Ich erkläre, daß ich

1. die Arbeit ohne unerlaubte fremde Hilfe angefertigt habe,
2. keine anderen als die von mir angegebenen Quelllen und Hilfsmittel benutzt habe und
3. die den benutzten Werke wörtlich oder inhaltlich entnommenen Stellen als solche kenntlich gemacht habe.

Bremerhaven, 21.02.2003

Thomas Mock

In memoriam Gerhard Mock

TABLE OF CONTENTS

1 INTRODUCTION

Photosynthesis is the process by which higher plants, algae and some bacteria transform and store solar energy in the form of energy-rich organic molecules. These compounds are in turn used as the energy source for growth and reproduction in these organisms. As such, virtually all life on the planet depends on photosynthetic energy conversion. Thus each ecosystem on earth, which receives solar irradiance in a sufficient dose, is inhabited by photoautotrophic organisms. The genetic diversity of aquatic photoautotrophs is extremely high (Medlin et al. 1995), whereas the basic process of photosynthetic energy conversion is highly conserved. Superimposed on the basic molecular mechanisms are variations in light harvesting, electron transport and carbon fixation (Falkowski & Raven 1995).

Antarctic sea ice represents one of the largest and most unique ecosystems on earth, inhabited predominantly by psychrophilic diatoms (Bacillariophyceae). Due to logistical and methodological constraints, this ecosystem also still is one of the most poorly investigated on earth. Consequently, how changes of environmental conditions influence photosynthesis and how these diatoms are generally adapted to their habitat still remained unresolved.

The mechanisms of adaptation and regulation of photosynthesis in Antarctic sea-ice algae are under debate (e.g. Palmisano et al. 1987, Bartsch 1989, Cota & Sullivan 1990, Kirst & Wiencke 1995, Gleitz et al. 1995, Robinson et al. 1997, Thomas & Dieckmann 2002). Only few *in situ* measurements have confirmed that sea ice algae still actively assimilate dissolved inorganic carbon ($H_2{}^{14}CO_3$) at temperatures as low as –15 °C, 1.5 µmol photons m^{-2} s^{-1} and a salinity of 150 PSU (e.g. Mock & Gradinger 1999) Photosynthesis under such conditions requires special acclimation or even adaptation including light harvesting, electron transport and carbon fixation, each with different sensitivities to environmental conditions and cellular controls.

The environmental conditions that have been studied thus far include light intensity and spectral quality, temperature, salinity and nutrient depletion. Growth kinetics (Bartsch 1989, Fiala & Oriol 1990, Aletsee & Jahnke 1992), photosynthesis vs irradiance (PE) response curves have so far

been the most popular methods to study photoacclimation in sea ice algae (Palmisano et al. 1987, Robinson et al. 1995, Glud et al. 2002). Derived parameters included the light limited slope (α, where photosynthesis is limited primarily by light harvesting mechanisms), the maximum photosynthetic rate (P_m, where enzymatic processes of carbon and nitrogen fixation limit photosynthesis) and the photoadaption parameter (E_k, the quotient P_m/α). These parameters revealed that ice algae are good adapted to low light (Cota 1985). The algae flourish under several meters of ice and snow at less than 1 % of surface scalar irradiance (Eicken 1992). They already show severe photoinhibition at moderate light levels (Cota 1985). The low light adaptation is accomplished by an increase in α along with an even larger reduction in P_m.(e.g. Robinson et al. 1997). Accessory photosynthetic pigment concentrations (e.g. fucoxanthin and chlorophyll *c* in diatoms) are elevated relative to the main photosynthetic pigment, chlorophyll *a* (chl *a*) (Boczar & Palmisano 1990). This adaptation allows the algae to enhance light harvesting at the wavelengths of light penetrating the ice and snow (Chl *a* is poorly efficient in absorbing green light (e.g. Falkowski & LaRoche 1991). The number of reaction centers, preferably photosystem II (PS II) also increase under light limited growth (Falkowski 1980, Richardson et al. 1983, Dubinsky et al. 1986).

Carbon acquisition in ice algae has received relatively little attention (Gleitz et al. 1995, Mitchell & Beardall 1996, Gleitz et al. 1996), although dissolved CO_2 [CO_2 (aq)] and O_2 concentrations can differ significantly from other aquatic ecosystems. Dissolved CO_2 and O_2 present in air-saturated sea water at the freezing point and 34 PSU (practical salinity units) are physically 1.5 times greater than in the same sea water at 15 °C. However, dissolved CO_2 and O_2 concentrations are influenced by photosynthetic active algae. In semi-closed or closed systems such as brine pockets dissolved CO_2 can be rapidly exhausted due to carbon acquisition by ice algae. The ability to utilise HCO_3 and to accumulate DIC (e.g. Kaplan & Reinhold 1999, Thoms et al. 2001) and/or store carbon in organic acids as observed in C4 plants (e.g. Sage 2001, Hibberd & Quick 2002) is likely more important in ice algae than in micro-algae from other marine habitats (Gleitz et al. 1995, Gleitz et al. 1996). In contrast dissolved oxygen concentrations my increase due to accumulation of photosynthetic oxygen under the ice cover (McMinn et al. 2000). Detoxification of molecular oxygen therefore is essential in sea ice diatoms

(Schriek 2000). Antioxidative enzymes (e.g. catalase, peroxidases, superoxide dismutase) increase their activity at low temperatures regardless of the light intensity (Schriek 2000).

Cold exposure is known to have an overall impact on light harvesting, electron generation at PS II and carbon fixation in temperate algae and plants (Raven & Geider 1988, Davidson 1991, Allen & Ort 2001, Stitt & Vaughan 2002, Jeong et al. 2002). The D1 protein of PS II as well as the carbon fixation enzyme RUBISCO (ribulosebisphosphate-carboxylase/oxy-genase) are damaged by cold exposure (e.g. Gombos et al. 1994, Allen & Ort 2001, Sitt & Vaughan 2002). How photosynthesis in psychrophilic algae responses to cold exposure in the light or in the dark is still unknown. Increasing salinity in contrast is known to influence photosynthesis in sea ice algae by increasing cyclic electron transport and cell dehydration (Bates & Cota 1986). Photoautotrophs in general have established mechanisms to reduce water loss by increasing their cellular concentrations of osmolytes, so as to restore the osmotic balance between the external medium and the inside of the cell. Osmolytes (e.g. proline, mannitol, glycine, betaine) accumulate under hypersaline conditions (e.g. Thomashow 2001, Girija et al. 2002, Sairam & Srivastava 2002) Dimethyl-sulfoniopropionate (DMSP) is known to be an important osmolyte in sea ice algae (Kirst & Wiencke 1995).

Field investigations revealed that growth of Antarctic sea ice diatoms seems to be frequently limited by a depletion of certain nutrients particularly during summer, when the resupply of new nutrients from sea water is less than the requirements for growth (e.g. Maestrini et al. 1986, McMinn et al. 1999). How diatoms cope their photosynthesis and thus growth at freezing temperatures under such resource limitations is still under debate (e.g. Reay et al. 1999, Lomas & Glibert 1999). Nutrient uptake experiments could recently been shown that growth of diatoms even may be limited by reduced affinity for some dissolved nutrients. Nitrate affinity for example is reduced as the temperature becomes suboptimal for growth (Lomas & Glibert 1999).

Consequently, there is an urgent need to improve our understanding of growth and success of Antarctic sea ice diatoms. Photosynthesis is a key process for growth and therefore systematically investigated ranging from new experiments under natural conditions in the field to *in situ* gene expression studies in an Antarctic sea ice diatom.

Photosynthesis measurements in an Antarctic sea ice floe conducted with an improved incubator confirmed the ability of ice algae to grow under extreme environmental conditions of sea ice. I introduced new sensors (oxygen micro-optodes) into sea ice research. Oxygen micro-optodes were used for the first time to measure oxygen dynamics of photosynthetically active diatoms directly within the microstructure of sea ice. Investigations of photosynthesis under simulated *in situ* conditions with this optode were attained by the development of a new microcosm, which enabled the cultivation of micro-algae under simulated natural conditions directly within sea ice. The results of these investigations, as well as physiological investigations in conventional liquid cultures (chemostats) raised the question of the molecular regulation of photosynthesis under sea ice conditions. Therefore molecular acclimation to freezing conditions was investigated by partial sequencing of an EST (EST = expressed sequence tag) library from a psychrophilic diatom acclimated to the freezing point of sea water. This approach provided the first genome informations of an obligate psychrophilic eucaryotic organsism. Expression of genes related to cold acclimation, photosynthesis, respiration and other important metabolic pathways in this diatom were investigated during cold exposure.

2 RESULTS

In situ measurements of photosynthesis are still vital to determine the physiological capacity of sea ice diatoms in their natural habitat and to quantify community primary production. To date there have been no *in situ* techniques capable of measuring primary production in Antarctic sea ice throughout the ice column without severe disruption of ice morphology, chemistry and ambient light field. I have therefore modified and improved a method described by Mock & Gradinger (1999) to measure primary production in thinner Antarctic sea ice - publication 1: Mock T (2002). This method is well suited to determine photosynthetic carbon assimilation (via $^{14}CO_2$ assimilation) in the interior of the floes. The rates of carbon assimilation of the interior algal assemblage in the ice floe (top to 5 cm from the bottom) was 0.25 mg C $m^{-2}d^{-1}$ whereas the bottom algal community (lowest 5 cm) attained only 0.02 mg C $m^{-2}d^{-1}$. Chlororophyll *a* (chl *a*) specific production rates (P^{chl}) for bottom algae revealed strong light limitation, whereas photosynthesis in the interior was probably limited by low temperatures and high salinities.

However, this new technique still does not enable the determination of photosynthetic activity directly in undisturbed brine channels. Our knowledge is therefore mainly restricted to bulk parameters. Conditions, which actually prevail within the network of brine channels, pockets or bubbles are not known. The main reason for this shortcoming is the inaccessibility of the interior due to the texture and rigid nature of sea ice. However, new microsensors (optodes) were deployed for the first time within the brine channels - publication 2: Mock T, Dieckmann GS, Haas C, Krell A, Tison JL, Belem AL, Papadimitiou S, Thomas DN (2002). Oxygen micro-optodes (PreSens GmbH, Germany) were used to measure oxygen in artificial sea ice in order to further develop our understanding of oxygen dynamics and thus photosynthesis under extreme conditions within the undisturbed micro-habitat of sea ice. Sensors were frozen into the ice during its formation. Increasing oxygen concentrations were measured during ice crystal formation at the water surface, which revealed a inclusion of oxygen by physical entrapment from the atmosphere and by oxygen producing diatoms. The major proportion of oxygen within brine channels was present as gas bubbles due to supersaturation. An increase in salinity due to a decrease in ice temperatures during subsequent sea ice development caused a reduction in the maximum concentration of dissolved oxygen within brine. Thus, dissolved

oxygen concentrations decreased over time, whereas gaseous oxygen was released to the atmosphere and sea water. The optodes are a significant advance over conventional microelectrodes, because the recordings can be temperature and salinity compensated in order to obtain precise measurements of oxygen dynamics with regard to total (dissolved and gaseous) and dissolved oxygen in sea ice. Optodes do not consume oxygen during measurement over a long period under extreme conditions.

A laboratory sea ice microcosm was developed for systematic investigations of photosynthesis with oxygen micro-optodes under simulated *in situ* conditions – publication 3: Mock T, Kruse M, Dieckmann GS (2003). This new microcosm is a break-through in cultivation of sea ice algae *in situ* (here *Fragilariopsis cylindrus*), because they can now be cultivated, and their photosynthetic activity investigated, under different abiotic conditions (e.g. low and high light intensity; melting or freezing of sea ice; nutrient limitation) directly within sea ice. First, measurements with oxygen micro-optodes were conducted to measure micro profiles through the ice-water interface and between the ice lamellae of the skeletal layer. The algal biomass in terms of chl *a* increased from the ice interior to the ice-water interface. Net oxygen production at the ice-water interface at an irradiance of 40 µmol photons $m^{-2}s^{-1}$ and –1.9°C, ranged between 0.0064 and 0.225 nmol O_2 $cm^{-2}s^{-1}$. Diffusive boundary layers (DBLs) were detected between ice lamellae, the periphery of the ice water interface and extending from the water below the ice through the ice-water interface into the spaces between ice lamellae. An additional small-scale horizontal variability of DBLs was also reflected in the net photosynthetic activity. The small-scale patchiness of algae and the differences in DBL thickness were caused by physico-chemical processes (e.g. turbulence, water flow velocity), which in turn were influenced by ice lamellar structure at the ice-water interface. These factors were the reasons for the observed variability in net-photosynthesis.

However, how changes of environmental conditions influence photosynthesis and how these diatoms are generally adapted to their habitat still remains unresolved. In addition to these oxygen measurements, I have therefore studied several diatom species in order to unravel common mechanisms of photosynthetic energy conversion under light and nitrate limitation by biophysical and biochemical measurements - publication 4 + 5: Mock T, Kroon BMA (2002); Mock T, Kroon BMA (2002). Both papers reveal that lipids are

important components, required to increase photosynthetic electron transport under light limitation and to sustain chloroplast membrane structure under a deficiency of integral bound proteins and pigments due to N-limitation. Monogalactosyl-diacylglycerol (MGDG) and digalactosyl-diacylglycerol (DGDG) are the main lipid classes of chloroplast membranes, especially thylakoid membranes. When nitrogen is limiting, pigment-protein complexes are one of the most affected structures. These complexes are reduced in the thylakoid membranes under N-limitation due to the reduced availability of nitrogen which is an essential component of proteins and pigments. However, pigment-protein complexes are responsible for thylakoid membrane bilayer formation. Thus, N-limitation destabilised the bilayer structure of the membrane which however is stabilised again by changes in the lipid composition and the degree of fatty acid desaturation. N-limitation caused a decrease in non-bilayer forming MGDG and a simultaneous increase in bilayer forming DGDG. Their ratio (MGDG:DGDG) decreased from 3.4 ± 0.1 to 1.1 ± 0.4, while 20:5 n-3 fatty acids of chloroplast related phospholipid classes (e.g. phosphatidylglycerol) increased under N-limitation. Extreme low light (e.g. 2 µmol photons $m^{-2}s^{-1}$) in contrast to N-limitation resulted in higher amounts of the non-lipid bilayer forming MGDG in relation to other bilayer forming lipids, especially DGDG. The ratio of MGDG:DGDG increased from 3.4 ± 0.1 to 5.7 ± 0.3. The existence of bilayer thylakoid membranes with high proportions of non-bilayer forming lipids is only possible when sufficient thylakoid pigment-protein complexes are present. These data reveal that lipids are important components, required to sustain membrane structure under a deficiency of integral membrane bound proteins and pigments regardless of the algal or plant species, because both chloroplast lipid classes (MGDG and DGDG) with their physical charcteristics are present in all photoautotrophic organisms.

The modulation of cellular structures, such as chloroplast membranes is based on emzyme reactions which lead to an acclimation to new environmental conditions. These basic processes start by signal perception and a cascade of signal transductions, which culminate in gene expression and translation of enzymes necessary for acclimation. The Antarctic diatom *Fragilariopsis cylindrus* was selected as a key organism to study molecular regulation of cold adaptation and photosynthesis - publications 6 + 7: Mock T, Valentin K (2003); Mock T, Valentin K (2003). This diatom is unique

due to its ability to survive extreme fluctuations of temperature (+8°C to ca. –20°C), salinity (0 – 150) and pH (7-11). Publication 6 describes an EST (expressed sequence tag) approach under cold shock to discover genes which are potentially involved in cold adaptation of *F. cylindrus*. Cells were grown at optimal conditions (+5°C and 35 µmol photons $m^{-2}s^{-1}$) and then transferred to the freezing point of sea water, simulating freezing into sea ice. After complete acclimation (5 days) mRNA was isolated and the complementary DNA cloned. Six hundred clones were analysed for insert sizes and those between 564 and 2500 base pairs were chosen for partial sequencing, producing 260 interpretable sequences. Forty % of the contigs (continuous sequences) could be identified by gene bank comparison. Among these, 7% were plastid-localised proteins potentially involved in photosynthesis and 5% were found to be involved in psychrophily or acclimation to cold conditions. Among genes identified, there was at least one of possible red algal origin indicating secondary gene transfer. Interestingly, the most abundant ESTs could not be identified, indicating the presence of yet unknown cold tolerance genes.

A subset of genes from the EST analysis was used and additional relevant genes for photosynthesis, respiration, and cold acclimation, not found by random sequencing of the cDNA-library were cloned and composed to macro-array for expression analysis (publication 7). The simultaneous expression of 44 *F. cylindrus* genes (macro-array) was analysed during simulated freezing at unchanged light intensity (35 µmol photons $m^{-2}s^{-1}$), at extreme low light intensity (3 µmol photons $m^{-2}s^{-1}$), and the results were compared to optimal growth conditions (35 µmol photons $m^{-2}s^{-1}$ at +5°C). Gene expression studies were paralleled by biophysical and –chemical investigations relevant for photosynthesis. When temperatures are reduced to the freezing point of sea water a molecular cold shock response is induced, also known from warm climate plants, which results in an increased expression of chaperons accompanied by dynamic photoinhibition of photosystem II with a strong reduction in RUBISCO gene expression. Recovery of photosynthesis and thus growth is only possible with a constantly high expression of chaperons and of genes necessary for repair and synthesis of chloroplast proteins. The degree of this cold shock response in an obligate psychrophilic diatom is reduced under extremely low light conditions. Photoautotrophs in polar oceans and sea ice are, therefore, probably highly susceptible to photo damage at

increasing light intensities and decreasing temperatures, particularly in the top layers of sea ice, where higher brine salinities also inhibit photosynthesis. Assimilated carbon under such conditions is probably completely used to repair photo damaged proteins (see above). However, at extreme low light conditions, such as in deep water, or in and underneath sea ice, metabolic costs for plastid repair are low. Only when temperatures increase, as the polar oceans become warmer, can growth proceed under high light intensities if enough resources (nutrients, CO_2) are available. Photosynthesis was investigated on a broad scale from community based investigations in the field to approaches of gene expression in a model organism cultured under simulated *in situ* conditions. The outcome of this thesis are new mechanisms of photosynthesis regulation under extreme polar conditions obtained by using new methods which help to understand how small scale cellular processes influence the energy flow on a broader ecosystem scale.

3 PUBLICATIONS

3.1 List of publications

Publication **1**

Mock, T., 2002.
In situ primary production in young Antarctic sea ice.
Hydrobiologia. 470, 127-132

Publication **2**

Mock, T., Dieckmann, G.S., Haas. C., Krell. A., Tison. J.L., Belem. A.L., Papadimitiou. S., Thomas. D.N., 2002. Micro-optodes in sea ice: a new approach to investigate oxygen dynamics during sea ice formation.
Aquatic Microbial Ecology 29, 297-306

Publication **3**

Mock, T., Kruse, M., Dieckmann, G.S., 2003. A new microcosm to investigate oxygen dynamics at the sea-ice water interface.
Aquatic Microbial Ecology 30, 197-205

Publication **4**

Mock, T., Kroon, B.M.A., 2002.
Photosynthetic energy conversion under extreme conditions-I: important role of lipids as structural modulators and energy sink under N-limited growth in Antarctic sea ice diatoms.
Phytochemistry 61, 41-51

Publication **5**

Mock, T., Kroon, B.M.A., 2002
Photosynthetic energy conversion under extreme conditions-II: the significance of lipids under light limited growth in Antarctic sea ice diatoms.
Phytochemistry 61, 53-60

Publication **6**

Mock, T., Valentin, K., 2003.
EST analysis of freezing tolerance in the Antarctic diatom *Fragilariopsis cylindrus*: Detection of numerous cold acclimation-related genes and a gene transfer event.
submitted

Publication **7**

Mock, T., Valentin, K., 2003.
Molecular cold acclimation in a polar diatom - requirement for low light at low temperatures.
submitted

3.2 Erklärung über den von mir geleisteten Anteil an den Publikationen

Publikation **1**

Die Weiterentwicklung dieser neuen Meßmethode, die Datenerhebung und die Datenauswertung wurden von mir durchgeführt. Auch das Manuscript wurde von mir selbst verfaßt.

Publikation **2**

Das wissenschaftliche Konzept dieser Arbeit stammt von mir. Die Installation der Sensoren, die Auswertung der Daten und die Verfassung des Manuskriptes wurden ebenfalls von mir durchgeführt. Alle beteiligten Koauthoren waren für die Erhebung der Daten verantwortlich.

Publikation **3**

Diese Arbeit beruht auf meinem Ansatz, wobei mir der Ingenieur Marcel Kruse bei der technischen Umsetzung meiner Ideen geholfen hat. Die Daten wurden von mir ausgewertet und auch ich habe das Manuskript geschrieben.

Publikation **4**

Bernd Kroon hat mich in die Fluoreszenztheorie eingewiesen und in die Kultivierarbeit von Mikroalgen. Die wissenschaftliche Fragestellung stammt von mir und auch ich habe sie methodisch umgesetzt, sowie alle Daten erhoben, ausgewertet und das Manuskript verfaßt.

Publikation **5**

Wie Publikation **4**

Publikation **6**

Die wissenschaftliche Intention zu dieser Arbeit kommt von mir, wobei der Weg der Umsetzung im engen Austausch mit Klaus Valentin stattfand. Die EST-Bank wurde von mir erstellt und Klaus Valentin übernahm die Auswertung der Sequenzen. Das Manuskript wurde hauptsächlich von Klaus Valentin verfaßt, wobei ich Teile der Einleitung und des Material und Methoden Teils sowie einen Teil der Diskussion geschrieben habe.

Publikation **7**

Dieses Experiment beruht auf meiner Idee, wobei das Konzept der Ausführung mit Klaus Valentin erarbeitet wurde. Ich habe die meisten Daten erhoben und ausgewertet. Das Manuskript wurde überwiegend von mir geschrieben.

Hydrobiologia **470:** 127–132, 2002.

In situ primary production in young Antarctic sea ice

Thomas Mock
Alfred-Wegener-Institute for Polar and Marine Research, Am Handelshafen 12, 27570 Bremerhaven, Germany
Tel: 0471-4831-1893. Fax: 0471-4831-1425. E-mail: tmock@awi-bremerhaven.de

Received 28 March 2001; in revised form 20 November 2001; accepted 19 December 2001

Key words: Antarctica, algae, carbon assimilation, chlorophyll *a*, growth, *in situ* primary production, methods, photosynthesis, sea ice

Abstract

An *in situ* incubation technique used successfully to measure the photosynthetic carbon assimilation of internal algal assemblages within thick multiyear Arctic ice was developed and improved to measure the photosynthetic carbon assimilation within young sea ice only 50 cm thick (Eastern Weddell Sea, Antarctica). The light transmission was improved by the construction of a cylindrical frame instead of using a transparent acrylic-glass barrel. The new device enabled some of the first precise measurements of *in situ* photosynthetic carbon assimilation in newly formed Antarctic sea ice, which is an important component in the sea ice ecosystem of the Antarctic Ocean. The rates of carbon assimilation of the interior algal assemblage (top to 5 cm from bottom) was 0.25 mg C m^{-2} d^{-1} whereas the bottom algal community (lowest 5 cm) attained only 0.02 mg C m^{-2} d^{-1}. Chl *a* specific production rates (P^{Chl}) for bottom algae (0.020 – 0.056 μg C μg chl a^{-1} h^{-1}) revealed strong light limitation, whereas the interior algae (P^{Chl} = 0.7 – 1.2 μg C μg chl a^{-1} h^{-1}) were probably more limited by low temperatures (< –5 °C) and high brine salinities.

Introduction

The *in situ* incubation technique developed by Mock & Gradinger (1999) provided the first precise measurements of an actively growing and photosynthesising algal community within the interior of first and multi year sea ice in the Arctic Ocean. The method permits carbon assimilation to be measured at a fine-scale of 1 cm thick vertical sections throughout the ice column, without severe disruption of ice morphology, geochemistry and light field. These results led to revised estimates of Arctic sea ice algal production, because until these measurements had been made, primary production within the interior of sea ice had been mostly neglected (e.g. Clasby et al., 1973; Smith & Herman, 1991, Gosselin et al., 1997). This is also true for Antarctic sea ice, where rich infiltration / freeboard, bottom and platelet algal communities are well studied, but not integrated production estimates that take into account ice interior carbon assimilation (e.g. Sullivan et al., 1985; Arrigo et al., 1997; Trenerry et al., 2002). Consequently, new methodologies for determining *in situ* profiles of photosynthesis and respiration within Antarctic sea ice are highly pertinent. Therefore, I improved the method described by Mock & Gradinger (1999) and adjusted the device for measurements in young sea ice stages (< 1 m thick), which are more representative for the seasonal Antarctic pack ice, than for the Arctic which is mostly covered by thick multi-year ice (Melnikov, 1997).

Material and methods

Site and sampling

Sea ice algae were collected in the Weddell Sea (Antarctica) during the RV Polarstern expedition ANT XVI / 3 from 18 March 1999 to 10 May 1999. The continuous decrease of sea water temperature in autumn 1999 caused sea ice formation from the middle of February close to the continental ice shelf at ca. 70°

S, 06° W. Thus, the sampled ice floe was estimated to be 2 months old on 17 April 1999. All samples were taken from one young ice floe of 50 cm thickness with a 5 cm snow cover (station PS 53 177, day of the year 107) at 70° 02′ 04″ S, 06° 00′ 06″ W using a 12 cm ice auger. Sampling of ice cores as well as light and photosynthesis measurements were done at this one station. Three ice cores were drilled for the *in situ* determinations: one for temperature profile measurements and pigment concentrations and two for determination of carbon assimilation parameters. All ice cores were taken in proximity to each other, about 100 m away from the research vessel. Care was taken to avoid disturbance of the site.

Irradiance

Total photosynthetically active radiation (PAR) was measured with a 2π sensor (LICOR 193) on the sea ice surface and a 4π sensor (LICOR 193 SB) positioned directly underneath the ice floe and recorded with a data logger (LICOR LI 1000) from 07:00 am to 16:00 pm (UTC). The ice core was returned into the original core hole and covered with snow to the original snow depth after installation of the sensors. The 2π sensor was placed approximately 10 m away from this hole. In order to calculate PAR in sea ice, we used the 4π data and Beer's law. The PAR flux on the top of each algal layer was calculated upward back to the surface using the equation:

$$E_o\,(z + \mathrm{d}z) = E_\circ\,(\mathrm{z})\,\mathrm{e}^{[-(k_i \cdot \mathrm{d}z + k\mathrm{chl} \cdot\ chl(z))]} \qquad (1)$$

where $E_\circ\,(z)$ is the PAR on the top of the algal layer (μmol m^{-2} s^{-1}); $E_\circ\,(z + \mathrm{d}z)$ is the PAR penetrating through the algal layer (μmol m^{-2}s^{-1}); k_i is the diffuse attenuation coefficient for ice (1.5 m^{-1}) (Maykut, 1985); dz is the ice layer thickness (m); $k$chl is the mean spectral attenuation coefficient for chlorophyl *a* (0.035 m^{2}mg^{-1}) (Smith et al., 1988); Chl (z) = chlorophyll *a* (chl *a*) concentration in each ice slice (mg m^{-2}).

Physico-chemical parameters and pigments

Snow depth was measured prior to coring. Ice core temperature (Testotherm 700 thermometer) was recorded on core 1, which immediately after coring was placed in an insulated tube to avoid rapid cooling. Temperature was measured at 1–10 cm intervals by inserting the thermometer through the walls of the insulating tube into holes drilled into the interior of the ice core. The core was then sawed into 1–10 cm

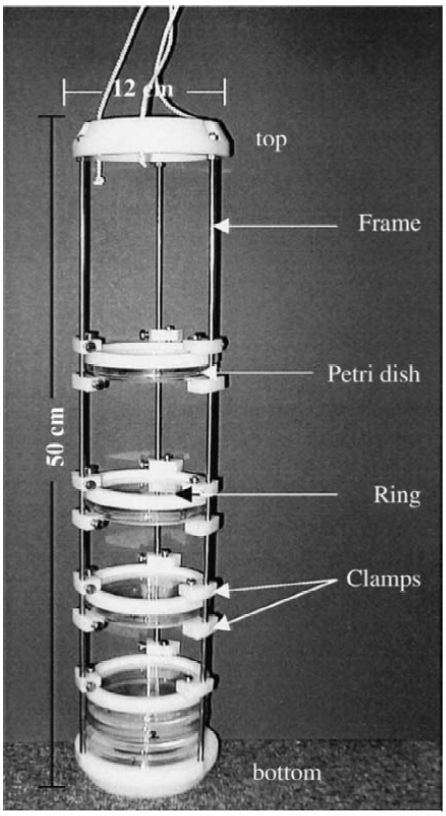

Figure 1. Photo of the new incubation system. Each petri dish serves as one incubation chamber.

long sections using a stainless steel saw. These were transferred into clean polyethylene cans and transported to the ship, and thawed (4 °C over night) for the determination of algal pigment concentration (chl a and phaeopigments). Thawed core sections were filtered onto Whatman GF/F filters and the pigments retained on the filters analysed, following extraction in acetone, with a Turner Designs Model 10-AU digital fluorometer according to Arar & Collins (1992).

Algal carbon production and growth rates

The second core was carefully extracted to avoid loss of the bottom portion. To minimise exposure of the shade-acclimated cells to the higher irradiances above

the ice, all ice core-handling processes took place under dark foil. Using a stainless steel saw, 6 slices of 1 cm thickness were cut from the following ice depths, beginning from the bottom of the core: (1) 0–1 cm, (2) 1–2 cm, (3) 2–3 cm, (4) 11–12 cm, (5) 20–21 cm, (6) 30–31 cm. Each of these 1 cm thick 6 slices was put into a glass petri dish, inoculated with 15 ml pre-filtered (0.2 μm) brine (obtained by sack hole drilling) at *in situ* temperature and 50 μl (15 μCi) $NaH^{14}CO_3$ (Amersham International plc, Little Chalfont, UK). The petri dish was sealed with a small transparent non-toxic silicon ring and clamps. The remaining core sections together with the 6 petri dishes were placed in a cylindical frame (Figure 1), in their original positions. These new developments increased light transmission when compared with the acrylic-glass barrel used by Mock & Gradinger (1999). The frame was then returned into the original core hole and secured with ropes. The core hole was then covered with snow to the original snow depth. In order to determine the dark carbon fixation, the bottom segment (0–1 cm) of a parallel core was incubated in a black petri dish whithin a sack hole of 20 cm depth. The sack hole was closed with the drilled ice core and covered with snow. After 8 h incubation, the black petri dish and the frame was removed from the floe and immediately covered with black plastic foil and transported to the laboratory on RV 'Polarstern'. Each incubation was terminated by adding 500 μl DCMU, final concentration ca. 2 mg l^{-1}, after the contents of the dish had melted (ca. 30 min) in the dark at room temperature. Three 15 ml aliquots of each sample were acidified with 150 μl 1 N HCl (pH <2). Non-fixed ^{14}C was removed by bubbling with air for 20 min. Ten ml of each aliquot were dispensed into 20 ml plastic vials and mixed with 10 ml scintilation cocktail (Packard). The samples were radio-assayed in a Packard TriCarb liquid scintillation counter. Quench correction was performed by automatic external standardisation. Dark carbon fixation was between 5 and 15% of light carbon fixation. Carbon production was calculated according to Strickland & Parsons (1972). The chl *a* specific photosynthetic rate P^{chl} was calculated by dividing the primary production (μg C l^{-1} h^{-1}) with the chl *a* concentration (μg chl *a* l^{-1}). Gross algal growth rates (μ+r), which are the sum of the specific growth rate of dark respiration (d^{-1}), were estimated from the P^{Chla} data (Sakshaug et al., 1989). A factor of 0.03 was used for chl *a* C^{-1} ratio (Mock & Gradinger, 2000).

Results and discussion

In situ photosynthetic rates of ice algae throughout ice floes was determined successfully using a new incubation method that can be deployed in first and multi year sea ice in the Arctic ocean. However, significant modifications were necessary before this technique could be deployed for measurements in young ice with a thickness below 1 m. This was mostly achieved by designing a new supporting frame (Fig. 1) which increased the light transmission incident on the radiolabelled incubations avoiding an underestimation by light absorption of the acrylic-glass barrel. The rods and all other holders that make up the frame frame were as thin as possible to avoid shading of the petri-dishes with the samples inside, at the same time being strong enough for deployment within the ice core hole. These improvements are vital for measurements at low incident light conditions such as during autumn or under thick snow cover. Frames of different length (25, 50, 100 cm) enabled measurements in young ice, which would have been too complicated with the previously used acrylic-glass barrels. The black petri dish for determination of dark carbon assimilation was not included in the new device, but was incubated elsewhere. This avoided the problems of the dark petri dish shading incubations beneath it in the incubation array.

The absolute measured range of surface irradiance at Stn. 107 was 28–194 μmol photons m^{-2} s^{-1}, and the mean under-ice irradiance was below 1.2% of the incident surface irradiance (Table 1). The modeled PAR values inside the ice floe over the entire incubation period decreased with depth (Table 1), which depends on attenuation and absorption of light by ice crystals, gas bubbles, brine, particles and micro-algae (e.g. Perovich & Grenfell, 1981; Mobley et al., 1998). The temperatures of new ice ranged between –2.4 and –11.3 °C and decreased with the distance from the ice–water interface. Ice salinity ranged from 7.9 to 10.8 in characteristic C-profile with increasing salinity to the top and the bottom of sea ice and minimum salinities in the middle. This pattern is probably the result of rapid freezing near the surface trapping larger amounts of salt (Martin, 1974). When the cold, dense brine from the upper layer of the ice fills the brine channels, the equilibrium brine level is lower than when warmer, and less saline seawater fills the channels. This small mass perturbation results in a large pressure imbalance within the brine drainage tube, which accelerates seawater up the tube until the second higher equilibrium level is reached (Martin, 1974).

Table 1. In situ variables of station 107; Light intensities are given as means ± standard deviations of 360 measurements over a time of 8 h

Distance to ice water interface [cm]	Light [μmol photons m^{-2} s^{-1}]	Temperature [°C]	Salinity [PSU]	Chl *a* [μg l^{-1}]	Phaeo / Chl *a* [μg l^{-1}]
40–50	2.9 ± 0.9	–11.3	10.8	0.01	0.23
30–40	2.5 ± 0.8	–8.3	9.5	0.05	0.02
20–30	2.2 ± 0.7	–6.1	7.8	0.03	0.03
10–20	1.9 ± 0.6	–4.6	6.4	0.10	0.06
5–10	1.6 ± 0.5	–4.0	7.4	0.14	0.10
3–5	1.5 ± 0.5	–3.7	6.9	1.18	0.06
2–3	1.4 ± 0.5	–3.7	6.6	4.09	0.07
1–2	1.4 ± 0.4	–3.1	6.5	6.32	0.02
0–1	1.4 ± 0.4	–2.4	7.9	1.13	0.02

Table 2. In situ variables of station 107: ice and snow thickness (cm), under ice irradiance (% of surface), incubation period ($T_{incubation}$; UTC), carbon assimilation (mg C m^{-2} d^{-1}), chl *a* specific photosynthetic rate (P^{chla}) (μg C μg chl a^{-1} h^{-1}), growth rate ($\mu + r$), which is the sum of the specific growth rate of dark respiration (d^{-1}) and chl *a* (mg m^{-2}); values represent means or ranges

Parameter	Ice habitat	Data
Ice type		Young ice
Ice thickness		50
Snow thickness		5
Under-ice irradiance		1.2
$T_{incubation}$		07: 42 – 15: 45
Carbon assimilation	Interior (>5–50 cm)	0.25
	Bottom (0–5 cm)	0.03
$P^{Chl\,a}$	Interior (>5–50 cm)	0.700 – 1.170
	Bottom (0–5 cm)	0.020 – 0.056
Growth rate	Interior (>5–50 cm)	0.140 – 0.230
	Bottom (0–5 cm)	0.004 – 0.013
Chl *a*	Interior (>5–50 cm)	0.03
	Bottom (0–5 cm)	0.14

High brine salinities, extremly cold temperatures and reduced light supply limits primary production of ice algae (Kottmeier & Sullivan, 1988; Gleitz & Thomas, 1993; Arrigo et al., 1993; Kirst & Wiencke, 1995), but each factor probably has a different significance relative to the others and depending on depth in sea ice (Arrigo et al., 1993). *In situ* carbon assimilation in general was relatively low, ranging between 0.04 and 0.15 μg C l^{-1} h^{-1} (Fig. 2). High rates were recorded in the bottom 1–2 cm at the chl *a* maximum (6.32 μg l^{-1}) and in the middle of the ice core.

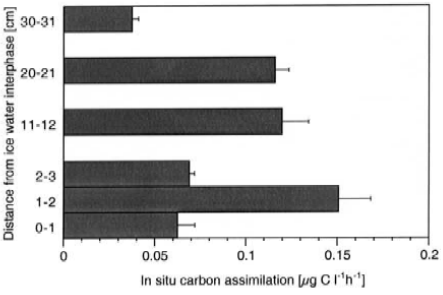

Figure 2. Vertical profiles of *in situ* carbon assimilation. *n*=3; error bars denote standard deviations; depth intervals are given relative to the bottom of the ice floe.

Integrated production rates of interior sea ice algae (<5–50 cm) exceeded the production of the bottom algal communities (Table 2). The same pattern was observed for chl *a* specific primary production ($P^{Chl\,a}$, Table 2). The opposite was observed for integrated chl *a* concentration of 0.03 mg m^{-2} in the interior (>5–50 cm), whereas the bottom layers (0–5 cm) contributed 0.14 mg m^{-2} (Table 2). Maximum growth rates of the algae (0.23 d^{-1}) occurred in the interior parts of sea ice, whereas the growth of bottom ice algae was negligible (Table 2). Low chl *a* specific production rates of ice algae in the bottom few centimetres, which was responsible for low growth rates, indicate a strong light limitation of primary production, whereas $P^{Chl\,a}$ rates in the middle and top of the ice flow were more than 10 fold higher despite temperatures down to –7 °C (Table 2). Light seems to be the most limiting factor in the bottom of sea ice, whereas

temperature in conjunction with increasing salinities limit algal productivity in the middle and especially in the top of sea ice (Arrigo et al., 1993). Low downwelling irradiance in autumn and 5 cm snow cover were responsible for relatively low light intensities within young sea ice, whereby the largest uncertainty is probably the snow cover. Nevertheless, Hoshiai (1985) found an unstable snow cover ranging between 5 and 20 cm on the top of autumn Antarctic sea ice. However, the actual growth rate of 0.004–0.013 d^{-1} is far too low in order to build up 6.32 μg chl *a* l^{-1} in 2 months with an assumed initial chl *a* concentration of 0.2 μg l^{-1} (Hoshiai, 1985). Nonetheless, algae in the upper parts received irradiances about twice as high as in the bottom of sea ice.

The ice algae are still active in autumn sea ice and low temperatures, irradiance and high brine salinities are most limiting algal photosynthesis and growth (e.g. Palmisano et al., 1985a, b, 1987; Sullivan et al., 1985; Grossi et al., 1987). Consequently autumn ice algae only remain photosynthetically active if they are able to continuously adapt to increasing brine salinities and decreasing light intensity until the light decreases below the threshold value for positive net photosynthesis. And this adaptation has to be even stronger in bottom of sea ice, where self-shading is also important for the reduction of light intensity (Palmisano et al., 1987).

With this improved *in situ* method, it is now able to make measurements even in young Antarctic sea ice. Nevertheless, this investigation is only another small step towards obtaining a realistic, precise and logistically cost effective estimates of sea ice primary production. Despite these improvements, such measurements remain unsatisfactory and creative methodologies need to be designed that enable photosynthetic and respiration measurements to be made in undisturbed *in situ* conditions (Mock & Gradinger, 1999). There is much promise in the adaptation of microelectrode techniques (McMinn & Ashworth, 1998; McMinn et al., 2000), although due to fragility, the methodologies for deploying these within the interior of the ice remains elusive. *In situ* incubations with radio-labelled tracers will remain a key tool in the study of ice productivity for the foreseeable future, and will generate key information, especially if they can be combined with parallel incubations to determine *in situ* heterotrophic activity.

Acknowledgements

I am grateful to the crew of the RV 'Polarstern' for their assistance during the expedition and I thank all the numerous people who helped me during the fieldwork. David Thomas and Gerhard Dieckmann are thanked for reviewing an earlier version of the manuscript, and making suggestions for its improvement.

References

Arar, E. J. & G. B. Collins, 1992. *In vitro* determination of chlorophyll *a* and phaeophytin *a* in marine and freshwater phytoplankton by fluorescence. Method 445.0. In: USEPA, Methods for the Determination of Chemical Substances in Marine and Estuarine Environmental Samples. EPA Cincinnati OH.

Arrigo, K. R., J. N. Kremer & C. W. Sullivan, 1993. A simulated Antarctic fast ice ecosystem. J. Geophys. Res. 98: 6929–6946.

Arrigo, K. R., D. L. Worthen, M. P. Lizotte, P. Dixon & G. Dieckmann, 1997, Primary production in Antarctic sea ice. Science 276: 394–397.

Clasby, R. C., R. Horner & V. Alexander, 1973. An *in situ* method for measuring primary production of Arctic sea ice algae. J. Fish. Res. Brd. Can. 30: 635–638.

Gleitz, M. & D. N. Thomas, 1993. Variation in phytoplankton standing stock, chemical composition and physiology during sea ice formation in the southeastern Weddell Sea, Antarctica. J. exp. mar. Biol. Ecol. 173: 211–230.

Gosselin, M., M. Levasseur, P. A. Wheeler, R. A. Horner & B. C. Booth, 1997, New measurements of phytoplankton and ice algal production in the Arctic Ocean. Deep-Sea Res 44: 1623–1644.

Grossi, S. M., S. T. Kottmeier, R. L. Moe, G. T. Taylor & C. W. Sullivan, 1987. Sea ice microbial communities. VI. Growth and primary production in bottom ice under graded snow cover. Mar. Ecol. Prog. Ser. 35: 153–164.

Hoshiai, T., 1985. Autumn proliferation of ice algae in Antarctic sea ice. In Siegfried, W. R., P. R. Condy & R. M. Laws (eds), Antarctic Nutrient Cycles and Food Webs. Springer Verlag Berlin, Heidelberg: 89–92.

Kirst, G. O. & C. Wiencke, 1995. Ecophysiology of polar algae. J. Phycol. 31: 181–199.

Kottmeier, S. T. & C. W. Sullivan, 1988. Sea ice microbial communities (SIMCO), 9. Effects of temperature and salinity on rates of metabolism and growth of autotrophs and heterotrophs. Polar Biol. 8: 293–304.

Martin, S., 1974. Ice stalactites: comparison of a laminar flow theory with experiment. J. Fluid. Mech. 63: 51–79.

Maykut, G. A., 1985. The ice environment. In Horner, R. (ed.), Sea Ice Biota. CRC Press, Boca Raton: 21–82.

McMinn, A. & C. Ashworth, 1998. The use of oxygen microelectrodes to determine the net production by Antarctic sea ice algal communities. Antarctic Sci. 10: 39–44.

McMinn, A., C. Ashworth & K. G. Ryan, 2000. *In situ* primary production of an Antarctic fast ice bottom algal community. Aquat. Microb. Ecol. 21: 177–185.

Melnikov, I., 1997. The Arctic Sea Ice Ecosystem. Gordon and Breach Science Publishers, Amsterdam.

Mobley, C. D., G. F. Cota, T. C. Grenfell, R. A. Maffione, W. S. Pegau & D. K. Perovich, 1998. Modeling light propagation in sea ice. IEEE Transact. Geosci. and Remote Sens. 36: 1743–1749.

Mock, T. & R. Gradinger, 1999. Determination of Arctic ice algal production with a new in situ incubation technique. Mar. Ecol. Prog. Ser. 177: 15–26.

Mock, T. & R. Gradinger, 2000. Changes in photosynthetic carbon allocation in algal assemblages of Arctic sea ice with decreasing nutrient concentrations and irradiance. Mar. Ecol. Prog. Ser. 202: 1–11.

Palmisano, A. C., J. Beeler SooHoo & C. W. Sullivan, 1985a. Photosynthesis-irradiance relationship in sea ice microalgae from McMurdo sound, Antarctica. J. Phycol. 21: 341–346.

Palmisano, A. C., S. Kottmeier, R. L. Moe & C. W. Sullivan, 1985b. Sea ice microbial communities. IV. Effect of light perturbation on microalgae at the ice water interface. Mar. Ecol. Prog. Ser. 21: 37–45.

Palmisano, A. C., J. Beeler SooHoo, R. L. Moe & C. W. Sullivan, 1987. Sea ice microbial communities. VII. Changes in under ice spectral irradiance during the development of Antarctic sea ice microalgal communities. Mar. Ecol. Prog. Ser. 35: 165–173.

Perovich, D. K. & T. C. Grenfell, 1981. Laboratory studies of the optical properties of young sea ice. J. Glaziol. 27: 331–346.

Smith, R. E. H. & A. W. Herman, 1991. Productivity of sea ice algae: *In situ* vs. incubator methods. J. mar. Syst. 2: 97–110.

Smith, R. E. H., J. Anning, P. Clement & G. Cota, 1988. Abundance and production of ice algae in Resolute Passage, Canadian Arctic. Mar. Ecol. Prog. Ser. 48: 251–263.

Strickland, J. D. H. & T. R. Parsons, 1972. A practical handbook of sea water analysis. Bull. Fish. Res. Bd Can: 167 pp.

Sullivan, C. W., A. C. Palmisano, S. Kottmeier, S. M. Grossi & R. Moe, 1985. The influence of light on growth and development of sea ice microbial communities in McMurdo Sound. In Siegfried, W. R., P. R. Condy & R. M. Laws (eds), Antarctic Nutrient Cycles and Food Webs. Springer, Berlin: 78–83.

Trenerry, L. J., A. McMinn & K. G. Ryan, 2002. *In situ* microelectrode measurements of bottom-ice algal production in McMurdo Sound, Antarctica. Polar Biol. 25: 72–80.

Vol. 29: 297–306, 2002 | AQUATIC MICROBIAL ECOLOGY
Aquat Microb Ecol | Published October 23

Micro-optodes in sea ice: a new approach to investigate oxygen dynamics during sea ice formation

Thomas Mock[1,*], Gerhard S. Dieckmann[1], Christian Haas[1], Andreas Krell[1], Jean-Louis Tison[2], Andre L. Belem[1], Stathis Papadimitriou[3], David N. Thomas[3]

[1]Alfred-Wegener-Institute for Polar and Marine Research, Am Handelshafen 12, 27570 Bremerhaven, Germany
[2]Département des Sciences de la Terre et de l'Environnement, Université Libre de Bruxelles, 50 Avenue Franklin D. Roosevelt, 1050 Bruxelles, Belgium
[3]School of Ocean Sciences, University of Wales-Bangor, Menai Bridge, Anglesey LL59 5AB, Wales, UK

ABSTRACT: Oxygen micro-optodes were used to measure oxygen dynamics directly within the microstructure of sea ice by freezing the sensors into the ice during its formation. The experiment was conducted in a 4 m^3 mesocosm filled with artificial seawater and inoculated with a unialgal culture of the common Antarctic ice diatom *Fragilariopsis cylindrus* (Bacillariophyceae) to a final chlorophyll *a* (chl *a*) concentration of 11 µg l^{-1}. Ice growth was initiated 7 d after inoculation by reducing the air temperature to –10 ± 2°C and terminated 17 d later. The final ice thickness was 27 cm. One optode was frozen into grease ice and 2 others into the skeletal layer of the growing ice sheet. Increasing oxygen concentrations during ice crystal formation at the water surface and the ice-water interface revealed a strong inclusion of oxygen, which was either physically trapped and/or the result of photosynthesising diatoms. The major portion of oxygen was present as gas bubbles due to supersaturation as a result of increasing salinity and oxygen production by diatoms. An increase in salinity due to a concurrent decrease in ice temperatures during subsequent sea ice development reduced the maximum concentration of dissolved oxygen within brine. Thus, dissolved oxygen concentrations decreased over time, whereas gaseous oxygen was released to the atmosphere and seawater. The sensors are a significant advance on more conventional microelectrodes, because the recordings can be temperature and salinity compensated in order to obtain precise measurements of oxygen dynamics with regard to total (dissolved and gaseous) and dissolved oxygen in sea ice. Optodes do not consume oxygen during measurement over a long period under extreme conditions, which is another advantage for long-term deployment in the field.

KEY WORDS: *Fragilariopsis cylindrus* · Oxygen · Methods · Micro-optodes · Sea ice · Biogeochemistry

INTRODUCTION

Ecology of sea ice has been studied intensively for several decades (e.g. Meguro 1962, Bunt & Lee 1970, Alexander et al. 1974, Horner 1985, Dieckmann et al. 1991, Legendre et al. 1992, Gleitz et al. 1995, Arrigo et al. 1997, Melnikov 1997, Mock & Gradinger 1999, Lizotte 2001, Brierley & Thomas 2002, Trenerry et al. 2002), but it is only in recent years that sea ice biogeochemistry has received attention (Günther & Dieckmann 1999, Günther et al. 1999, Thomas et al. 2001, Thomas & Dieckmann 2002). Due to the lack of comprehensive temporal studies, the relationships between abiotic factors (e.g. irradiance, temperature, nutrients, ice texture, ice thickness) and biological processes (e.g. carbon uptake by algae, remineralisation), are still unclear. For instance, several workers (Gleitz

*E-mail: tmock@awi-bremerhaven.de

et al. 1995, Günther et al. 1999) measured phosphate accumulation as a consequence of heterotrophic production in combination with substantial dissolved inorganic carbon (DIC) depletion and strong oxygen oversaturation. This is contradictory to the expected oxygen consumption by microzooplankton and bacteria, of which the latter frequently exceeds primary production of microalgae (Grossmann & Dieckmann 1994). Such discrepancies can be best addressed by defined laboratory ice experiments where the concepts of brine channel architecture and internal surface area as the basis for interactions of organisms, colonisation and biogeochemical processes can be studied in detail (Krembs et al. 2000, 2001). Cryo-microscopical methods are now available which enable the visualisation of microorganisms in their brine channel habitat (Junge et al. 2001). Such developments are superb aids to define complex physicochemical and biogeochemical interactions within the intricate sea ice microbial networks. However, despite these developments, we are still unable to determine chemical or physical conditions in undisturbed brine channels. Consequently, our knowledge is mainly restricted to bulk parameters resulting in the development of concepts with unclear details about prevailing environmental conditions in the network of brine channels, pockets or bubbles. The main reason for this serious shortcoming is the inaccessibility of the ice interior due to texture and rigid nature of the ice.

Many of the problems facing the sea ice researcher are similar to those encountered when measuring production processes and fluxes across biological films and surface sediments (Krembs et al. 2000, 2001). The technological progress that has been revolutionary in the study of biofilms and sediments is the most appropriate source of tools for a new era in sea ice research. One of the most striking advances in the past 15 yr has been the development of microelectrodes for the study of diffusive boundary layers and profiles of dissolved gases with remarkably fine scale resolution (Herman & Rechnitz 1974, Revsbech et al. 1980, Jörgensen & Revsbech 1985, Revsbech & Jörgensen 1986, Klimant et al. 1995, De Beer et al. 1997).

Several studies have used microelectodes in sea ice investigations (McMinn & Ashworth 1998, McMinn et al. 2000, Kühl et al. 2001, Rysgaard et al. 2001, Glud et al. 2002, Trenerry et al. 2002). These microelectrodes were constructed exclusively to measure dissolved oxygen, however, they were not deployed directly in brine channels (McMinn et al. 2000). They are able to penetrate loose layers of ice crystals at the ice-water interface and the bottom few millimetres of sea ice which encompasses the bottom sea ice assemblages that are common in land fast ice (Rysgaard et al. 2001). *In situ* determination of dissolved oxygen, and therefore photosynthesis and respiration, is of fundamental importance in understanding the driving forces behind biogeochemical cycling within ice assemblages (Gleitz et al. 1995, Günther et al. 1999, Glud et al. 2002). Chemical processes such as redox-reactions are strongly influenced by the presence or absence of oxygen. The oxygen concentration is also influenced by physical processes within brine channels (Tsurikov 1979). Thus, oxygen is central in the interaction between physicochemical and biological processes (Jörgensen & Revsbech 1985).

Unfortunately, there are major limitations to the use of microelectrodes within brine channels of sea ice. They are not flexible and consume oxygen, which results in a strong influence on oxygen concentrations within small pore spaces (Klimant et al. 1995, 1997, Gouin et al. 1997). To overcome these constraints and to further develop our understanding of oxygen dynamics, we have investigated the use of oxygen micro-optodes in artificially produced sea ice. An array of micro-optodes was frozen into the ice as it was growing. Temperature and salinity compensation of the signals was possible by simultaneous freezing of a chain of thermistors in the same sea ice depth. Salinity was calculated based on temperature (Assur 1960). The deployment of the sensors within the brine channels for ca. 17 d indicated that oxygen concentrations were influenced by freezing of sea water, brine salinity, diffusive gas exchange and biological activity.

MATERIALS AND METHODS

Set-up of mesocosm experiment. The optodes were tested in a 4 m^3 polyethylene tank (mesocosm without exchange of water) placed in a large environmental basin at HSVA (Hamburgische Schiffbau- und Versuchsanstalt) in Hamburg, Germany. The mesocosm was filled with artificial seawater (Instant Ocean Salt) to a final salinity of 34 and f/2 nutrients (Guillard & Ryther 1962). At all times, the water was well mixed using a filterless water pump. Light was provided from above by fluorescence tubes (Osram, ultra-white). Surface irradiance at the ice surface was adjusted to 34 µmol photons m^{-2} s^{-1} for the entire period of the experiment. The mesocosm (water temperature 0°C) was inoculated with batch cultures of non-axenic *Fragilariopsis cylindrus* (Bacillariophyceae), originally isolated from the Antarctic, to a final chlorophyll *a* (chl *a*) concentration of 11 µg l^{-1}. This relatively high initial algal concentration was chosen to initiate a dense algal bloom in the ice. Ice growth was initiated 7 d after inoculation by reducing the room temperature to −10 ± 2°C and initiating ice crystal formation by fine water spray over the water surface (Haas et al. 1999, Krembs et al. 2001).

Physical, chemical and biological measurements. Air temperatures were logged every 10 min using a TinyTalk thermometer located 20 cm above the ice surface in a parallel tank. Ice and water temperatures were measured at intervals of 6 s using 2 thermistor sticks deployed near the optode array. They were composed of 10 Siemens K17 thermistors with a vertical spacing of 2 cm beginning 2 cm above the air-water interface. The thermistor tips extended horizontally by about 1.5 cm away from the vertical stick to avoid ice growth artefacts. Ice thickness measurements were performed at irregular time intervals by inserting a dipstick inside small drill holes.

Surface irradiance (photosynthetically active radiation [PAR]) was measured with a Li-Cor 1000 radiometer and a 4π sensor, whereas the underwater light field was recorded with a miniature Fiber Optic Spectrometer (Ocean Optics) fitted with a CC-3 cosine-corrected irradiance probe. This probe was placed 30 cm below the water surface. Readings were taken at irregular time intervals but parallel to the oxygen measurements.

Ice cores for the determination of chl *a*, phaeopigments, and bulk ice and brine salinities were drilled manually with a 12 cm ice auger at irregular time intervals throughout the ice phase of the experiment. The cores were sectioned into 5 to 7 cm sections and centrifuged for 15 min at −5°C to extract the brine (Krembs et al. 2001). The salinities of the brine and remaining melted ice were measured using a WTW LF 191 conductivity meter. For the determination of chl *a* and phaeopigments, brine and the remaining melted ice were filtered onto Whatman GF/F filters and analysed fluorometrically with a Turner Designs Model 10-AU digital fluorometer after Arar & Collins (1992).

The Type A micro-optodes (PreSense, Precision Sensing GmbH) have a measuring range from 0 to 500% air saturation. They possess fibre tips of ca. 40 µm which were coated with black silicon to ensure stability and to suppress any optical effects from the surrounding sea ice. The optical fibre was fixed in a syringe and guided through the needle (10 cm length). The micro-optodes were 2 point calibrated at −1°C in aerated artificial sea water with a salinity of 34 (100% air saturation) and a solution of 0.5% $NaSO_3$ (0% oxygen) before starting the experiment. A re-calibration of the optodes was not possible because the cables had to be severed for the thin section analysis needed to determine the position of the optodes in the ice. Four sensors were deployed at discreet intervals attached to a wooden support placed in a corner of the mesocosm (Fig. 1). The first sensor was placed 4 cm below the surface of the water (Optode 4), the second 15 cm below (Optode 15), the third 25 cm (Optode 25) and one in 60 cm depth (Optode 60) (Fig. 1). The sensor tips extended horizontally by about 12 cm from the vertical stick. Readings were taken with a Microx I (PreSens) at irregular time intervals with a maximum frequency of 3 times a day. Microx I measures the luminescence lifetime of the immobilised luminophore as the oxygen dependent parameter. Measurements are not affected by bending the fibre or the optical properties of the sample. Furthermore, intensity fluctuations of the light sources or bleaching effects of the indicators have no impact on the lifetime measurements. The Microx I uses a phase-modulation technique to evaluate the lifetime of the indicators. The oxygen content as % air-saturation can be calculated using Eq. (1):

$$[O_2] = \frac{1 - \frac{\tan\Phi}{\tan\Phi_0}}{K_{SV}\left\{\frac{\tan\Phi}{\tan\Phi_0} - 0.11\right\}} \quad (1)$$

where Φ_0 is the phase angle of oxygen free water, Φ is the measured phase angle, K_{SV} is the Stern-Volmer constant and $[O_2]$ is the oxygen content in % air saturation.

The conversion of % air saturation into µmol O_2 l^{-1} can be calculated as in Eq. (2):

$$O_2\ (\mu mol\ l^{-1}) = \left[\frac{p_{atm} - p_w(T)}{p_N} \times \frac{\%\ \text{air saturation}}{100} \times 0.2095 \times \alpha(T;S) \times 1000 \times \frac{M(O_2)}{V_M}\right] \times 31.25 \quad (2)$$

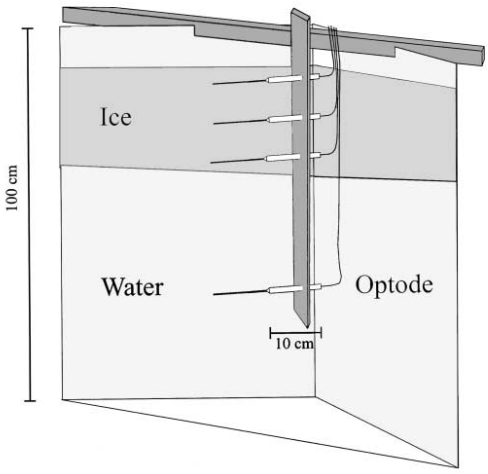

Fig. 1. Set-up of the oxygen micro-optode array in 1 corner of the mesocosm. The first sensor was placed 4 cm below the surface (Optode 4), the second 15 cm below (Optode 15), the third 25 cm (Optode 25) and one was placed at 60 cm depth (Optode 60). Ice thickness reached 27 cm at the end of the experiment

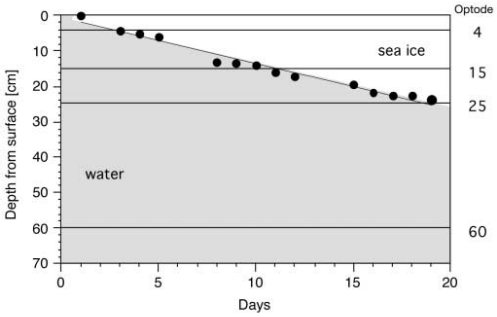

Fig. 2. Ice thickness during the experiment. Optode 4 was frozen on Day 3 in a grease ice layer, whereas Optode 15 was frozen on Day 10 and Optode 25 on Day 17 in the skeletal layer of sea ice. Optode 60 was the reference for seawater

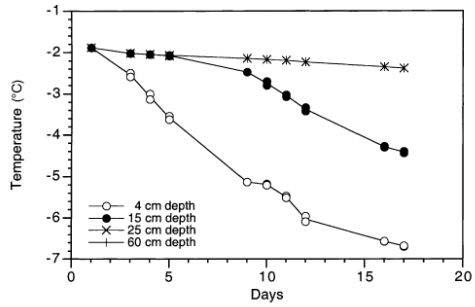

Fig. 3. Temperature shift during oxygen measurement in those depths where the optodes were placed. Optodes 4, 15, 25 and 60 are at 4, 15, 25 and 60 cm depth, respectively

where p_{atm} is the actual atmospheric pressure, p_N is the standard pressure (1013 mbar), 0.2095 is the volume content of oxygen in air, $p_w(T)$ is the vapour pressure of water at temperature T given in Kelvin, $M(O_2)$ is the molecular mass of oxygen (32 g mol^{-1}), V_M is the molar volume (22.414 l mol^{-1}), and $\alpha(T;S)$ is the Bunsen absorption coefficient at temperature T (Kelvin) and salinity S.

The conversion of % air saturation into µmol O_2 l^{-1} can only be calculated by considering the influence of temperature and salinity changes during sea ice formation and subsequent growth. Both parameters (T;S) have a strong influence on the concentration of dissolved oxygen in brine (Sherwood et al. 1991). The solubility of oxygen decreases with increasing salt concentrations and increases with decreasing temperatures. Consequently, a temperature compensation had to be conducted by using thermistors. The temperature data were also used to calculate brine salinity (Assur 1960) and chlorinity using Eq. (3):

$$[Cl^-] = \frac{S_b}{1.805} - 0.03 \quad (3)$$

where S_b is the brine salinity.

This is necessary to compensate for the salting-out effect with the Bunsen absorption coefficient $\alpha(T;S_b)$ using Eq. (4):

$$[\alpha(T;S_b)] = \exp\left[\left(A + \frac{B}{T} + C \times \ln T + D \times T\right) - [Cl^-] \times \left(P + \frac{Q}{T} + R \times \ln T + S \times T\right)\right] \quad (4)$$

where A is –7.424, B is 4.417×10^3, C is –2.927, D is 4.238×10^{-2}, P is -1.288×10^{-1}, Q is 53.44, R is -4.442×10^{-2} and S is 7.145×10^{-4}. A–D and P–S are coefficients based on measurements and polynomial fits (Instruction Manual for Microx TX, PreSence Precision Sensing).

Ten temperature measurements (60 s) were used for each reading point of oxygen. The average of the temperature/chlorinity data was used to compensate the oxygen measurements. More details on the measuring principle, calculation as well as the optodes themselves are available at www.PreSens.de. Oxygen titration according to the Winkler method (Strickland & Parsons 1972) was conducted on water samples from below sea ice at irregular time intervals in order to compare the water measurements taken with Optode 60. This comparison was not possible for the ice samples.

At the end of the experiment, an ice block in which the optodes were frozen was cut out from the ice sheet in order to determine the microstructure in which each sensor tip was embedded. In a –20°C cold room, thin cross sections of ca. 3 to 4 mm were cut to include and display the optode tips. Sections were photographed under ordinary light for best contrast between the black fibre tip and the pores or brine channels.

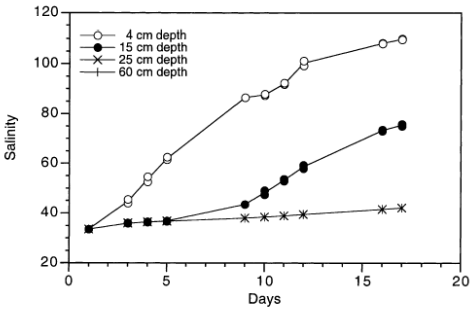

Fig. 4. Shift of calculated brine salinities in those depths where the optodes were placed. Optodes 4, 15, 25 and 60 are at 4, 15, 25 and 60 cm depth, respectively

Table 1. Chlorophyll *a* (chl *a*) concentration [µg l^{-1}] in brine. Chl *a* on Day 3 is given for the entire ice thickness (5 cm), on Day 10 for top (0 to 7 cm) and middle/bottom (7 to 14 cm) and on Day 17 for top (0 to 7 cm) and middle/bottom (7 to 21 cm)

Depth in sea ice	Day 3	Day 10	Day 17
Top	2.65	10.94	0.74
Middle/bottom		8.78	1.23

RESULTS

The ice grew at a rate of 0.54 mm h^{-1} after the reduction of room temperature and attained a thickness of 27 cm by the end of the experiment (Fig. 2). Ice growth was uniform over the surface of the mesocosm, and there were no signs of spatial heterogeneity in ice growth and properties. Consequently, Optodes 4, 15 and 25 were successively frozen into the ice. Optode 4 was frozen on Day 3, Optode 15 on Day 10 and Optode 25 on Day 17, whereas Optode 60 remained in the water as a reference probe. Each of the optodes experienced a different temperature shift during ice formation (Fig. 3). The temperature of Optode 4 decreased from –1.9 to –6.7°C, of Optode 15 from –1.9 to –3.4°C and for Optodes 25 and 60 from –1.9 to –2.2°C. This general decrease in ice temperatures resulted in an increase of calculated brine salinities from 34 to 110 at 4 cm depth and from 34 to 78 at 15 cm depth (Fig. 4). Measured salinities ranged within the same magnitude (Fig. 5). The increase was strongest in the upper parts (from 34 to 77), lower in the middle of the ice (from 34 to 62) and a slight increase was measured at the ice-water interface (from 34 to 42). Measured bulk salinities of the ice decreased inversely to the measured brine salinities indicating a desalination of the ice sheet.

The PAR was calculated from the entire under ice spectrum. It decreased from approximately 12 to below 1 µmol photons m^{-2} s^{-1} during the experiment, due to increasing ice thickness (Fig. 6).

Algal biomass in terms of chl *a* fluctuated during ice formation (Table 1). An initial enrichment in brine was measured in the early stages of ice formation especially in the upper parts of the ice (from 2.65 to 10.94 µg chl *a* l^{-1}) until Day 10. Thereafter, chl *a* concentrations decreased dramatically in the upper parts (from 10.94 to 0.74 µg chl *a* l^{-1}) and moderately in the middle and bottom portions (from 8.78 to 1.23 µg chl *a* l^{-1}).

Data obtained with the Microx I are calibrated but not corrected for temperature and salinity. The data are given in % air saturation and integrate both changes in temperature and salinity over time (Fig. 7). Optode 4 recorded oxygen oversaturation in the brine within the top of the sea ice (Fig. 7a), whereas relative oxygen concentrations in the bottom of sea ice, measured with Optode 15 after Day 10, were nearly identical to those of the water below (Fig. 7b,c,d). In general, the temporal trend of oxygen in the water decreased from 89 ± 4.0 to 60 ± 0.5 % air saturation. Temperature

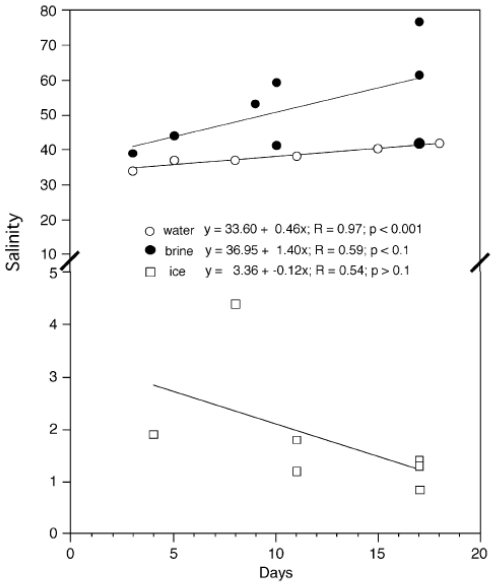

Fig. 5. Water, brine and bulk salinity during sea ice formation

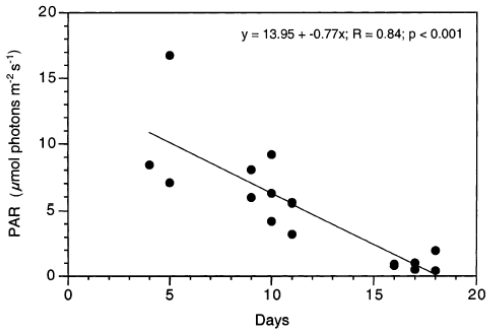

Fig. 6. Irradiance (photosynthetically active radiation = PAR) measured with a miniature fibre optic spectrometer suited 30 cm below the water surface

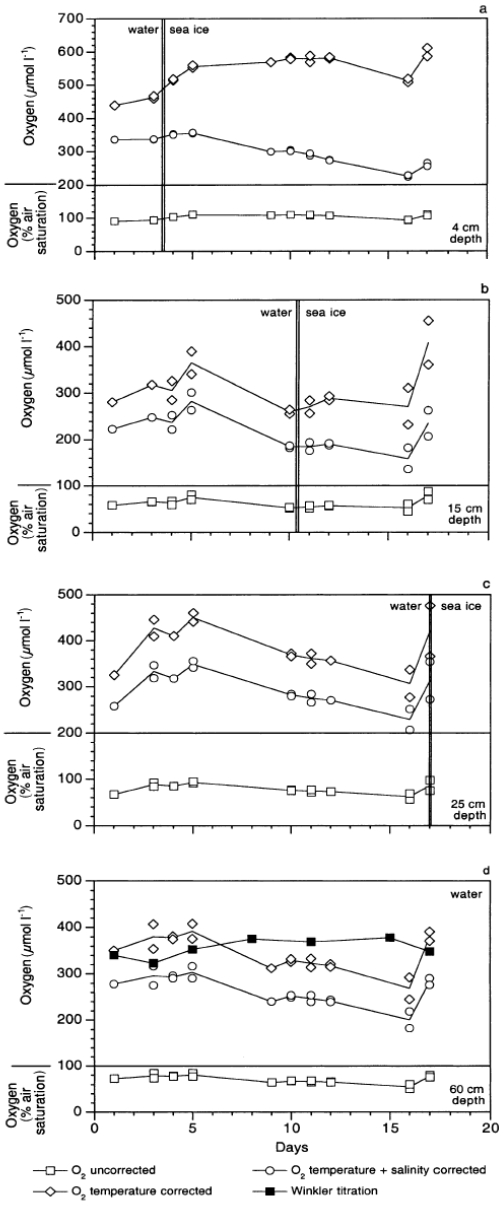

Fig. 7. Oxygen concentrations as % air saturation (O_2 uncorrected) and in µmol l^{-1} (O_2 temperature corrected; temperature + salinity corrected oxygen measurements) within sea ice and seawater below the ice for (a) Optode 4, (b) Optode 15, (c) Optode 25 and (d) Optode 60

compensation resulted in micromolar oxygen concentrations, which verified the uncorrected Microx I data with regard to the temporal trends. These data also indicated higher oxygen concentrations within the top of the ice compared to the water below. The first significant increase of oxygen occurred on Day 3 of freezing (Optode 4) and in the skeletal layer of the growing ice at Day 10 (Optode 15). The salinity correction takes into account the gassing out effect of oxygen with increasing salinity. This gives the dissolved oxygen concentration under this condition, whereas the temperature corrected as well as the uncorrected data represent both dissolved and gaseous oxygen. This phenomenon of oxygen out-gassing is most pronounced in the top of sea ice, where dissolved oxygen concentrations (temperature and salinity corrected) rapidly decreased with increasing brine salinities (Figs. 4 & 7a). A small out-gassing event probably also occurred during growth of the skeletal layer (Fig. 7b). Temperature and salinity corrected oxygen concentrations are almost constant over 3 d, whereas the temperature corrected data increased significantly, which was not observed at 25 and 60 cm water depth (Fig. 7c,d). The chemically determined oxygen concentrations in seawater corresponded well with optode measurements for the first 5 d of the experiment. Thereafter, Winkler oxygen increased, whereas Optode 60 recorded decreasing values.

Microscopic analyses reveal that each sensor tip was enclosed in a brine channel or pocket (Fig. 8a). Brine channels appear to be narrower in the top of the sea ice (Optode 4) than in the middle (Optode 15) or the skeletal layer (Optode 25). Also, small gas bubbles were more numerous in the top of sea ice than in the middle or bottom parts.

DISCUSSION

In situ determination of oxygen within a completely undisturbed brine channel system of sea ice has been impossible up to now. Although McMinn & Asworth (1998), Kühl et al. (2001), Rysgaard et al. (2001) and others, e.g. Trenerry et al. (2002), successfully introduced microelectrodes in sea ice ecology, these studies were either conducted in the diffusive boundary layer between sea ice and seawater with remote-controlled devices (McMinn et al. 2000, Trenerry et al. 2002) or with a tripod and divers (Kühl et al. 2001, Rysgaard et al. 2001). The latter technique enabled measurements of oxygen distribution within loose layers of microalgae just beneath the solid ice cover or even within the lowermost mm of the skeletal layer. However, both techniques have limitations, which are related to the measuring principle of electrodes, their stability, as

well as the constructions of the devices (Klimant et al. 1997). Oxygen optodes compared to oxygen electrodes do not consume oxygen (Klimant et al. 1995) and they are also able to measure gaseous oxygen. The electrode is immersed in an electrolyte and separated from interfering species by a membrane permeable to oxygen. A flow of dissolved oxygen through this membrane is induced by the consumption of oxygen by the electrode. Non-oxygen consuming sensors, however, are of paramount importance for long-term measurements in semi-enclosed brine channel systems of sea ice. The stability of the optode is guaranteed by the flexibility of the glass fibre and the coating of the sensor with silicon (PreSens). These advantages make the optodes an ideal instrument for determination of oxygen evolution or consumption in brine channels or even enclosed brine pockets. This is only possible by freezing of optodes during sea ice formation, a process, which results in a change of physical and biogeochemical properties of seawater. The effects of such changes on the dynamics of oxygen which is influenced by chemical as well as biological processes are still unknown.

Nevertheless, measurements in small brine channels or even spheres could reveal strong heterogeneity in oxygen concentrations caused by bubble formation and aggregates of either oxygen-producing (algae) or oxygen-consuming organisms (bacteria). One problem during long-term deployment could be the development of bacterial films on the sensor tip, which was not observed during our experiment. Nonetheless, the general differences in oxygen concentrations between the optodes at the beginning of the experiment remains to be resolved because all the optodes were still in the same well-mixed seawater (Fig. 7). With the exception of this problem, optode measurements are able to resolve small scale heterogeneity in sea ice. However, more sensor arrays would need to be deployed to obtain a representative overview of the oxygen dynamics within sea ice. Sack hole sampling of brine is not appropriate because brine collection takes too long, thereby enabling gassing out of hyperoxic brines (Gleitz et al. 1995). Optode measurements are more precise, leading to a better estimate of ecosystem productivity, which varies considerably during different stages of ice algal blooms and inducing dramatic changes in biogeochemical cycles (Günther et al. 1999, Thomas & Dieckmann 2002).

The discrepancy between temperature corrected (total oxygen: dissolved and gaseous) and salinity corrected oxygen (dissolved oxygen) during ice crystal formation at the water surface and the ice-water interface revealed a strong incorporation of gaseous oxygen, which could be the result of physical entrapment of oxygen producing algae and a salinity increase

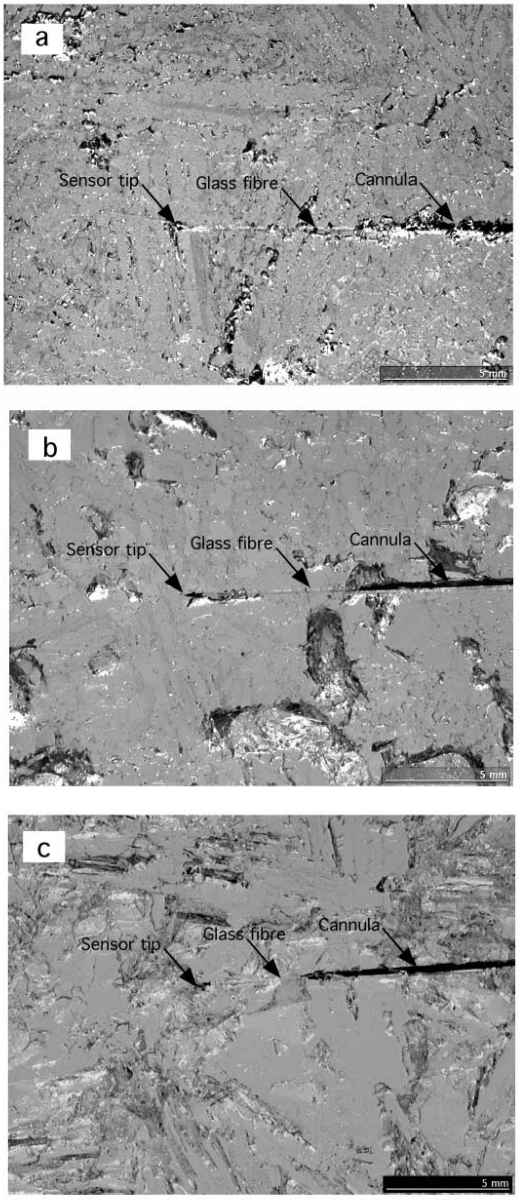

Fig. 8. Thin sections of frozen optodes at the end of the experiment. (a) Optode 4 (4 cm ice depth); (b) Optode 15 (15 cm ice depth); (c) Optode 25 (25 cm ice depth = skeletal layer)

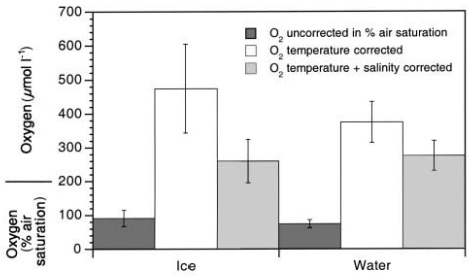

Fig. 9. Ice-water comparison of oxygen either as % air saturation (uncorrected measurements) or given in µmol oxygen l^{-1} (temperature corrected; temperature + salinity corrected oxygen measurements)

during freezing. The significantly higher concentration of gaseous oxygen in comparison to dissolved oxygen in sea ice could be elucidated by comparison of total oxygen data for ice and water (Fig. 9). In contrast to sea ice, no significant difference between gaseous and dissolved oxygen could be found in the seawater. It is reasonable to assume that the diatoms were passively accumulated by grease ice formation and that their photosynthetic activity under the higher light intensities at the surface, resulted in the elevated oxygen concentrations. The brine channels could therefore be oversaturated with oxygen, resulting in a release of gaseous oxygen from sea ice (see uncorrected data of Optode 4). This is also indicated by high concentrations of gas bubbles around Optode 4 (Fig. 8). A physical entrapment of oxygen within the primary ice layer at the water surface at a time when it consisted of separate crystals can also be assumed. The oxygen is probably incorporated partly from the atmosphere and partly from the water (Matsuo & Miyake 1966, Tsurikov 1979). Experiments with microelectrodes in artificial sea ice by Glud et al. (2002) confirmed the observation that brine is supersaturated while melt water is undersaturated with respect to dissolved oxygen. They speculated that the major portion of oxygen associated with the sea ice matrix is most likely trapped as gas bubbles that developed during the freezing process, which is confirmed by our measurements. Nevertheless, both physical and biological processes influence the gaseous oxygen in newly formed sea ice. Increasing salinities due to decreasing ice temperatures reduce the maximum concentration of dissolved oxygen within brine channels. The higher the brine salinity, the lower the maximum oxygen concentration which can be dissolved. This chemical relationship is assumed to be the reason for a temporal decrease in dissolved oxygen concentrations within sea ice (temperature and salinity corrected data of Optode 4). This salinity effect is most pronounced in the top of sea ice where ice is colder in comparison to the ice-water interface. However, the dynamics of oxygen at the ice-water interface is, in contrast, probably influenced by physically trapped oxygen and activity of algal communities, dominating the bottom habitat because the salinity difference to sea water was less pronounced here. Optode 15 recorded an increase in total oxygen (temperature corrected oxygen) during skeletal layer formation from Days 10 to 12. The highest biomass in terms of chl *a* in this layer and a strong reduction of biomass in the top layers was also recorded during this time. A release of gas from solution during subsequent freezing of sea water at the ice-water interface also occurs during ice growth (Tsurikov 1979). Winkler titrations and optode measurements (Fig. 7) confirmed the release of oxygen during sea ice formation between Days 3 and 5. However, the oxygen concentrations in water remained almost constant after Day 5 as determined by Winkler, whereas optode measurements revealed decreasing values (Fig. 7b,c,d; water).

Salinity and density of brine in the upper layer of the sea ice increase because of the rejection of salt by the growing ice sheet. This caused desalination of the ice, which is confirmed by decreasing bulk salinities during freezing (Fig. 5) and generated an unexpected high loss of initially trapped diatoms. Nevertheless, such changes in pigment concentration could also be caused by changes of chl *a*:carbon ratios, which probably decreased due to increasing irradiance in the top of sea ice. Photosynthesis of diatoms at the sea ice surface was more likely inhibited by high salinities and low temperatures, whereas diatoms at the sea ice-water interface were probably inhibited by low photon flux densities of not more than 1 µmol photons m^{-2} s^{-1} (Fig. 6). Nutrient limitation could be excluded in the artificial seawater enriched by f/2 nutrients.

The measurements with micro-optodes have improved our understanding of oxygen dynamics in sea ice, which is vital for modelling biogeochemical cycles (Thomas & Dieckmann 2002). This method combined with novel measurements by Eicken et al. (2000) using magnetic resonance imaging (MRI) to investigate small scale processes in changing temperature regimes occurring during sea ice formation may help to better understand the dramatic influence of gas dynamics in sea ice and related biological activity. Optical observations to investigate microstructural influences on the distribution of algae and bacteria (Junge et al. 2001) would complete the detailed investigation of small scale microstructural processes within sea ice brine channels and pockets.

CONCLUSIONS

This study demonstrated the first use of micro-optodes to investigate oxygen dynamics within undisturbed brine channels of sea ice. Although experiments were done in an artificial experimental tank, the results give reason to believe that further developments will enable their deployment in the field. The sensors are a significant advance over more conventional microelectrodes. They are ideal for long-term deployment in the field because they can be temperature and salinity compensated and do not consume oxygen during measurements over a long period under low temperatures. The optodes withstand freezing without damage to the sensor tip, an important prerequisite to measure directly within brine channels or brine pockets of sea ice without disturbing the ice texture or brine chemistry. Evidently, both physicochemical and biological processes influence the oxygen concentrations in sea ice. Oxygen is obviously incorporated during sea ice formation and enhanced by photosynthetic activity of micro-algae, resulting in supersaturation, especially in the top layers of sea ice. However, the major proportion of oxygen is not dissolved in brine, but is concentrated in the form of air bubbles or released to the seawater.

Acknowledgements. We would like to thank the Hamburg Ship Model Basin (HSVA), especially K. U. Evers and the ice tank crew, for hospitality, technical support and professional execution of the test programme in the ARTECLAB. The research activities carried out at the Major Research Infrastructure ARTECLAB were granted by the Human Potential and Mobility Programme from the European Union through grant: HPRI-CT-1999-00035. D.N.T. is grateful also to the support of the Hanse Institute of Advanced Study and a NERC small research grant to the Bangor group. Special thanks are given to Erika Allhusen for her excellent technical assistance.

LITERATURE CITED

Alexander V, Horner R, Clasby CR (1974) Metabolism of Arctic sea ice organisms, Rep R74–4. Institute of Marine Science, University of Alaska, Fairbanks, p 1–120

Arar EJ, Collins GB (1992) *In vitro* determination of chlorophyll *a* and phaeophytin *a* in marine and freshwater phytoplankton by fluorescence. Method 445.0. In: US EPA (ed) Methods for the determination of chemical substances in marine and estuarine environmental samples. US Environmental Protection Agency, Cincinnati

Arrigo KR, Worthen DL, Lizotte MP, Dixon P, Dieckmann G (1997) Primary production in Antarctic sea ice. Science 276:394–397

Assur A (1960) Composition of sea ice and its tensile strength. SIPRE Res, Rep 44, Wilmette, IL, p 1–49

Brierley AS, Thomas DN (2002) The ecology of Southern Ocean sea ice. Adv Mar Biol 43:171–276

Bunt JS, Lee CC (1970) Seasonal primary production in Antarctic sea ice at McMurdo Sound in 1967. J Mar Res 28:304–320

De Beer D, Glud A, Epping E, Kühl M (1997) A fast-responding CO_2 microelectrode for profiling sediments, microbial mats, and biofilms. Limnol Oceanogr 42(7):1590–1600

Dieckmann G, Lange M, Ackley SF, Jennings J Jr (1991) The nutrient status in sea ice of the Weddell Sea during winter: effects of sea ice texture and algae. Polar Biol 11:449–456

Eicken H, Bock C, Wittig R, Miller H, Poertner HO (2000) Magnetic resonance imaging of sea-ice pore fluids: methods and thermal evolution of pore microstructure. Cold Reg Sci Technol 31:207–225

Gleitz M, Vonderloeff MR, Thomas DN, Dieckmann GS, Millero FJ (1995) Comparison of summer and winter inorganic carbon, oxygen and nutrient concentrations in Antarctic sea ice brine. Mar Chem 51(2):81–91

Glud RN, Rysgaard S, Kühl M (2002) A laboratory study on O_2 dynamics and photosynthesis in ice algal communities: quantification by microsensors, O_2-exchange rates, ^{14}C incubation and PAM fluorometer. Aquat Microb Ecol 27:301–311

Gouin JF, Baros F, Birot D, Andre JC (1997) A fibre-optic oxygen sensor for oceanography. Sensors Actuators B 38–39: 401–406

Grossmann S, Dieckmann GS (1994) Bacterial standing stock, activity, and carbon production during formation and growth of sea ice in the Weddell Sea, Antarctica. Appl Environ Microbiol 60:2746–2753

Guillard RR, Ryther JH (1962) Studies of marine plankton diatoms. I. *Cyclotella nana* (Husted) and *Detonula confervacea* (Cleve). Can J Microbiol 8:229–239

Günther S, Dieckmann GS (1999) Seasonal development of algal biomass in snow-coverd fast ice and the underlying platelet layer in the Weddell Sea, Antarctica. Antarct Sci 11(3):305–315

Günther S, Gleitz M, Dieckmann GS (1999) Biogeochemistry of Antarctic sea ice: a case study on platelet ice layers at Drescher Inlet, Weddell Sea. Mar Ecol Prog Ser 177:1–13

Haas C, Cottier F, Smedsrud LH, Thomas D and 7 others (1999) Multidisciplinary ice tank study shedding new light on sea ice growth processes. EOS 80(43):507–513

Herman HB, Rechnitz GA (1974) Preparation and properties of a carbonate ion-selective membrane electrode. Anal Chim Acta 76:155–164

Horner R (1985) Sea ice biota. CRC, Boca Raton

Jörgensen BB, Revsbech NP (1985) Diffusive boundary layers and the oxygen uptake of sediments and detritus. Limnol Oceanogr 30:111–122

Junge K, Krembs C, Deming J, Stierle A, Eicken H (2001) A microscopic approach to investigate bacteria under *in situ* conditions in sea ice samples. Ann Glaciol 33:304–310

Kirst GO, Wiencke C (1995) Ecophysiology of polar algae. J Phycol 31:181–199

Klimant I, Meyer V, Kühl M (1995) Fiber-optic oxygen microsensors, a new tool in aquatic biology. Limnol Oceanogr 40:1159–1165

Klimant I, Kühl M, Glud RN, Holst G (1997) Optical measurement of oxygen and temperature in microscale: strategies and biological applications. Sensors Actuators B 38–39: 29–37

Krembs C, Gradinger R, Spindler M (2000) Implications of brine channel geometry and surface area for the interaction of sympagic organisms in Arctic sea ice. J Exp Mar Bio Ecol 243:55–80

Krembs C, Mock T, Gradinger R (2001) A mesocosm study of physical-biological interactions in artificial sea ice: effects of brine channel surface evolution and brine movement on algal biomass. Polar Biol 24:356–364

Kühl M, Glud RN, Borum J, Roberts R, Rysgaard S (2002)

Photosynthetic performance of surface associated algae below sea ice as measured with a pulse amplitude modulated (PAM) fluorometer and O_2 microsensors. Mar Ecol Prog Ser 223:1–14

Legendre L, Ackley SF, Dieckmann GS, Gulliksen B and 6 others (1992) Ecology of sea ice biota. 2. Global significance. Polar Biol 12:429–444

Lizotte M P (2001) The contributions of sea ice algae to Antarctic marine primary production. Am Zool 41:57–73

Matsuo S, Miyake Y (1966) Gas composition in ice samples from Antarctica. J Geophys Res 71(22):5235–5241

McMinn A, Ashworth C (1998) The use of oxygen microelectrodes to determine the net production by an Antarctic sea ice algal community. Antarct Sci 10:39–44

McMinn A, Ashworth C, Ryan KG (2000) *In situ* net primary productivity of an Antarctic fast ice bottom algal community. Aquat Microb Ecol 21:177–185

Meguro H (1962) Plankton ice in the Antarctic ocean. Antarct Rec 14:1192–1199

Melnikov IA (1997) The Arctic sea ice ecosystem. Gordon and Breach Science Publishers, Amsterdam

Mock T, Gradinger R (1999) Determination of Arctic ice algal production with a new *in situ* incubation technique. Mar Ecol Prog Ser 177:15–26

Revsbech NP, Jörgensen BB (1986) Microelectrodes: their use in microbial ecology. In: Marshall KC (ed) Advances in microbial ecology, Vol 9. Plenum Press, New York, p 293–352

Revsbech NP, Jörgensen BB, Blackburn TH (1980) Oxygen in the sea bottom measured with a microelectrode. Science 207:1355–1356

Rysgaard S, Kühl M, Glud RN, Hansen JW (2001) Biomass, production and horizontal patchiness of sea ice algae in a high-Arctic fjord (Young Sound, NE-Greenland). Mar Ecol Prog Ser 223:15–26

Sherwood JE, Stagnitti F, Kokkin MJ, Williams WD (1991) Dissolved oxygen concentrations in hypersaline waters. Limnol Oceanogr 36(2):235–250

Strickland JD, Parsons TR (1972) A practical handbook of sea water analysis. Bull Fish Res Board Can 167:310

Thomas DN, Dieckmann GS (2002) Antarctic Sea Ice—a habitat for extremophiles. Science 295:641–644

Thomas DN, Kennedy H, Kattner G, Gerdes D, Gough C, Dieckmann GS (2001) Biogeochemistry of platelet ice: its influence on particle flux under fast ice in the Weddell Sea, Antarctica. Polar Biol 24:486–496

Trenerry LJ, McMinn A, Ryan KG (2002) *In situ* oxygen microelectrode measurements of the bottom-ice algal production in McMurdo Sound, Antarctica. Polar Biol 25:72–80

Tsurikov VL (1979) The formation and composition of the gas content of sea ice. Journal of Glaciology 22:67–81

Editorial responsibility: Karin Lochte, Kiel, Germany

Submitted: January 14, 2002; Accepted: June 14, 2002
Proofs received from author(s): September 19, 2002

Vol. 30: 197–205, 2003 | AQUATIC MICROBIAL ECOLOGY
Aquat Microb Ecol | Published January 7

A new microcosm to investigate oxygen dynamics at the sea ice water interface

Thomas Mock[1,*], Marcel Kruse[2], Gerhard S. Dieckmann[1]

[1]Alfred Wegener Institute for Polar and Marine Research, Am Handelshafen 12, 27570 Bremerhaven, Germany
[2]Denkmanufaktur GmbH, Vor der Reihe 1, 26197 Großenkneten, Germany

ABSTRACT: A laboratory sea ice microcosm was developed to enable the cultivation of the ice diatom *Fragilariopsis cylindrus* in the skeletal layer and bottom 10 cm of sea ice. Growth of diatoms was ensured by continuous flow of new medium beneath the ice. Light was provided from above by a metal halide lamp to simulate a typical natural daylight irradiance spectrum. Oxygen micro-optodes were deployed in the microcosm to measure micro-profiles through the ice water interface and between the ice lamellae of the skeletal layer. Net oxygen production at the ice water interface, at an irradiance of 40 µmol photons m^{-2} s^{-1} and –1.9°C, ranged between 0.0064 and 0.0225 nmol O_2 cm^{-2} s^{-1}. Algal biomass increased from 0.03 µg chlorophyll *a* (chl *a*) l^{-1} in the column interior to 42 µg chl a l^{-1} within 5 mm of the ice water interface. Oxygen micro-profiles revealed diffusive boundary layers (DBLs) which varied between ca. 460 and 1000 µm. DBLs were detected between ice lamellae, the periphery of the ice water interface and extending from the water below the ice through the ice water interface into the spaces between ice lamellae. An additional small-scale horizontal variability of DBLs was also reflected in the net photosynthetic activity. The small-scale patchiness of algae and the differences in DBL thickness were caused by physico-chemical processes (e.g. turbulence, water flow velocity), which in turn were influenced by ice lamellar structure at the ice water interface. These factors were the grounds for the observed variability in net-photosynthesis.

KEY WORDS: *Fragilariopsis cylindrus* · Methods · Microcosm · Micro-optodes · Oxygen · Photosynthesis · Sea ice

INTRODUCTION

The sea ice habitat is still a relatively under-explored research area. Although we have a reasonable understanding of the physics and ecology of sea ice-covered seas (Brierley & Thomas 2002, Thomas & Dieckmann 2002), biogeochemical processes taking place within the sea ice matrix are still largely unknown. This is due to limited access to sea ice throughout the year and the difficulties with sampling and *in situ* measurements (Smith & Hermann 1991, Mock & Gradinger 1999, McMinn et al. 2000, Kühl et al. 2001, Rysgaard et al. 2001). In the past decade, sea ice research has begun to benefit from the development of new technologies that enable the investigation of the sea ice interior (Mock & Gradinger 1999, Eicken et al. 2000, Junge et al. 2001) and the elucidation of small-scale oxygen distribution within brine channels during sea ice formation (Mock et al. 2002) and at the ice water interface (McMinn et al. 2000, Kühl et al. 2001, Rysgaard et al. 2001, Glud et al. 2002, Trenerry et al. 2002).

For the first time oxygen micro-optodes have enabled us to measure oxygen directly within sea ice brine channels or pockets without disturbing the ice matrix or the brine chemistry (Mock et al. 2002). However, this was only possible by freezing the sensors into growing ice. In consolidated ice, processes are best measured by adapting non-invasive methodologies such as NMR (nuclear magnetic resonance) (Eicken et al. 2000), cryo-microscopes (Junge et al. 2001) or PAM (pulse amplitude modulated fluorescence measurements) while sensors and microelectrodes are ideal for studying the ice water interface (McMinn et al. 2000,

*Email: tmock@awi-bremerhaven.de

Kühl et al. 2001, Rysgaard et al. 2001, Glud et al. 2002, Trenerry et al. 2002). Microelectrodes have been used to measure the diffusive boundary layer (DBL) of oxygen at the ice water interface in order to quantify net photosynthesis of algae (McMinn et al. 2000), which grow there. Sufficient nutrient supply, relatively constant temperatures and large spaces between the ice lamellae support the rich growth of sea ice algae within these few mm of sea ice called the skeletal layer (Horner et al. 1992). The most successful organisms living under these conditions are diatoms, which contribute a large proportion of the total polar primary productivity (e.g. Warwick 1988, Gleitz et al. 1998, Lizotte 2001).

The skeletal layer of sea ice consists of ice lamellae with pore spaces up to 1200 µm wide (Williams et al. 1992, Wettlaufer et al. 1997a, Krembs et al. 2000). The spacial complexity of this layer results from small-scale differences in pore space, which is related to lamellar growth and brine movement (Wettlaufer et al. 1997b). The skeletal layer and lamellae are a very dynamic interface due to fluctuating ice and water temperatures (Worster & Wettlaufer 1997). The critical factor affecting ice growth and the ablation of the skeletal layer is the flux of energy through the ice; hence, the steepness of the temperature gradient. Traditional investigations into ice cores or the use of divers to deploy chambers *in situ* have not yet been able to explain the complex processes at the ice water interface. There is an evident need for laboratory experiments and defined conditions to understand the consequences of variability of the ice water interface (Worster & Wettlaufer 1997) and the photosynthetic dynamics of ice-algae under simulated *in situ* conditions.

The aim of this study was to cultivate ice algae at the ice water interface using a microcosm under simulated *in situ* conditions, and to investigate the variability of DBLs on small spatial scales to infer the net photosynthesis of ice algae using oxygen microsensors (optodes). This approach was a further step towards unravelling the effect of small-scale variability on primary productivity at the sea ice water interface.

MATERIALS AND METHODS

Microcosm experiment. Artificial sea ice was formed in a 25 l acrylic-glass cylinder (height = 80 cm; radius = 10 cm) fixed in a supporting frame and placed in a freezer room (Fig. 1). The microcosm was filled with 0.2 µm filtered Antarctic seawater and inoculated with f/2 nutrients (Guillard & Ryther 1962). The cylinder was insulated with polystyrene plates to ensure freezing from the water surface downwards and not from the sides. After a decrease in the air temperature to –20°C, the ice thickness reached 40 cm within 2 d. The seawater below the ice was then exchanged with nutrient-enriched seawater (f/2) of 34 salinity, using a flow-through system at the base of the cylinder. The circulation system ensured a homogenous salinity and nutrient regime below the ice. Once these conditions had been established, 50 ml of a dense axenic *Fragilariopsis cylindrus* culture (5×10^5 cells ml^{-1}) was added through a septum in the bottom of the cylinder. The polystyrene insulation was removed and subsequent cooling continued at –10°C air temperature. Further freezing was controlled by transparent heating foils (Minco Products) surrounding the bottom 7 cm of the cylinder. Freezing was continued and regulated to allow incorporation of algae into the growing skeletal layer. The continuous flow-through system ensured a stable salinity of ca. 36 and constant nutrient supply. Seawater below the ice (ca. 2.5 l) was exchanged completely every 3 d. Continuous illumination was provided from above by a 250 W metal halide lamp (Siemens). A heat cut-off filter (KG1 Schott) between the lamp and the cylinder prevented melting of the ice surface. A stable skeletal layer of approximately 1 cm thickness harbouring growing algae was established after ca. 6 mo, following which the micro-optode experiments were started.

Pumps, fresh medium and a bottle for the overflow were maintained at ca. +10°C air temperature in a room adjacent to the freezer. Flexible tubes (inlet and outlet) linking this room and the microcosm were insulated to avoid freezing of the flow-through system.

Temperature and light measurements. Ice and water temperatures were monitored at irregular intervals prior to the establishment of stable sea ice conditions using an array of thermistors on the inside of the cylinder wall. Temperature recordings and visual observation of the skeletal layer helped to maintain stable conditions therein. The thermistor array comprised 8 Siemens K17 thermistors with a vertical spacing of 9 cm, installed 3 cm above the bottom of the cylinder. The thermistors extended horizontally 1.5 cm into the ice column.

Scalar irradiance (PAR = photosynthetically active radiation [400 to 700 nm] in µmol photons m^{-2} s^{-1}) was measured on the top of sea ice with a LI-COR 1000 radiometer and a 4π sensor during each experiment. In order to determine PAR at the ice water interface, fluxes were calculated from the surface scalar irradiance using Beer's law:

$$E_i = E_t \times e^{[-a-k_i \times d_z + k_{chl} \times chl(z)]} \quad (1)$$

where E_t = PAR on the sea ice surface; E_i = PAR at ice water interface; a = albedo (0.7 for frozen white ice) (Perovich 1996); k_i = diffusive attenuation coefficient

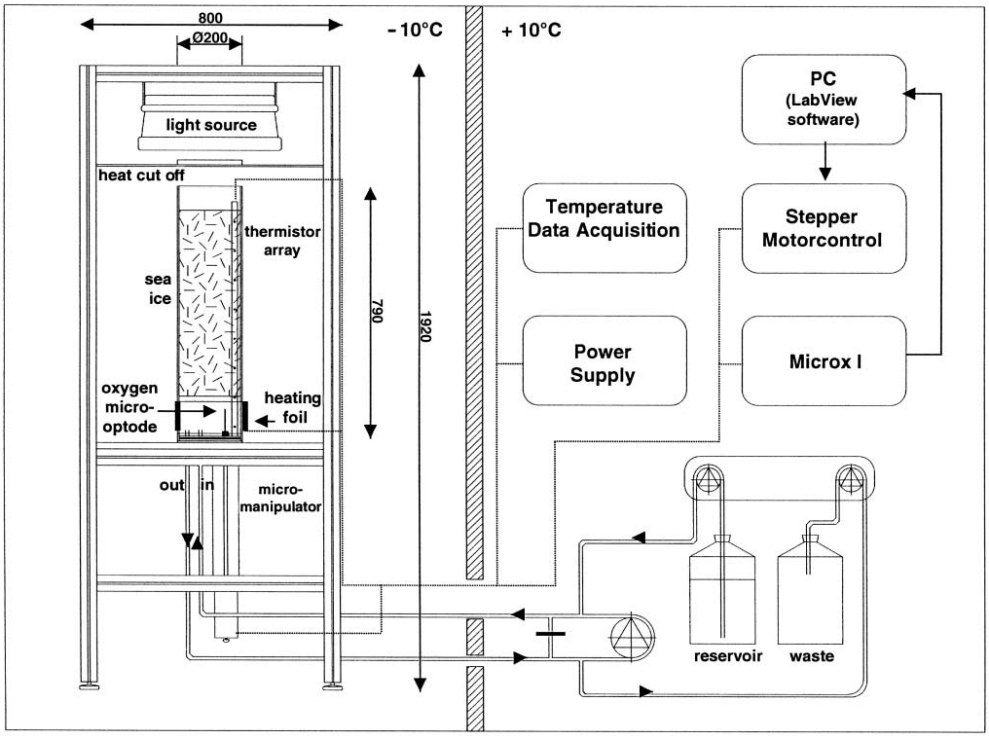

Fig. 1. Scheme of microcosm experiment. Scale given in mm

for ice (1.5 m^{-1}) (Maykut 1985); d_z = ice layer thickness (m); k_{chl} = mean spectral attenuation coefficient for chlorophyll *a* (chl *a*) (0.035 m^2 mg^{-1}) (Smith et al. 1988); chl(*z*) = chl *a* concentration in ice (mg m^{-2}).

Oxygen measurements. Micro-optodes of Type A, with a measuring range from 0 to 500 % air saturation (PreSens, Precision Sensing), were used to measure the oxygen dynamics within the skeletal layer, under ice water and the diffusive boundary layers. The sensor fibre has a diameter of 140 µm and is tapered to a tip of ca. 40 µm. This makes them ideal for inserting into the spaces (up to a diameter of 3000 µm) of the skeletal layer (ca. lowermost 10 mm of sea ice). To introduce the sensor into the ice, the optical fibre was passed through a standard syringe (1 ml) with a 30 cm needle. Micro-optodes were calibrated at −2°C in aerated seawater with a salinity of 36 and 100% air saturation and a solution of 0.5% $NaSO_3$ (0% oxygen). This calibration was conducted before and at the end of each measurement. The maximum sensor drift observed was a decrease of 7.3% air saturation (primary Microx meter signal), after 24 h sensor deployment in sea ice. A micro temperature sensor was pushed through a silicon septum into the lowermost mm of the skeletal layer to determine whether a temperature gradient, which would effect the optode signal, existed between the water below the ice and the lowermost mm of the skeletal layer. No gradient was measured. Since salinity and temperature are correlated we also ruled out a salinity gradient (Cox & Weeks 1983). Oxygen sensors were operated from below the cylinder using a motorised micromanipulator (NL4 Isel), to guide the sensors through the silicon septum visually to a position between the ice lamellae. The ice underside was defined as the zone where the micro-optode tip disappeared between ice lamellae. Visual guiding was possible because the ice water interface was relatively flat.

The micromanipulator was connected to a computer and a Microx I sensor control box (PreSens). Oxygen

measurements were based on the luminescence lifetime of the immobilised luminophore as the oxygen-dependent parameter (for further details see: www.presens.de). Signals of the micromanipulator (sensor depth) and the micro-optodes (oxygen as % air saturation) were processed and visualised using custom made Labview software (National Instruments), which also controlled the propulsion of the sensor into the ice.

The sensor was moved through the spaces between the ice lamellae in 6 to 100 µm steps with more than 4 measurements of oxygen per step and a temporal resolution of 1 s. A 24 h time series measurement of oxygen concentration was also conducted. Calculations of oxygen concentrations were made according to the Microx manual. The oxygen concentration as % air saturation was calculated according to Eq. (2):

$$[O_2] = \frac{1-\frac{\tan\Phi}{\tan\Phi_0}}{K_{SV}\times\left\{\frac{\tan\Phi}{\tan\Phi}-0.11\right\}} \quad (2)$$

where Φ_0 = phase angle of oxygen-free water; Φ = measured phase angle; K_{SV} = Stern-Volmer constant; $[O_2]$ = oxygen content as % air saturation.

The conversion of % air saturation into µmol O_2 l^{-1} is obtained with Eq. (3):

$$[O_2]\ (\mu mol\ l^{-1}) = \left[\frac{p_{atm}-p_w(T)}{p_N}\times\frac{\%\ \text{air saturation}}{100}\times 0.2095 \times\alpha(T;Cl^-)\times 1000\times\frac{M(O_2)}{V_M}\right]\times 31.25 \quad (3)$$

where p_{atm} = actual atmospheric pressure; p_N = standard pressure (1013 mbar); 0.2095 = volume content of oxygen in air; $p_w(T)$ = vapor pressure of water at temperature T (K); $M(O_2)$ = molecular mass of oxygen (31.25 g mol^{-1}); V_M = molar volume (22.414 l mol^{-1}); $\alpha(T;Cl^-)$ = Bunsen absorption coefficient at water temperature T (271°K) and chlorinity (20), which is assumed to be the same within the lowermost few mm of sea ice.

Photosynthesis. Net photosynthesis was calculated by using diffusive oxygen fluxes (J) based on the 1-dimensional version of Fick's first law of diffusion (Revsbech & Jørgensen 1986):

$$J = D_O\frac{dC(z)}{dz} \quad (4)$$

where D_O is the molecular diffusion coefficient (at –1.9°C = 1.11×10^{-5} cm^2 s^{-1}; Broecker & Peng 1974) and dC/dz is the concentration gradient.

Micro-optode experiments were conducted in a stable skeletal layer for a period of 5 d. This was an important prerequisite for the growth of diatoms. Without stable conditions the skeletal layer would either disappear by melting or advance by continuing lamellar growth. Both processes cause strong biomass fluctuation and changes in mass transfer of salt and gas (Glud et al. 2002). An outflow of dense brine was only observed during the initial stages of ice growth and not during oxygen measurements within the stable skeletal layer. The optode sensor tips were placed into the spaces of the skeletal layer up to a maximum distance of 2 mm without damage to the fragile tips or the ice lamellae. Whenever ice lamellae appeared to flake off, the measurements were abandoned. Sixteen micro-profiles were successfully completed, of which 3 examples are shown (see Fig. 4a,b,c). Five successful time series measurements were carried out, 1 of which is shown in Fig. 3.

Salinity, nutrient and pigment measurements. After the micro-optode experiments were completed, the sea ice column was removed from the cylinder. The bottom 10 cm of the ice column was cut into 5 and 10 mm horizontal sections using a stainless steel saw and melted at 4°C in the dark. Salinity of the melted ice sections was determined with a WTW (Wissenschaftlich Technische Werkstätten) salinometer and the brine volume fraction of ice was calculated according to Cox & Weeks (1983). Nutrient concentrations were determined according to standard seawater procedures in Grasshoff et al. (1983). For the determination of algal pigment concentrations (chl *a* and phaeopigments), thawed core sections were filtered onto Whatman GF/F filters extracted in 90% acetone and analysed fluorometically with a Turner Designs Model 10-AU digital fluorometer according to Arar & Collins (1992).

RESULTS

Sea ice formation began from the seawater surface after cooling below –2°C. A sea ice column of 60 cm had developed down to the heating foils after 8 d. The sea ice column was characterised by higher temperatures at the top and bottom with a minimum in the centre (Fig. 2). The air temperature increase from –20 to –10°C caused a general increase in sea ice temperatures and a reduction of the steep gradient in the bottom of the sea ice. A stable skeletal layer had developed ca. 1 mo later without any measurable variance in sea ice thickness. The micro-optode experiments were conducted 18 d later.

Dissolved oxygen concentrations between ice lamellae fluctuated over time as indicated by results obtained during 24 h period and under continuous light (Fig. 3). Strong fluctuations were recorded within the first 11 h, followed by a stable period for 5 h and a steep rise and continued increase in oxygen.

Oxygen microprofiles across the ice water interface and within the ice were highly variable. Three differ-

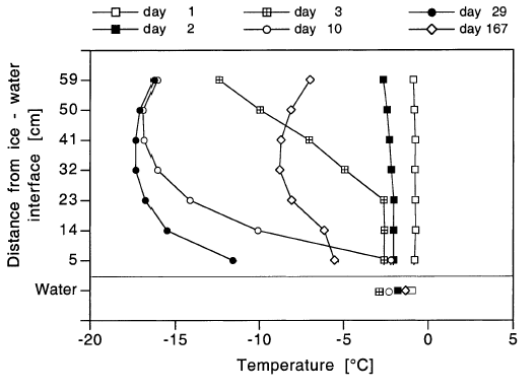

Fig. 2. Thermistor measurements in sea ice and seawater from the beginning of surface sea ice development at Day 1 to fully stabile ice conditions at Day 167

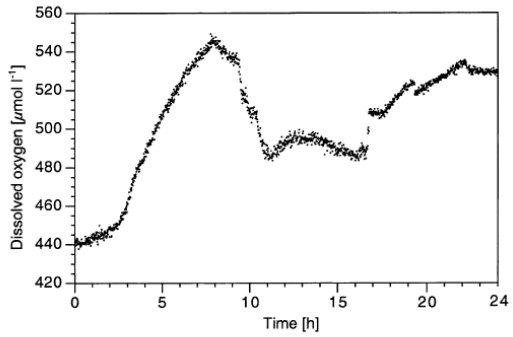

Fig. 3. Continuous measurements of dissolved oxygen concentrations within 1 brine channel of the skeletal layer measured over 24 h and continuous illumination

ent scenarios were observed: (1) a linear increase in oxygen concentration, which represented the diffusive boundary layers beginning with increasing concentrations in the water below the ice (Fig. 4a), (2) an increase beginning at the ice water interface (Fig. 4b) or (3) an increase beginning only between the ice lamellae (Fig. 4c). Only diffusive boundary layers within ice lamellae were used to determine net oxygen flux using Eq. (4). Net oxygen export ranged between 0.0064 and 0.0225 nmol O_2 cm^{-2} s^{-1} depending on the steepness of the dissolved oxygen gradient. The strongest gradient was measured within the ice, 1.5 mm from the ice water interface (Fig. 4c).

Chl *a* in the sea ice column was detectable to a distance of 100 mm from ice water interface (0.03 µg

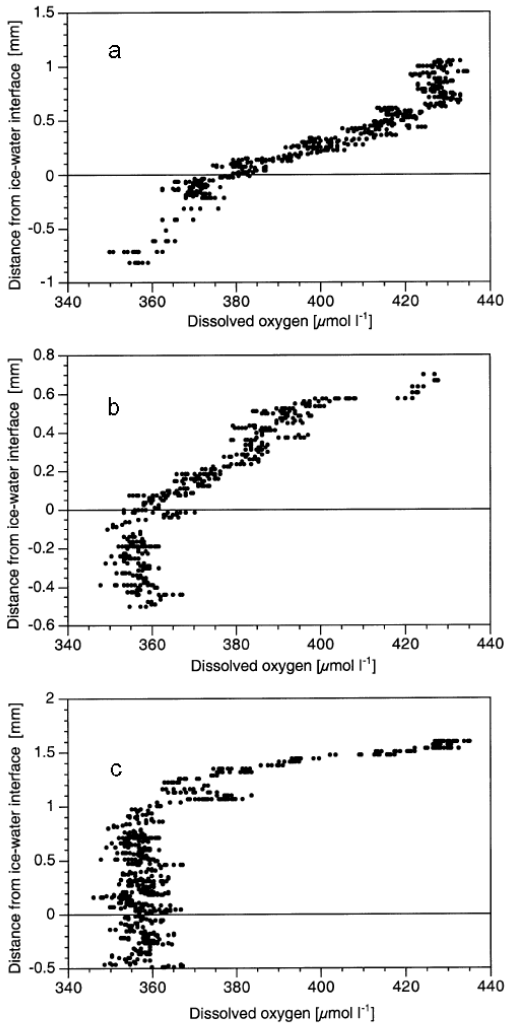

Fig. 4. Micro-profiles of dissolved oxygen measured at the sea ice water interface: (a) linear increase in oxygen concentrations, which represented the diffusive boundary layers beginning with increasing concentrations in the water below the ice; (b) increase beginning at the ice water interface; (c) increase beginning only between the ice lamellae

chl *a* l^{-1}) (Fig. 5) increasing steadily to a maximum of 42.06 µg chl *a* l^{-1} in the bottom 5 mm. The ice was characterised by a bulk salinity gradient (Fig. 6) with a minimum at 40 cm below the surface and a maximum

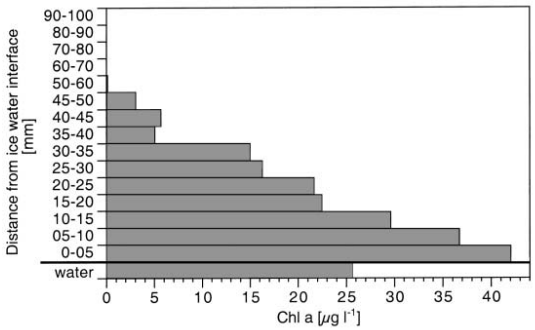

Fig. 5. Chl *a* distribution in the bottom 10 cm, where *Fragilariopsis cylindrus* was cultured

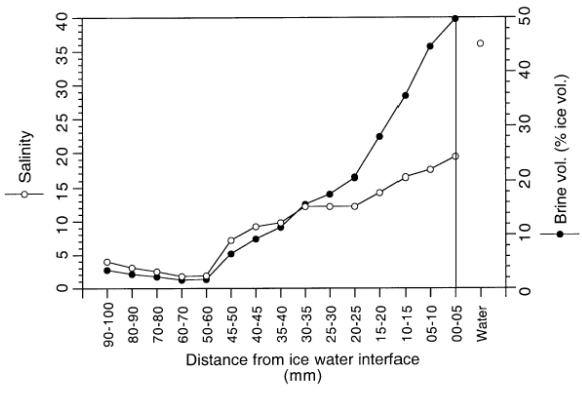

Fig. 6. Vertical profile of salinity in melted ice sections and relative brine volume as % of ice volume over the bottom 10 cm

at the ice water interface, which coincided with the biomass peak of *Fragilariopsis cylindrus*. The maximum brine volume of 50% also occurred at the ice water interface (Fig. 6). Nutrient concentrations were exceptionally high as expected for artificially enriched seawater (Fig. 7). The vertical distribution of nutrients through the bottom 100 mm of sea ice followed the bulk salinity profile with lowest nutrient concentrations in the interior and increasing concentrations towards the ice water interface.

Scalar irradiance at the top of the ice was 561 µmol photons m^{-2} s^{-1} during the experiments. Calculated scalar irradiance experienced by the algae at the ice water interface was 40 µmol photons m^{-2} s^{-1}.

DISCUSSION

The skeletal layer is characterised as a 3-dimensional network of ice lamellae, interspersed with layers of brine (e.g. Weissenberger et al. 1991), and differs structurally from sediment or stone surfaces. This was shown by our fluctuating oxygen measurements. Strongly fluctuating oxygen concentration in a brine channel, observed during a 24 h period of continuous illumination, is probably related to several factors. Percolation of brine occurred within the ice, which could cause a local decrease of oxygen concentration (Glud et al. 2002), although brine drainage was not observed. Brine from the interior of colder ice has a higher salinity and consequently lower oxygen concentration (Sherwood et al. 1991, Mock et al. 2002). Photosynthetic activity is reduced as salinity increases (Bates & Cota 1986, Mock &

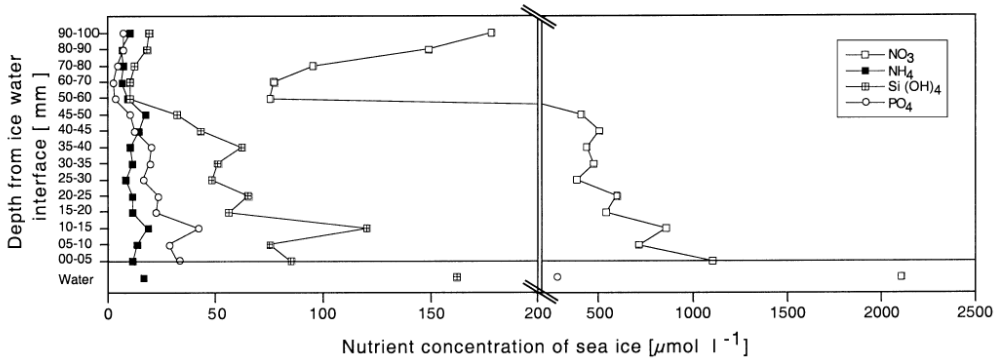

Fig. 7. Vertical profiles of nutrients in melted ice sections over the bottom 10 cm

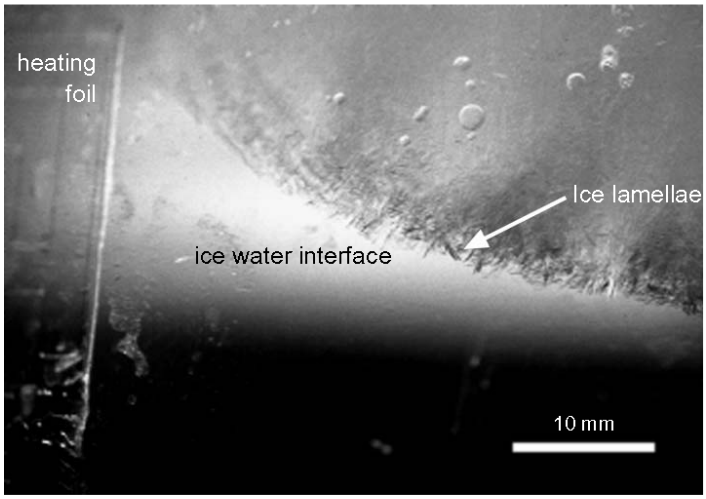

Fig. 8. ice water interface with large ice lamellae in the skeletal layer (bottom 10 mm of sea ice)

Gradinger 1999). The general trend, however, was an increase in oxygen concentration over time due to photosynthetic activity of *Fragilariopsis cylindrus*.

Oxygen micro-profiles revealed varying thicknesses of the DBL within a distance of a few cm. This implies a complex surface topography and thus an intricate DBL topography (Jørgensen & DesMaris 1990). We assume that DBLs develop at the base of each ice lamella, which also appears to be the locality of the algae. Thus a 1-dimensional geometry for 1-dimensional diffusion calculations still exists, albeit on a small scale. The 1-dimensional geometry changes to a radial geometry with increasing distance from the ice water interface, where vein-like brine channels dominate. The DBL thickness ranged from ca. 460 µm to >1000 µm across the ice water interface (Fig. 4). Differences in DBL thickness of the ejected seawater are affected by flow velocities and turbulence which are dependent on surface roughness (Jørgensen & Revsbech 1985). The roughness of the ice water interface which existed over different metric scales is assumed to be the main reason for strong variability of the boundary layer thickness. Our results demonstrate that the DBLs at the ice water interface and below the ice are in fact influenced by different sizes of ice lamellae (Fig. 8). It is well known from sediment studies that grains or pellets above 0.2 to 0.4 mm in size cause measurable deviations of the DBL thickness (Jørgensen & Revsbech 1985). The ice lamellae at the ice water interface were longer than 0.4 mm (Fig. 8). Gas bubbles, which formed during ice formation as a result of increasing salinities (salting-out effect) could also have contributed to the complex behaviour of oxygen at the ice water interface (Tsurikov 1979). However, this physical effect is assumed to be small within the stable skeletal layer.

The complex DBL topography can affect the transport coefficient and thus would invalidate the use of a 1-dimensional diffusion approach to estimate solute fluxes (M. Kühl pers. comm.) This is obviously even more the case under natural conditions. For instance, a significant mass transfer of salt and gases occurs, particularly during sea ice growth or melt or any other physical force, which causes advection of brine at the sea ice water interface. Such processes are probably negligible in our microcosm. Nonetheless, our calculated fluxes are comparable to oxygen fluxes measured under natural conditions (Table 1) (McMinn & Ashworth 1998, McMinn 2000, Buffan-Dubau 2001, Trenerrry et al. 2001). This could possibly be related to similar stable conditions whenever these natural oxygen fluxes were measured.

Strong differences in net photosynthesis determined in studies of natural sea ice populations were related to differences in assimilation numbers. The reported assimilation numbers for sea ice studies ranged from 0.0002 (Trenerry et al. 2001) to 2.0100 mg C mg^{-1} chl *a* h^{-1} (McMinn 2000), which was attributed to large differences in algal biomass between studies and large spatial heterogeneity of the sea ice algae. In future, we will have to measure chl *a* in the spatially confined areas in which we have determined the oxygen distribution (Kühl & Fenchel 2000). As the chl *a* measurements were imprecise, we did not attempt to calculate assimilation numbers for the algae.

Table 1. Net photosynthesis (nmol O_2 cm^{-2} s^{-1}) measured by microsensors in different microbial mats. Irradiance is given as photosynthetic active radiation (PAR) in µmol photons m^{-2} s^{-1} and temperature is given in °C

Type of measurement	Net photosynthesis	Irradiance	Temp.	Area	Source
Artificial	0.015–0.282	16–200	20–22	Skødstrup (Denmark)	Kühl et al. (1996)
Artificial	0–0.0042	0.1–33.1	–1.0	Davis (Antarctica)	McMinn & Ashworth (1998)
Natural	0.2	180	21	Wismar Bay (Germany)	Epping et al. (1999)
Natural	0.10–0.38	425	25–40	Solar Lake (Egypt)	Wieland & Kühl (2000)
Artificial	0.12	413	20	Niva Bay (Denmark)	Kühl & Fenchel (2000)
Natural	0.0084–0.0440	3–55	–1.8	Cap Evans (Antarctica)	McMinn et al. (2000)
Artificial	0.0083–0.0517	70	6	Lake Fryxell (Antarctica)	Buffan-Dubau et al. (2001)
Natural	0.0001–0.0034	0.2–7	–1.9	Cap Evans (Antarctica)	Trenerry et al. (2001)
Artificial	0.0064–0.0225	40	–1.9	Artificial substrate	This study

The multi-factorial influence of oxygen distribution debilitates the quantification of photosynthesis or the estimation of overall large-scale productivity from microprofiles. Primary production estimates of natural ice algal communities should therefore, in the foreseeable future, be conducted with radio-labelled tracers under *in situ* conditions (Mock 2002).

CONCLUSION

Fine-scale studies of oxygen measurements at the ice water interface, especially within the undisturbed sea ice skeletal layer, are still rare (McMinn et al. 2000, Kühl et al. 2001, Rysgaard et al. 2001, Glud et al. 2002). The described culture chamber used to grow sea ice and microalgae within sea ice over an extended time period (1 yr and longer) enables visible and mechanical access with micro-optodes to an undisturbed ice water interface. This preliminary investigation opens new perspectives in the use of new sensors such as micro PAM (pulse amplitude modulated fluorometer) sensors (Walz), CO_2 and pH sensors (PreSens) in sea ice research. The microcosm also enabled us to study ice algal photosynthesis, simulation of ice melt processes, changes in light intensity/spectrum (UV) and nutrient limitation via the flow-through system. Chemical processes in sea ice can be studied without the influence of biology (Glud et al. 2002). Consequently this microcosm is a tool for future research to bridge gaps in our knowledge of micro-environmental controls at the sea ice water interface.

Acknowledgements. David N. Thomas is thanked for reviewing an earlier version of the manuscript, and making suggestions for its improvement. We are also grateful to Michael Kühl and Andrew McMinn and 1 anonymous reviewer for helpful comments about an earlier version of this article. Special thanks to Erika Allhusen for her excellent technical assistance.

LITERATURE CITED

Arar EJ, Collins GB (1992) *In vitro* determination of chlorophyll *a* and phaeophytin *a* in marine and freshwater phytoplankton by fluorescence: method 445.0. In: US EPA (ed) Methods for the determination of chemical substances in marine and estuarine environmental samples. US EPA, Cincinnati, OH, p 1–22

Bates SS, Cota GF (1986) Fluorescence induction and photosynthetic response of Arctic ice algae to sample treatment and salinity. J Phycol 22:421–429

Brierley AS, Thomas DN (2002) The ecology of Southern Ocean sea ice. Adv Mar Biol 43:171–276

Broecker WS, Peng TH (1974) Gas exchange rates between air and sea. Tellus 26:21–35

Buffan-Dubau E, Pringault O, de Wit R (2001) Artificial cold-adapted microbial mats cultured from Antarctic lake samples. 1. Formation and structure. Aquat Microb Ecol 26:115–125

Cox GFN, Weeks WF (1983) Equations for determining the gas and brine volumes in sea ice samples. J Glaciol 29: 306–316

Eicken H, Bock C, Wittig R, Miller H, Poertner HO (2000) Magnetic resonance imaging of sea-ice pore fluids: methods and thermal evolution of pore microstructure. Cold Reg Sci Technol 31:207–225

Epping EHG, Khalili A, Thar R (1999) Photosynthesis and the dynamics of oxygen consumption in a microbial mat as calculated from transient oxygen microprofiles. Limnol Oceanogr 44:1936–1948

Gleitz M, Bartsch A, Dieckmann GS, Eicken H (1998) Composition and succession of sea ice diatom assemblages in the eastern and southern Weddell Sea, Antarctica. In: Lizotte MP, Arrigo KR (eds) Antarctic sea ice: biological processes, interactions and variability. Antarc Res Ser (AGU) 73:107–120

Glud RN, Rysgaard S, Kühl M (2002) A laboratory study on O_2 dynamics and photosynthesis in ice algal communities: quantification by microsensors, O_2 exchange rates, ^{14}C incubations and PAM fluorometer. Aquat Microb Ecol 27: 301–311

Grasshoff K, Erhard M, Kremling K (1983) Methods of sea water analyses, 2nd edn. Verlag Chemie, Weinheim

Guillard RR, Ryther JH (1962) Studies of marine plankton diatoms. I. *Cyclotella nana* (Husted) and *Detonula confervacea* (Cleve). Can J Microbiol 8:229–239

Horner R, Ackley SF, Dieckmann GS, Gulliksen B and 6 others (1992) Ecology of sea ice biota. 1. Habitat, terminology, and methodology. Polar Biol 12:417–427

Jørgensen BB, Des Marais DJ (1990) The diffusive boundary layer of sediments: oxygen microgradients over a microbial mat. Limnol Oceanogr 35:1343–1355
Jørgensen BB, Revsbech NP (1985) Diffusive boundary layers and the oxygen uptake of sediments and detritus. Limnol Oceanogr 30:111–122
Junge K, Krembs C, Deming J, Stierle A, Eicken H (2001) A microscopic approach to investigate bacteria under in situ conditions in sea ice samples. Ann Glaciol 33:304–310
Krembs C, Gradinger R, Spindler M (2000) Implications of brine channel geometry and surface area for the interaction of sympagic organisms in Arctic sea ice. J Exp Mar Bio Ecol 243:55–80
Krembs C, Tuschling K, Juterzenka KV (2002) The topography of the ice water interface — its influence on the colonization of sea ice by algae. Polar Biol 25:106–117
Kühl M, Fenchel T (2000) Bio-optical characteristics and the vertical distribution of photosynthetic pigments and photosynthesis in an artificial cyanobacterial mat. Microb Ecol 40:94–103
Kühl M, Glud RN, Ploug H, Ramsing NB (1996) Microenvironmental control of photosynthesis and photosynthesis-coupled respiration in an epilithic cyanobacterial biofilm. J Phycol 32:799–812
Kühl M, Glud RN, Borum J, Roberts R, Rysgaard S (2001) Photosynthetic performance of surface associated algae below sea ice as measured with a pulse amplitude modulated (PAM) fluorometer and O_2 microsensors. Mar Ecol Prog Ser 223:1–14
Lizotte MP (2001) The contributions of sea ice algae to Antarctic marine primary production. Am Zool 41:57–73
Maykut GA (1985) The ice environment. In: Horner R (ed) Sea ice biota. CRC Press, Boca Raton, FL, p 21–82
McMinn A, Ashworth C (1998) The use of oxygen microelectrodes to determine the net production by an Antarctic sea ice algal community. Antarct Sci 10:39–44
McMinn A, Ashworth C, Ryan KG (2000) *In situ* net primary productivity of an Antarctic fast ice bottom algal community. Aquat Microb Ecol 21:177–185
Mock T (2002) In situ primary production in young Antarctic sea ice. Hydrobiologia 470:127–132
Mock T, Gradinger R (1999) Determination of Arctic ice algal production with a new in situ incubation technique. Mar Ecol Prog Ser 177:15–26
Mock T, Dieckmann GS, Haas C, Krell A, Tison JL, Belem AL, Papadimitriou S, Thomas DN (2002) Micro-optodes in sea ice: a new approach to investigate oxygen dynamics during sea ice formation. Aquat Microb Ecol 29:297–306
Perovich DK (1996) The optical properties of sea ice. Cold Regions Research and Engineering Laboratory Monograph, Office of Naval Research, Arlington, VA, p 1–24
Revsbech NP, Jørgensen BB (1986) Microelectrodes: their use in microbial ecology. In: Marshall KC (ed) Advances in microbial ecology, Vol 9. Plenum Press, New York, p 293–352
Rysgaard S, Kühl M, Glud RN, Hansen JW (2001) Biomass, production and horizontal patchiness of sea ice algae in a high-Arctic fjord (Young Sound, NE-Greenland). Mar Ecol Prog Ser 223:15–26
Sherwood JE, Stagnitti F, Kokkin MJ, Williams WD (1991) Dissolved oxygen concentrations in hypersaline waters. Limnol Oceanogr 36(2):235–250
Smith REH, Herman AW (1991) Productivity of sea ice algae: In situ vs. incubator methods. J Mar Syst 2:97–110
Smith REH, Anning J, Clement P, Cota G (1988) Abundance and production of ice algae in Resolute Passage, Canadian Arctic. Mar Ecol Prog Ser 48:251–263
Trenerry LJ, McMinn A, Ryan KG (2002) In situ oxygen microelectrode measurements of the bottom-ice algal production in McMurdo Sound, Antarctica. Polar Biol 25: 72–80
Tsurikov VL (1979) The formation and composition of the gas content of sea ice. J Glaciol 22(86):67–81
Warwick VF (1988) Microbial ecosystems of Antarctica. Cambridge University Press, Cambridge
Weissenberger J, Dieckmann GS, Gradinger R, Spindler M (1991) Sea ice: a cast technique to examine and analyze brine pockets and channel structure. Limnol Oceanogr 37: 179–183
Wettlaufer JS, Worster MG, Huppert HE (1997a) The phase evolution of young sea ice. Geophys Res Lett 23: 1251–1254
Wettlaufer JS, Worster MG, Huppert HE (1997b) Natural convection during solidification of an alloy from above with application to the evolution of sea ice. J Fluid Mech 344: 291–316
Wieland A, Kühl M (2000) Short-term temperature effects on oxygen and sulfide cycling in a hypersaline cyanobacterial mat (Solar Lake, Egypt). Mar Ecol Prog Ser 196:87–102
Williams KL, Garrison GR, Mourad PD (1992) Experimental examination of growing and newly submerged sea ice including acoustic probing of the skeletal layer. J Acoust Soc Am 92:2075–2092
Worster MG, Wettlaufer JS (1997) Natural convection, solute trapping, and channel formation during solidification of saltwater. J Phys Chem 101:6132–6136

Editorial responsibility: Karin Lochte, Kiel, Germany

Submitted: April 22, 2002; Accepted: September 12, 2002
Proofs received from author(s): December 2, 2002

PERGAMON

Phytochemistry 61 (2002) 41–51

PHYTOCHEMISTRY

www.elsevier.com/locate/phytochem

Photosynthetic energy conversion under extreme conditions—I: important role of lipids as structural modulators and energy sink under *N*-limited growth in Antarctic sea ice diatoms

Thomas Mock[a,*], Bernd M.A. Kroon[a,b]

[a] *Alfred-Wegener-Institute for Polar and Marine Research, Am Handelshafen 12, D-27570 Bremerhaven, Germany*
[b] *KroonAqa GmbH, Kurrhahnstraße 9, D-27572 Bremerhaven, Germany*

Received 14 December 2001; received in revised form 2 May 2002

Abstract

The availability of dissolved nutrients such as nitrate under extreme low temperatures is a strong determinant in the development and growth of ice diatoms. Consequently we investigated regulation of photosynthesis in a mixed culture of three diatom species, which grew in chemostats at −1 °C, 15 μmol photons m^{-2} s^{-1} under *N*-limitation. When nitrogen is limiting, pigment–protein complexes are one of the most affected structures under low-light conditions. The loss of integral polar thylakoid components destabilized the bilayer structure of the membrane with consequences for lipid composition and the degree of fatty acid desaturation. *N*-Limitation caused a decrease in monogalactosydiacylglycerol (MGDG) and a simultaneous increase in bilayer forming digalactosyldiacylglycerol (DGDG). Their ratio MGDG:DGDG decreased from 3.4±0.1 to 1.1±0.4, while 20:5 n-3 fatty acids of chloroplast related phospholipid classes such as phosphatidylglycerol (PG) increased under *N*-limitation. These data reveal that lipids are important components, required to sustain membrane structure under a deficiency of integral membrane bound proteins and pigments. Nonetheless, energy conversion at photosystem II is still affected by *N*-limitation despite this structural regulation. Photosynthetic quantum yield (F_v/F_m) and electron transport rates decreased under *N*-limitation caused by an increasing amount of electron acceptors (second stable electron acceptor = Q_B) which had slower reoxidation kinetics. The energy surplus under these conditions is stored in triacylglycerols, the main energy sink in Antarctic sea ice diatoms under *N*-limitation.

Keywords: Bacillariophyceae; Carbohydrates; Fatty acids; Fluorescence; Lipids; Low temperature; Nitrogen limitation; Pigments; Proteins; Sea ice

1. Introduction

A dominant feature of the Southern Ocean is the sea ice canopy, which has been recognized as an important habitat that significantly contributes to Southern Ocean productivity (Arrigo et al., 1997). Productivity in sea ice is mainly based on micro-organisms, living in a network of brine channels and pockets, which have an average diameter of 200 μm (Weissenberger et al., 1992). This narrow space is characterized by low temperature, low photon flux densities and a reduced resupply of nutrients from seawater (e.g. Eicken, 1992; McMinn et al., 1999). Sea ice is therefore an environment, where organisms are always colimited by more than one resource and temperature, which allows the coexistance of species (Hutchinson, 1961).

Studies with green algae and higher plants have shown that cold adapted enzymes and an increase in membrane fluidity are important prerequisites for optimal photosynthesis and growth under polar conditions (Thomashow, 1998; Routaboul et al., 2000; Allen and Ort, 2001). Obviously only those diatom species can probably persist in Antarctic sea ice, which are cold adapted and able to regulate photosynthesis efficiently under simultaneous light and *N*-limitation. Ecophysiological investigations based on both limitations are still rare for sea ice diatoms and have been either conducted with natural communities or with single species (Tillmann et al., 1989; Kirst and Wiencke, 1995; Taguchi and Smith, 1997; McMinn et al., 1999). Our approach

* Corresponding author. Tel.: +49-471-4831 1893; fax: +49-471-4831-425.
E-mail address: tmock@awi-bremerhaven.de (T. Mock).

0031-9422/02/$ - see front matter
PII: S0031-9422(02)00216-9

Nomenclature

RC	reaction centre
PS II, I	photosystem II, I
LHC	light harvesting complex
D1/D2	PS II reaction centre proteins
Q_A	quinone A, first stable electron acceptor of PS II
Q_B	quinone B, second stable electron acceptor
F	fluorescence. Subscripts **o**, **v**, **m** represent the fluorescent level during light induction at the origin, variable and maximum levels, respectively.
F_v/F_m	quantum yield
q	reaction centers
p	connectivity between PS II units
Φ_f	fluorescence yield
Φ_P	quantum yield
$q1$	open reaction centres
$q0$	closed reaction centres
σ	effective cross section of PS II
A	fraction of PS II characterized by a fast fluorescence decay after turnover saturation flashes at a rate of K_A
B	fraction of PS II characterized by a middle fluorescence decay after turnover saturation flashes at a rate of K_B
C	craction of PS II characterized by a slow fluorescence decay after turnover saturation flashes at a rate of K_C
P vs I	photosynthesis (P) versus irradiance (I)
α	light limited slope of the P vs I curve/ light utilization effiziency
Ik	light level at which photosynthesis saturates
P_{max}	mximum rate of photosynthesis
K	rate constant for fluorescence decay measurements
A, B, C_{comp}	amplitudes of fluorescence decay rate constants (K)
J_{con}	connectivity between reaction centres (PS II)
FA	fatty acid
PUFA	polyunsaturated fatty acid
MGDG	monogalactosyldiacylglycerol
DGDG	digalactosyldiacylglycerol
PC	phosphatidylcholine
PG	phosphatidylglycerol
PE	phosphatidylethanolamin
PI	phosphatidylinositol
TAG	triacylglycerol
SQDG	sulfoquinovosyldiacylglycerol
NADPH	nicotinamide-adenine-dinucleotide-phosphate
ATP	adenosine-tri-phosphate
POC	particulate organic carbon
PON	particulate organic nitrogen
DIN	dissolved inorganic nitrogen

studies the mechanisms of photosynthesis regulation in diatom species, which coexist in the natural sea ice community (*Fragilariopsis curta, Navicula gelida* var. *antarctica, Nitzschia medioconstricta*) observed during an Antarctic expedition ("Polarstern" ANT XVI). We assume, that these diatoms share similar regulation mechanisms that are responsible for their success. Consequently, we investigated regulation of photosynthesis in a mixed culture of these three diatom species, which grew in chemostats at −1 °C under *N*-limitation. Defined conditions and the restricted number of diatom species in one chemostat enabled us to investigate processes of regulation, which might be universal for this group of diatoms. One of these fundamental processes is the regulation of photosynthetic energy conversion by chloroplast lipids, an unknown process in Antarctic sea ice diatoms. It has been pointed out that the degree of fatty acid desaturation and the lipid composition in thylakoide membranes is critical in maintaining optimal photosynthesis (Siegenthaler and Murata, 1998). This study focusses on nitrogen stress and its consequences for energy conversion at photosystem II (PS II) and the associated lipid classes as well as the desaturation of their fatty acids. Additionally, we present a concept of lipids as structural modulators and energy sink in *N*-limited Antarctic sea ice diatoms.

2. Results

2.1. Physiology

PS II related parameters of continuous cultures were significantly influenced by nitrogen availability (Table 1). Under nitrogen deplete conditions, during a 50% reduction in growth rate (0.28 day^{-1}), F_v/F_m decreases by 30% whereas connectivity between reaction centres decreased by at least 10%. Reoxidation kinetics of Q_A (first stable electron acceptor) were also negatively influenced by *N*-limitation for all three processes (Table 1). The electron transport is slower under *N*-limitation although more Q_B (second stable electron acceptor) was bound at D1 (reaction center protein of PS II), which is indicated by the fluorescent amplitude A (A_{comp}) (Table 2). This amount of bound Q_B was not influenced by 30 min dark adaptation of samples, which

was revealed in the comparison to measurements made only 90 s after sampling. Nevertheless, the rate constants remained high in comparison to other algae (Kroon 1994; Kroon and Prezelin, 1995).

Photosynthesis (P) defined as F_v/F_m*photon flux density (PFD) vs irradiance (I) measurements revealed that P_{max} (maximum of P), Ik (irradiance where P saturates) as well as α (light utilization efficiency defined as the slope of the P vs I curve) were negatively effected by N-limitation (Fig. 1). Each of these parameters was calculated on the basis of quantum yield (F_v/F_m) measurements, which were generally higher under nitrogen replete conditions (Fig. 2). This is primarily caused by a higher amount of oxidized reaction centres (K_{open}). Nitrogen limitation resulted in a stronger reduction of reaction centres because of reduced availability of nitrate as a very important electron sink. Consequently, the electrons can not be efficiently used for the reduction of nitrate and thus accumulate within the plastoquinone pool (PQ).

Pigment concentrations were affected by N-limitation. Chlorophyll (Chl) c, a and fucoxanthin decreased by about 50% (Fig. 3) with simultaneous changes in their

Table 1
Fluorescence variables for dissolved inorganic nitrogen (DIN) replete growth (0.55 day^{-1}) and deplete growth (0.28 day^{-1})

Variable	DIN replete	DIN deplete
J_{con}	0.341±0.010	0.308±0.017
K_{open}	0.408±0.015	0.255±0.021
F_v/F_m (yield)	0.337±0.009	0.236±0.025
K_A (m s^{-1})	11.16±1.34	4.24±1.01
K_B (m s^{-1})	0.42±0.12	0.16±0.08
K_C (m s^{-1})	0.02±0.02	0.00±0.01
r^2 (n=5)	0.966	0.797

Connectivity (J_{con}) between reaction centres (RC), open (K_{open}) RC and quantum yield are based on DCMU induction measurements. Fluorescence decay rate constants for fast K_A, middle K_B and slow K_C component. Values are given as relative units; n=5; r^2=model fit.

Table 2
Amplitudes of fluorescence decay rate constants for fast K_A (A_{comp}), middle K_B (B_{comp}) and slow K_C (C_{comp}) component for dissolved inorganic nitrogen (DIN) replete growth (0.55 day^{-1}) and deplete growth (0.28 day^{-1})[a]

Variable	DIN replete		DIN deplete	
	90 s	30 min	90 s	30 min
A_{comp}	0.011 0.012	0.012 0.012	0.018 0.022	0.017 0.018
B_{comp}	0.006 0.010	0.004 0.006	0.027 0.025	0.024 0.025
C_{comp}	0.001 0.001	0.001 0.001	0.002 0.009	0.006 0.002

[a] They were determined 90 s and 30 min after sampling; n=2.

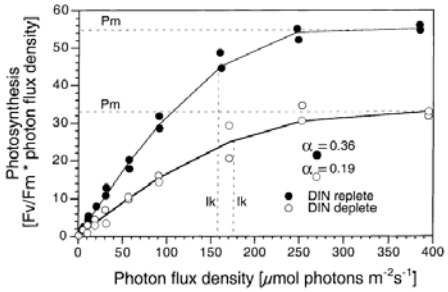

Fig. 1. Photosynthesis as F_v/F_m*photon flux density vs irradiance in ice diatoms under dissolved inorganic nitrogen (DIN) replete (μ=0.55 day^{-1}) and DIN deplete conditions (μ=0.28 day^{-1}) are based on DCMU induction measurements. Photosynthetic parameters α (light utilization effiziency), Ik (quantum flux of PAR at onset of light saturation), P_{max} (maximum photosynthetic rate) were calculated after Eilers and Peeters (1988); n=2.

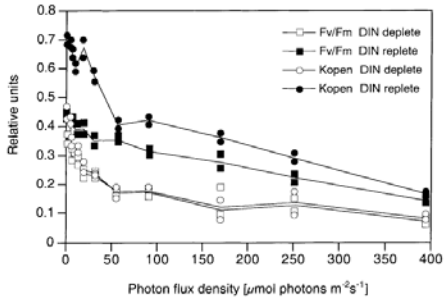

Fig. 2. Photophysiological parameters of photosynthesis vs irradiance curves based on DCMU induction measurements under dissolved inorganic nitrogen (DIN) replete (μ=0.55 day^{-1}) and DIN deplete (μ=0.28 day^{-1}) conditions. Kopen=relative proportion of oxidized reaction centres; F_v/F_m=quantum yield of photosynthesis; n=2.

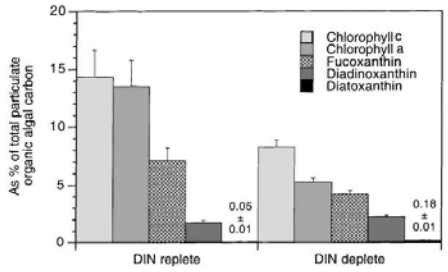

Fig. 3. Pigment composition of sea ice diatoms as% of total particulate organic algal carbon under dissolved inorganic nitrogen (DIN) replete and DIN deplete conditions with corresponding growth rates of 0.55 and 0.28 day^{-1}, respectively. Carotene was always below detection limit. Error bars denote standard deviations; n=3.

relative ratios, chl *c*:*a* from 1.0 to 1.6, and fucoxanthin:chl *a* from 0.5 to 0.8. Other carotenoids (diadinoxanthin, diatoxanthin) increased slightly, whereas β-carotene was always below the detection limit.

2.2. Biochemistry

N-Limitation imposed a potential problem for the algae: The protein pathway is partially blocked by a lack of sufficient dissolved nitrogen relative to the light input. Thus, the biochemical composition of the cell changed dramatically, which is already known from many other investigations (e.g. Pohl and Zurheide, 1979; Shifrin and Chisholm, 1981). The most frequently observed phenomenon under *N*-limitation is a proportional reduction of intracellular proteins to the reduced external availability of dissolved inorganic nitrogen (Fig. 4). Consequently the energy surplus from photosynthesis is stored or exudated in form of reduced substances, which contain no or only less nitrogen as in carbohydrates and lipids. Sea ice diatoms are known to store energy in the form of lipids, which was confirmed in our experiment. Lipids increased dramatically during *N*-limitation (Fig. 4). This was mainly caused by triacylglycerol production but also by production of polar lipids constituting diverse kinds of membranes (Fig. 5). The well known glycolipids, monogalactosyldiacylglycerol (MGDG) and digalactosyldiacylglycerol (DGDG), which are exclusively present in chloroplasts, were the dominant polar lipid classes in sea ice diatoms (Fig. 6). Their ratios changed during nitrate limitation due to a decrease in MGDG and an increase in DGDG (Fig. 7). Phospholipids phosphatidylcholine (PC), phosphatidylglycerol (PG) and phosphatidylinositol (PI) were preferentially synthesized during nitrogen limitation, whereas phosphatidylethanolamin (PE) decreased. PC was more concentrated under nitrogen limited growth, despite the presence of methylated nitrogen in the molecule, which probably indicates an

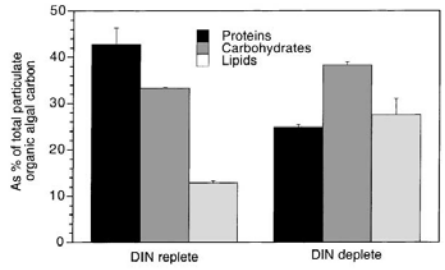

Fig. 4. Macromolecular composition of sea ice diatoms as% of total particulate organic algal carbon under dissolved inorganic nitrogen (DIN) replete and DIN deplete conditions with corresponding growth rates of 0.55 and 0.28 day^{-1}, respectively. Error bars denote standard deviations; $n = 3$.

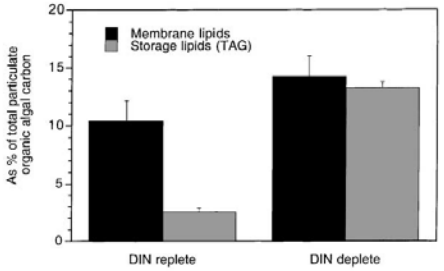

Fig. 5. Polar membrane lipids and storage lipids (triacylglycerol TAG) as% of total particulate organic algal carbon under dissolved inorganic nitrogen (DIN) replete and DIN deplete conditions with corresponding growth rates of 0.55 and 0.28 day^{-1}, respectively. Error bars denote standard deviations; $n = 3$.

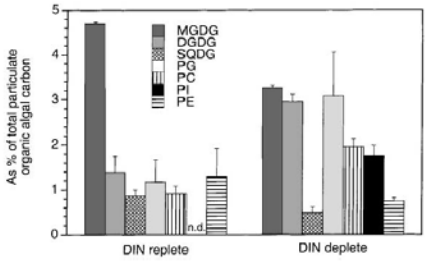

Fig. 6. Glyco- and phospholipid classes of sea ice diatoms in% of total particulate organic algal carbon under dissolved inorganic nitrogen (DIN) replete and DIN deplete conditions with corresponding growth rates of 0.55 and 0.28 day^{-1}, respectively. Error bars denote standard deviations; n.d. = not detectable; $n = 3$.

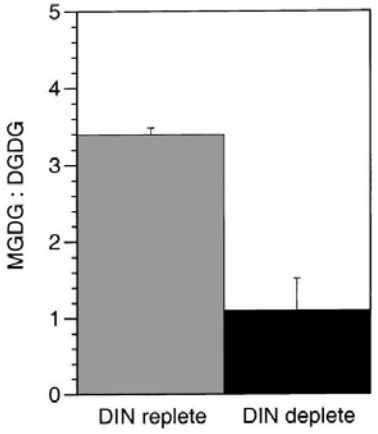

Fig. 7. Ratio of monogalactosyldiacylglycerol (MGDG) to digalactosydiacylglycerol (DGDG) under dissolved inorganic nitrogen (DIN) replete and DIN deplete conditions with corresponding growth rates of 0.55 and 0.28 day^{-1}, respectively. Error bars denote standard deviations; $n = 3$.

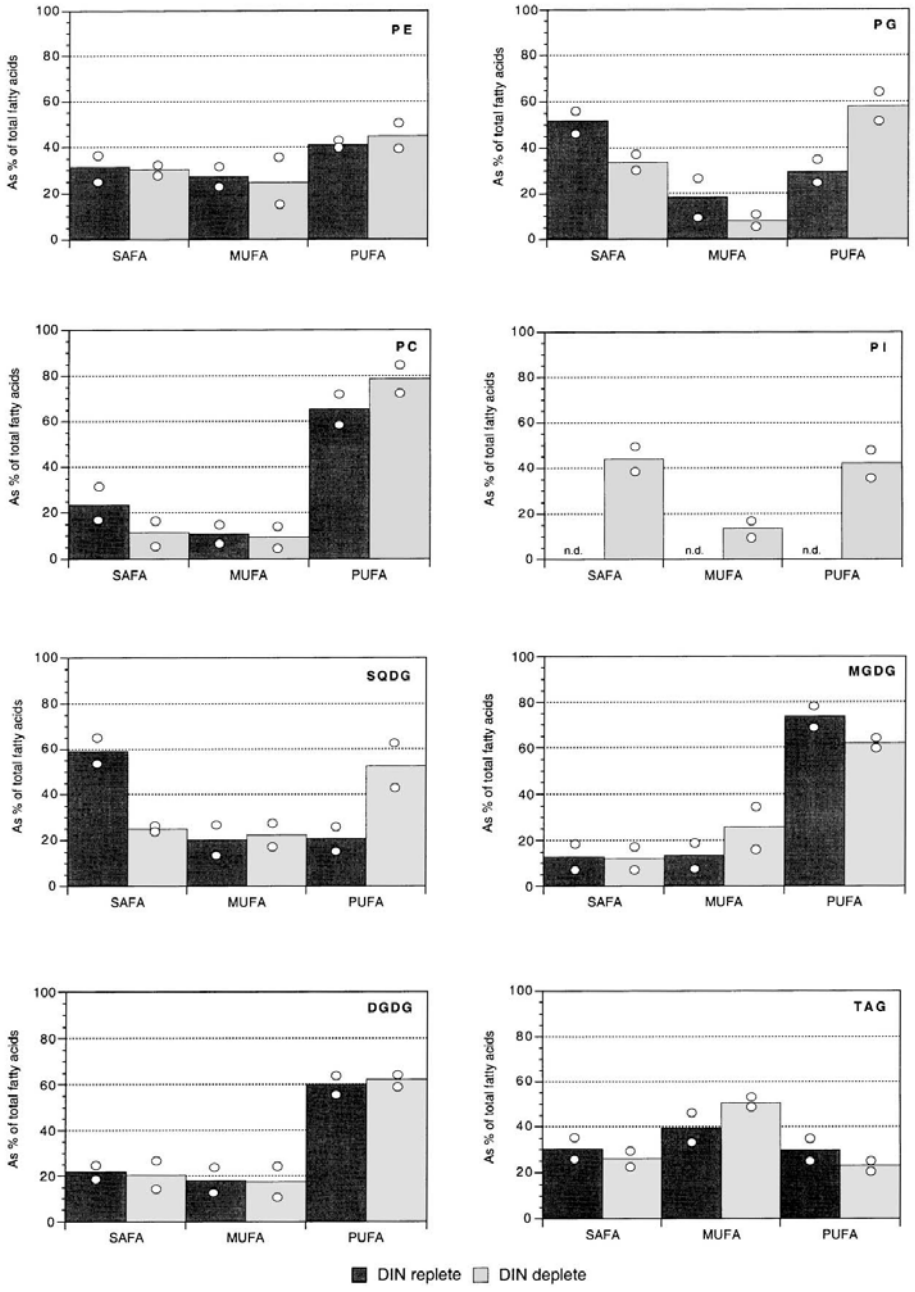

Fig. 8. Distribution of saturated (SAFA), monounsaturated (MUFA) and polyunsaturated fatty acids (PUFA) in lipid classes of sea ice diatoms as% of total particulate organic algal carbon under dissolved inorganic nitrogen (DIN) replete and DIN deplete conditions with corresponding growth rates of 0.55 and 0.28 day^{-1}, respectively; n.d. = not detectable; $n = 2$.

Table 3
Fatty acid composition in lipid classes of sea ice diatoms during dissolved inorganic nitrogen (DIN) replete (growth rate 0.55 day^{-1}) and deplete growth (growth rate 0.28 day^{-1})

Fatty acid	PC		PI		PE		PG		SQDG		DGDG		MGDG		TAG	
	DIN replete	DIN deplete	DIN replete	DIN deplete	DIN replete	DIN deplete	DIN replete	DIN deplete	DIN replete	DIN deplete	DIN replete	DIN deplete	DIN replete	DIN deplete	DIN replete	DIN deplete
14:0	7.46	4.08		8.06	8.40	6.66	21.37	5.72	22.80	5.57	8.17	10.75	4.66	5.64	9.65	6.59
15:0					1.24	0.47						0.26	3.32	0.61	0.43	0.71
16:0	14.12	7.08		36.06	21.02	23.27	30.60	28.14	28.58	17.32	10.81	9.32	3.50	5.78	19.34	18.55
18:0	2.04	0.46			0.95				7.67	2.08	2.89		1.37	0.18	1.11	0.39
16:1n-7	7.30	4.58		13.67	23.53	23.06	11.88	8.00	20.21	15.72	8.45	11.56	8.72	16.65	36.02	45.46
18:1n-9	1.66	1.99								2.77	6.37	1.18	0.96	3.83	3.02	4.34
18:1n-7	1.82	1.16			3.77	1.74	6.60			2.31			0.83	0.23		0.38
20:1n-9		1.83								1.66	3.30	4.69	2.96	5.04	0.50	0.39
16:2n-?	2.87										10.59	6.62	2.48	2.99	1.69	1.06
16:3n-?												0.50	8.45	3.17	1.12	0.35
16:4n-1									9.46	11.41	4.45	2.89	35.41	27.38	1.57	1.29
18:2n-6	5.55	3.45			0.80	0.64				14.17		1.04	1.84	4.02	2.18	1.44
18:3n-3	2.98	2.54										1.10	2.38	0.50	0.91	1.50
18:4n-3	7.6	6.72				0.81	6.65			2.06	11.81	17.78		2.76	6.38	5.97
20:2n-?					13.36	8.37									1.47	
20:4n-6		0.94												0.38		0.07
20:4n-3	1.62	1.48		23.98	3.20	2.745						1.00		0.33	1.08	0.29
20:5n-3	37.16	51.54		18.23	20.56	27.90	22.91	58.14	11.28	21.39	33.19	29.22	23.10	19.98	12.49	10.26
22:6n-6	7.82	12.14			3.15	4.32				3.55		2.09		0.53	1.04	0.96

Results are reported as % of total fatty acids. PC = phosphatidylcholine; PE = phosphatidylethanolamin; PG = phosphatidylglycerol; SQDG = sulfoquinovosyldiacylglycerol; DGDG = digalactosyldiacylglycerol; MGDG = monogalactosyldiacylglycerol; TAG = triacylglycerol; – not detected; $n=2$.

important function of this lipid class in membranes of sea ice diatoms. Changes also occurred in fatty acid composition of each lipid class which has implications for the degree of lipid saturation and thus for membrane fluidity (Fig. 8, Table 3). Our data reveal that the proportion of polyunsaturated fatty acids under nitrogen limited growth increased in most of the lipid classes, except for dominant chloroplast related MGDG and triacylglycerol (TAG) where they decreased or remained constant.

3. Discussion

Sea ice diatoms appear to have sophisticated mechanisms for photosynthetic energy conversion under dynamic *N*-supply in order to regulate (i) underlying structural components which are dependent on proteins and *N*-containing molecules and (ii) the discrepancy between energy input and the potential to use this energy for growth. In plants, the most affected structures under *N*-limitation are photosystems within the thylakoid membranes. Under such conditions it is likely that light-harvesting-protein complexes and reaction centre proteins like D1/D2 (reaction center proteins of PS II) are only poorly assimilated (e.g. Falkowski et al., 1989) and consequently less concentrated in the thylakoid membrane. This loss of integral polar membrane components has consequences for membrane structure and thus lipid composition as well as the degree of fatty acid desaturation. Low light acclimated microalgae used here were characterized by large chloroplasts. Consequently, the most membrane systems were related to chloroplasts and particular thylakoid membranes (Forde and Steer, 1976) which explains the dominance of MGDG. Typical chloroplast related lipid classes for microalgae are MGDG, DGDG, SL, PG with minor amounts of PC and PI (Mendiola-Morgenthaler et al., 1985). Significant changes in concentration were probably the result of physiological reactions in order to sustain the optimal structure and function of chloroplast membranes even under sub-optimal conditions of nitrogen limitation at low temperature. The overall reduction of proteins was accompanied by an increase in membrane lipids which caused an increased lipid/protein ratio also in thylakoid membranes (Block et al., 1983). This physiological acclimation may compensate structural changes of the thylakoid membrane because of reduced pigments and proteins within the membrane. Pigments and proteins are normally responsible for bilayer formation at unusually high concentrations of non-bilayerforming MGDG (Quinn and Williams, 1985; Murphy, 1984; Webb and Green, 1991). The precise role of non-bilayer lipids in membranes is still unclear. Early suggestions that they facilitate the sealing of proteins into membranes remain extremely plausible

but detailed evidence is still missing. When less proteins and pigments are available, the thylakoid membrane has to be stabilized in a bilayer-state by increasing the concentrations of bilayer forming lipids such as DGDG and phospholipids. Hexagonal structures of MGDG would develop micelles, which destroy the thylakoid lipid bilayer (Williams, 1998). Highly unsaturated PG is normally a functional effector for charge separation at the D1/D2-heterodimer, electron flow and a membrane anchor for the D1-core peptide (Kruse and Schmidt, 1995; Duchene et al., 2000). Either the assembly of new D1 protein into active PS II reaction centers or the processing of the pre-D1 protein appears to depend on the degree of unsaturation of the thylakoid lipids, particularly at low temperatures (Murata and Wada, 1995; Nishida and Murata, 1996). Increasing concentrations of PG PUFAs under *N*-limitation was probably an instrument for improving the incorporation of D1 proteins into the thylakoid membrane. Additionally, the PUFA content (20:5 n-3) of most phospholipid classes increased under *N*-limitation. Decreasing MGDG PUFAs like 20:5 n-3, during *N*-limitation, is probably related to decreasing chl *a*, because there is a strong association between both substances (e.g. Cohen et al., 1988) *N*-limitation would disrupt the entire chloroplast membranes and thus photosynthesis if the cell was not able to compensate the reduction of pigments and proteins inside the thylakoid membrane. These regulating mechanisms are probably universal to establish membrane integrity and consequently active photosynthesis in sea ice diatoms or even other algae or higher plants.

The light energy which was absorbed per unit chl *a* in nitrogen limited cells increased because of decreasing chl *a* contents. The incoming energy is therefore concentrated in a few PS II reaction centres. The electron transport from PS II to triacylglycerols, the primary electron sink, is dependent on the amount of Q_A and Q_B, their mobility through the membrane and the amount of redox-equivalents (NADPH) as electron acceptors. Fluorescence amplitudes indicated that the amount of bound Q_B at D1 increased during *N*-limitation, but that the rate constants decreased. The binding site of D1 therefore does not seem to be negatively influenced by *N*-limitation so that only less Q_B can be bound but the exchange of reduced against oxidized Q_B and the mobility of Q_B is more likely responsible for the reduced rate constants. One consequence of this reduced flow of electrons is a tailback of electrons within the transport chain, including Q_A. Under sufficient nitrogen availability these electrons are normally used for a reduction in nitrate. Here they are used more for intense carbon assimilation in the form of triacylglycerols.

Nevertheless, the PQ pool remained reduced, indicating an inbalance between electron generation and all processes that remove electrons such as reduced substances or enzymes, which require electrons for their reactions. This highly reduced state of the plastoquinone pool is probably the trigger for production of diatoxanthin and diadinoxanthin which protects the reaction centre from photoinhibition by exciton dissipation.The strongly reduced plastoquinone pool also inhibits de novo LHC (light harvesting complex) synthesis (Falkowski et al., 1989). Consequently, the response to nitrogen limitation is similar to the high light response (Kolber et al., 1988; Herzig and Falkowski, 1989).

4. Experimental

4.1. Site and sampling

Sea ice algal assemblages were collected in the Weddell Sea (Antarctica) during the RV 'Polarstern' expedition ANT XVI/3 from 18 March to 10 May 1999. Samples were taken from one first year sea ice floe of 37 cm thickness (station PS 53 177) at 70°02′04″S, 06°00′06″W using a 9 cm ice auger. Only the bottom 5 cm of several ice cores, containing the highest density of algae, was used. The segments were placed into clean 5-l polyethylene containers and returned to the ship where they were transferred into 0.2 μm pre-filtered seawater (defined as sterile) with a final dilution of 4:1 (volume sea water:volume sea ice) at 0 °C to avoid osmotic stress during the melting procedure (Garrison and Buck, 1986). They were allowed to melt at 0 °C and a light intensity of approx. 7 μmol photons m^{-2} s^{-1}.

4.2. Experimental set-up

After melting (ca. 24 h), the sedimented algae were drawn up by a sterile syringe and transferred into 10 ml "petri" dishes of sterile F/2 medium (Guillard and Ryther, 1962). Representatives of the dominant diatom species: *Fragilariopsis curta, Navicula gelida* var.-*antarctica, Nitzschia medioconstricta* were picked up by a glass pipette. These species were transferred into aerated 1-l glass bottles containing F/2 medium. Illumination (cool white fluorescent tubes, Philips TL 33) was provided from above and the photon flux density within the bottles was adjusted to 15 μmol photons m^{-2} s^{-1} and a light-dark cycle of 20:4 h. Growth of unialgal cultures with respect to irradiance was similar to that often observed under low temperature and light conditions (e.g. Fiala and Oriol, 1990). After 1 week, all the exponentially growing diatoms were transferred into 5-l bottles for continuous cultures under the same light conditions used in the batch cultures. Antarctic sea water was enriched with F/2 nutrients twice as high as recommended by Guillard and Ryther (1962) in order to avoid nutrient limitation. F/2 medium with a reduced nitrate concentration was used for nitrogen limited

growth experiments. Nutrient concentrations were checked daily and immediately determined after sampling according to standard seawater procedures (Grasshoff et al., 1983). The pH of the cultures was kept constant at 8.00±0.15 by bubbling air at a rate of 270-ml min^{-1}. The airflow was used to vigorously mix the culture. Temperature was kept constant at −1±0.5 °C by cooling the entire laboratory. Steady state cell concentrations were checked at 750 nm with a Shimadzu Photometer and microscopical analyses of species composition were carried out according to Utermöhl (1958). Under nutrient replete conditions, the maximal attained dilution rate for steady state growth was 0.55 day^{-1} whereas steady state growth under nitrogen limitation was adjusted to 0.28 day^{-1}. The average photon flux densities for both experimental conditions was 15.0±5.0 μmol photons m^{-2} s^{-1} with an optical density (OD) of 0.11±0.01 at 0.55 day^{-1} and an OD of 0.08±0.01 at 0.28 day^{-1}. The algal composition at a growth rate of 0.55 day^{-1} was 66±11% *Navicula gelida* var. *antarctica*, 20±7% *F. curta* and 14±9% *N. medioconstricta* after ca. 1 week under steady state cell concentrations. During nitrate deplete growth and a growth rate of 0.28 day^{-1} *N. gelida* var. *antarctica* contributed 61±8%, *F. curta* 27±9% and *N. medioconstricta* 12±4% to the total community based on cell numbers.

4.3. Bio-optics

Pigment composition was determined by High Performance Liquid Chromatography (HPLC). Samples of 20 ml were filtered through Whatmann GF/C filters, which were placed in cryo vials and immediately frozen in liquid nitrogen. They were then stored at −80 °C for about 4 months prior to pigment extraction in 100% DMF (dimethylformamide) and subsequent HPLC analysis. HPLC protocols followed Karsten and Garcia-Pichel (1996) with some modification. Pigments were separated using a Waters Associates HPLC system which includes a 600 MS gradient module with system controller and a Model 996 photodiode array detector. Samples (50 μl) were injected into a HPLC column by an autosampler (717 plus). The column was a stainless steel Merck LiChrospher RP 18 (5 μm packing; 125×4 mm I.D.) behind a Merck RP 18 guard column (4×4 mm I.D.), filled with the same material. Pigments were monitored at 436 nm and separated by a binary gradient system of helium-degassed solvents. The mobile phase of solvent A (distilled water) and solvent B (acetonitrile methanol tetrahydrofuran, 75:15:10 vol:vol) was regulated at a flow rate of 1.5 ml min^{-1} using the following program: 0 15 min for a linear increase from 15% solvent A to 100% solvent B and 15 24 min for 100% solvent B. The individual pigments were identified by their absorption spectra in a mixture of solvent A and solvent B at the appropriate retention time. Their identification was evaluated against co-chromatography with commercially available standards (International Agency for ^{14}C Determination VKI). Pigments were quantified by peak area at 436 nm with reference to response signals obtained from the standards using the Waters 996 photodiode array detector and integrator.

Chl *a* fluorescence measurements were conducted with a Dual-Modulation LED Kinetic Fluorometer (Trtilek et al., 1997). Fluorescence induction measurements were done on samples (11.5±2.1 μg total chl *a*) that had been dark adapted for 30 min in the presence of DCMU [3-(3,4-dichlorophenyl)-1,1-dimethylurea, 20 μmol l^{-1} final concentration]. Consequently DCMU induction kinetics reveal the potential maximum of photosynthetic performance and not in situ kinetics. Reoxidation kinetics of Q_A were determined as soon as possible after sampling (90 s) and after 30 min in order to test the influence of dark adaptation on the amount of bound Q_B. When dark adapted DCMU containing cells are light-exposed, fluorescence will increase from a minimum level F_o (Q_A fully oxidized, PS II reaction centres open) to a maximum level Fm (Q_A fully reduced, i.e. all PS II reaction centres closed). These cells displayed a fast fluorescence increase upon illumination because electron transport between the primary stable electron acceptor Q_A and the secondary acceptor Q_B was blocked. Normalized DCMU induction curves were fitted to a set of equations (Trissl and Lavergne, 1995; Lavergne and Trissl, 1995). Any increase from F_o is termed variable fluorescence [F_v (q)] and can be described as

$$F_v(q) = \Phi_f(q0) - F_o \quad (1)$$

where Φ_f ($q0$) is the fluorescence yield which is defined as

$$\Phi_f(q0) = F_m - q_{(t)}(F_m - F_o(1+J))/1 + Jq_{(t)} \quad (2)$$

where J is a measure of the connectivity between PS II centres and is related to Joliot's connection parameter p by

$$J = p/(1-p) \quad (3)$$

where p was defined as the probability that an exciton hitting a closed reaction centre will be transmitted to an open reaction centre (Joliot and Joliot, 1964). The $q_{(t)}$ is calculated from the fraction of open centre at time t_{-1} and the change in open centres in dt

$$q_{(t)} = q(t-1) + \mathrm{d}q \quad (4)$$

where dq can be described as

$$\mathrm{d}q = \sigma p_{(t-1)}{}^{*}(1+J)/\left(1+Jq_{(t-1)}\right)^{*}\mathrm{d}t \quad (5)$$

and σ is a relative measure of the cross section of PS II. Photochemical quantum yield of PS II from fluorescence levels is expressed as (Schreiber et al., 1986; Genty et al., 1989)

$$\Phi_p(q) = F_m - \Phi_f(q1)/F_m \quad (6)$$

Reoxidation kinetics of Q_A were measured by decay of variable fluorescence back to the F_o state in absence of DCMU with decreasing resolution during 100 s, starting 120 μs after firing of six single turnover flashes to saturate all reaction centres. The decay kinetics reflects the re-oxidation of Q_A by Q_B. Complete Q_A reoxidation can be described by a triphasic exponential decay function for F_v

$$F_v = A_e^{-Ka*t} + B_e^{-Kb*t} + C_e^{-Kc*t} + F_o \quad (7)$$

where A, B and C are the amplitudes and K_A, K_B and K_C the decay rate constants for the fast (<10 ms), middle (10–50 ms) and slow (>50 ms) phase, respectively. The fast phase is attributed to electron transport from Q_A to Q_B in centres that possess bound Q_B. The middle phase is thought to represent those centres that had no bound Q_B before the flash. Thus this phase may indicate the kinetics of equilibration of PQ binding to the Q_B site of the D1 protein. The third, very slow component seems to represent the decay of PS II centres that are unable to transmit electrons to the PQ pool. The slow Q_A reoxidation apparent from this phase is thought to result from recombination between Q_A and the water oxidation system in the S_2 state.

P vs I curves were done on 10 ml algal samples filled into 10 ml transparent polycarbonate cuvettes lined up and illuminated by a slide projector. Photon flux density within the cuvettes was adjusted with neutral density filters, which covered the cuvette side in front of the slide projector. The photon flux density determined within filled cuvettes ranged between 0.5 and 395 μmol photons m^{-2} s^{-1}. The illumination time was 2 h at −1 °C with regular stirring every 15 min. The quantum yield was measured with a Dual-Modulation LED Kinetic Fluorometer (Trtilek et al., 1997). Fluorescence induction measurements were done on samples (11.5±2.1 μg total chl *a*) that had been dark adapted for 30 min in the presence of DCMU. P vs I parameters α, P_{max}, and Ik were determined by a fit according to Eilers and Peeters (1988).

4.4. Biochemistry

For particulate organic carbon (POC) and nitrogen (PON), carbohydrate, protein and lipid analyses, samples of 40 ml were filtered through precombusted Whatmann GF/C filters. Filters for POC/PON, carbohydrates and proteins were kept frozen at −80 °C for further processing. The thawed filters for POC/PON were dried (12 h at 60 °C), transferred to pewter foil and combusted in oxygen enriched helium atmosphere in a Heraeus CHN-O-Rapid analyzer. Concentrations of carbohydrates were determined after Holland and Gabbott (1971) and proteins were determined after Smith et al. (1985) with a BCA Protein Assay Kit (Pierce, Rockford, IL 61105) which has serum albumin as standard. Filters for lipid analyses were immediately aerated with N_2 after filtration and stored in dichlormethane:methanol (2:1, by vol.) at −80 °C for further processing. Algal cells together with the filter were sonicated for 5 min with a stainless-steel probe and extracted in the storage solution (Folch et al., 1957). Lipid class composition was measured by quantitative thin-layer chromatography densitometry (HPTLC) as described by Olsen and Henderson (1989) with some modifications. Individual lipid classes were isolated on precoated HPTLC silica gel 60 plates (20×10 cm, Merck, Darmstadt, Germany). Lipid standards for each lipid class were obtained from Sigma Chemical Pool, U.K. Lipid samples (100 μl) were added with a Linomat (Carmag, CH) as a sharp line over nearly the full width (8 cm) of the plates. All developments were performed at room temperature in saturated standard chambers for 20×10 cm HPTLC plates loaded with standards or samples. The first development ran to a distance of 12 cm from the origin using methyl acetate:isopropanol:chloroform: methanol:0.25% KCl (25:25:25:10:4 by vol.) as the solvent system. After evaporation of the solvents at 110 °C for 5 min, the plates were dried under a stream of N_2. Plates were then developed in hexane:diethyl ether:glacial acetic acid (70:30:2 by vol.) to 17 cm from the origin. Separated lipid classes or standards were detected by spraying the plates with 3% H_2SO_4, followed by charring at 200 °C for 15 min. Quantification was performed on a Carmag TLC scanner. Preparation of individual fatty acids (FAs) for each lipid class were conducted on parallel samples using 400 μl instead of 100 μl to ensure sufficient material for gas chromatography analyses. The separated lipid classes were directly scraped off after both developments using a standard plate with detected lipid classes for orientation. FAs were resuspended in 5 ml dichlormethane:methanol (2:1 by vol.) and then separated from silica gel by centrifugation (2000 rpm for 5 min). Thereafter FAs were transmethylated in methanol containing 2% sulphuric acid for 4 h at 80 °C to generate fatty acid methyl esters (FAME) which were extracted with hexane and analysed by gas liquid chromatography with a Carlo Erba gas chromatograph. FAs were identified with a standard mixture.

Acknowledgements

We are grateful to the crew of the RV *Polarstern* for their assistance during the expedition. We thank Gerhard

Kattner and Martin Graeve for valuable discussions and for kind assistance with the lipids. Gerhard Dieckmann is thanked for reviewing an earlier version of the manuscript, and making suggestions for its improvement.

References

Allen, D.J., Ort, D.R., 2001. Impacts of chilling temperatures on photosynthesis in warm-climate plants. Trends in Plant Sci. 6 (1), 36–42.

Arrigo, K.R., Worthen, D.L., Lizotte, M.P., Dixon, P., Dieckmann, G., 1997. Primary production in Antarctic sea ice. Science 276, 394–397.

Block, M.A., Dorne, A.J., Joyard, J., Douch, R., 1983. Preparation and characterization of membrane fractions enriched in outer and inner envelope membranes from spinach chloroplasts. II Biochemical characterization. J. Biol. Chem. 258, 13281–13286.

Cohen, Z., Vonshak, A., Richmond, A., 1988. Effect of environmental conditions on fatty acid composition of the red alga *Porphyridium cruetum*: correlation to growth rate. J. Phycol. 24, 328–332.

Duchene, S., Smutny, J., Siegenthaler, P.A., 2000. The topology of phosphatidylglycerol populations is essential for sustaining photosynthetic electron flow activities in thylakoid membranes. Biochim. Biophys. Acta 1463, 115–120.

Eicken, H., 1992. The role of sea ice in structuring Antarctic ecosystems. Polar Biol. 12, 3–13.

Eilers, P.H., Peeters, J.C.H., 1988. A model for the relationship between light intensity and the rate of photosynthesis in phytoplankton. Ecol. Model. 42, 199–215.

Falkowski, P.G., Sukinek, A., Herzig, R., 1989. Nitrogen limitation in *Isochrysis galbana* (Haptophyceae). II. Relative abundance of chloroplast proteins. J. Phycol. 25, 471–478.

Fiala, M., Oriol, L., 1990. Light-temperature interactions on the growth of Antarctic diatoms. Polar Biol. 10, 629–636.

Folch, J., Lees, M., Sloane-Stanley, G.H., 1957. A simple method for the isolation and purification of total lipids from animal tissues. J. Biol. Chem. 226, 497–509.

Forde, J., Steer, M.W., 1976. The use of quantitative electron microscopy in the study of lipid composition of membranes. J. Exp. Bot. 27, 1137–1141.

Garrison, D.L., Buck, K.R., 1986. Organism losses during ice melting: a serious bias in sea ice community studies. Polar Biol. 6, 237–239.

Genty, B., Briantais, J.M., Baker, N.R., 1989. The relationship between the quantum yield ofphotosynthetic electron transport and quenching of chlorophyll fluorescence. Biochim. Biophys. Acta 90, 87–92.

Guillard, R.R., Ryther, J.H., 1962. Studies of marine plankton diatoms. I. *Cyclotella nana* (Husted) and *Detonula confervacea* (Cleve). Can. J. Microbiol. 8, 229–239.

Grasshoff, K., Ehrhard, M., Kremling, K., 1983. Methods of Sea Water Analyses, 2nd ed. Verlag Chemie, Weinheim.

Herzig, R., Falkowski, P.G., 1989. Nitrogen limitation in *Isochrysis galbana* (Haptophyceae) I. Photosynthetic energy conversion and growth efficiencies. J. Phycol. 25, 462–471.

Holland, D.L., Gabbott, P.A., 1971. A micro-analytical scheme for determination of proteins, carbohydrates, lipid and RNA levels in marine invertebrate larvae. J. Mar. Biol. Assoc. UK 51, 659–668.

Hutchinson, G.E., 1961. The paradox of the plankton. Am. Nat. 95, 135–137.

Joliot, P., Joliot, A., 1964. Études cinétique de la réaction photochimique libérant l'oxygene au cours de la photosynthese. C. R. Acad. Sci. Paris 258, 4622–4625.

Karsten, U., Garcia-Pichel, F., 1996. Carotenoids and mycosporine-like amino acid compounds in members of the genus *Microcoleus* (cyanobacteria): a chemosystematic study. System Appl. Microbiol. 19, 285–294.

Kirst, G.O., Wiencke, C., 1995. Ecophysiology of polar algae. J. Phycol. 31, 181–199.

Kolber, Z., Zehr, J., Falkowski, P.G., 1988. Effects of growth irradiance and nitrogen limitation on photosynthetic energy conversion in photosystem II. Plant Physiol. 88, 923–929.

Kroon, B.M.A., 1994. Variability of photosystem II quantum yield and related processes in *Chlorella pyrenoidosa* (Chlorophyta) acclimated to an oscillating light regime simulating a mixed photic zone. J. Phycol. 30, 841–852.

Kroon, B.M.A., Prézelin, B.B., 1995. Temperature dependency of fluorescence decay parameters in an Antarctic isolate of the diatom *Thalassiosira* sp. Antarct. J. US. 159–160.

Kruse, O., Schmidt, G.H., 1995. The role of phosphatidylglycerol as a functional effector and membrane anchor of the D1-core peptide from photosystem II-particles of the cyanobacterium *Oscillatoria chalybea*. Z. Naturforsch. 50c, 380–390.

Lavergne, J., Trissl, H.W., 1995. Theory of fluorescence induction in photosystem II: derivation of analytical expressions in a model including exciton-radical-pair equilibrium and restricted energy transfer between photosynthetic units. Biophys. J. 88, 2474–2492.

McMinn, A., Skerratt, J., Trull, T., Ashworth, C., Lizotte, M., 1999. Nutrient stress gradient in the bottom 5 cm of fast ice, McMurdo Sound, Antarctica. Polar Biol. 21, 220–227.

Mendiola-Morgenthaler, L., Eichenberger, W., Boschetti, A., 1985. Isolation of chloroplast envelopes from *Chlamydomonas*. Lipid and polypeptide composition. Plant Sci. 41, 97–104.

Murata, N., Wada, H., 1995. Acyl-lipid desaturases and their importance in the tolerance and acclimatization to cold of cyanobacteria. Biochem. J. 308, 1–8.

Murphy, D., 1984. Structural properties and molecular organization of the acyl lipids of photosynthetic membranes. In: Staehelin, L.A., Arntzen, C.J. (Eds.), Encyclopedia of Plant Physiology. Photosynthesis III: Photosynthetic Membranes and Light-Harvesting Systems, Vol. 19. Springer-Verlag, Berlin, pp. 713–725.

Nishida, I., Murata, N., 1996. Chilling sensitivity in plants and cyanobacteria: the crucial contribution of membrane lipids. Annu. Rev. Plant. Physiol. Plant. Mol. Biol. 47, 541–568.

Olsen, R.E., Henderson, R.J., 1989. The rapid analysis of neutral and polar marine lipids using double-developmant HPTLC and scanning densitometry. J. Exp. Mar. Biol. Ecol. 129, 189–197.

Pohl, F., Zurheide, 1979. Fatty acids and lipids of marine algae and the control of their biosynthesis by environmental factors. In: Hoppe, H.A., Levring, T., Tanaka, Y. (Eds.), Marine Algae in Pharmaceutical Science. Walter de Gruyter, Berlin, pp. 473–523.

Quinn, P.J., Williams, W.P., 1985. Environmentally induced changes in chloroplast membranes and their effects on photosynthetic function. In: Barber, J. (Ed.), Topics in Photosynthesis, Vol. 6. Elsevier, Amsterdam, pp. 1–47.

Routaboul, J.M., Fischer, S.F., Browse, J., 2000. Trienoic fatty acids are required to maintain chloroplast function at low temperatures. Plant Physiol. 124, 1697–1705.

Schreiber, U., Schliwa, U., Bilger, W., 1986. Continuous recording of photochemical and non-photochemical chlorophyll fluorescence quenching with a new type of modulation fluorometer. Photosynth. Res. 10, 51–62.

Shifrin, N.S., Chisholm, S.W., 1981. Phytoplankton lipids: interspecific differences and effects of nitrate, silicate and light-dark cycles. J. Phycol. 17, 374–384.

Siegenthaler, P.A., Murata, N., 1998. Lipids in Photosynthesis: Structure, Function and Genetics, Advances in Photosynthesis, Vol. 6. Kluwer Academic Publishers, Dordrecht.

Smith, P.K., Krohn, R.I., Hermanson, G.T., Mallia, A.K., Gartner, F.H., Provenzano, M.D, Fujimoto, E.K., Goecke, N.M., Olson, B.J., Klenk, D.C., 1985. Measurement of protein using bicinchoninic acid. Anal. Biochem. 150, 76–85.

Taguchi, S., Smith, R.E.H., 1997. Effects of nitrogen and silicate enrichment on photosynthate allocation by ice algae from Resolute Passage, Canadian Arctic. J. Mar. Syst. 11, 53–61.

Thomashow, M.F., 1998. Role of cold-responsive gene in plant freezing tolerance. Plant Physiol. 118, 1 7.

Tillmann, U., Baumann, M.E.M., Aletsee, L., 1989. Distribution of carbon among photosynthetic end products in the bloom-forming diatom *Thalassiosira antarctica* COMBER. Polar Biol. 10, 231 238.

Trissl, H.W., Lavergne, J., 1995. Fluorescence induction from photosystem II: analytical equations for the yields of photochemistry and fluorescence derived from analysis of a model including exciton-radical pair equilibrium and restricted energy transfer between units. Aust. J. Plant Physiol. 22, 183 193.

Trtilek, M., Kramer, D.M., Koblizek, M., Nedbal, L., 1997. Dual-modulation LED kinetic fluorometer. J. Lumin. 72 74, 597 599.

Utermöhl, H., 1958. Zur Vervollkommnung der quantitativen Phytoplankton-Methodik. Mitt. Int. Ver. Theor. Angew. Limnol. 9, 1 38.

Webb, M.S., Green, B.R., 1991. Biochemical and biophysical properties of thylakoid acyl lipids. Biochim. Biophys. Acta 1060, 133 158.

Weissenberger, J., Dieckmann, G., Gradinger, R., Spindler, S., 1992. Sea ice: a case technique to examine and analyze brine pockets and channel structure. Limnol. Oceanogr. 37 (1), 179 183.

Williams, W.P., 1998. The physical properties of thylakoid membrane lipids and their relation to photosynthesis. In: Siegenthaler, P.A., Murata, N. (Eds.), Lipids in Photosynthesis: Structure, Function and Genetics, Vol. 6. Kluwer Academic, Dordrecht, pp. 21 52.

PERGAMON

Phytochemistry 61 (2002) 53–60

PHYTOCHEMISTRY

www.elsevier.com/locate/phytochem

Photosynthetic energy conversion under extreme conditions—II: the significance of lipids under light limited growth in Antarctic sea ice diatoms

Thomas Mock[a,*], Bernd M.A. Kroon[a,b]

[a]*Alfred-Wegener-Institute for Polar and Marine Research, Am Handelshafen 12, D-27570 Bremerhaven, Germany*
[b]*KroonAqa GmbH, Knurrhahnstraße 9, D-27572 Bremerhaven, Germany*

Received 14 December 2001; received in revised form 2 May 2002

Abstract

Low photosynthetic active radiation is a strong determinant in the development and growth of sea ice algae. The algae appear to have universal mechanisms to overcome light limitation. One important process, which is induced under light limitation, is the desaturation of chloroplast membrane lipids. In order to discover whether this process is universally valid in sea ice diatoms, we investigated three species coexisting in chemostats illuminated with 15 and 2 μmol photons $m^{-2} s^{-1}$ at −1 °C. Growth under 2 μmol photons $m^{-2} s^{-1}$ caused a 50% increase in monogalactosyldiacylglycerols (MGDG) thylakoid membrane related 20:5 *n*-3 fatty acids. This fatty acid supports the fluidity of the thylakoid membrane and therefore the velocity of electron flow, which is indicated by increasing rate constants for the electron transport between Q_A (first stable electron acceptor) and bound Q_B (second stable electron acceptor) (11.16±1.34 to 23.24±1.35 relative units). Two μmol photons $m^{-2} s^{-1}$ furthermore resulted in higher amounts of non-lipid bilayer forming MGDG in relation to other bilayer forming lipids, especially digalactosydiacylglycerol (DGDG). The ratio of MGDG:DGDG increased from 3.4±0.3 to 5.7±0.3. The existence of bilayer thylakoid membranes with high proportions of non. bilayer forming lipids is only possible when sufficient thylakoid pigment–protein complexes are present. If more thylakoid pigment–protein complexes are present in membranes, as found under extreme light limitation, less bilayer forming lipids such as DGDG are required to stabilize the bilayer structure. Differences in protein contents between both light intensities were not found. Consequently pigment contents which nearly doubled under 2 μmol photons $m^{-2} s^{-1}$ must be responsible in balancing the potential stability loss resulting from an increase in MGDG:DGDG ratio.

Keywords: Bacillariophyceae; Carbohydrates; Fluorescence induction; Lipids; Low temperature; Pigments; Proteins; Sea ice

1. Introduction

A number of sea ice diatom species coexist in the narrow space of brine channels (Krembs et al., 2000). This habitat is characterized by extreme conditions (low light intensities, low temperature, high salinities and limited supply of nutrients) which are strong selection factors for diatom species. Thus, only those species persist in this polar ecosystem which are able to acclimate or adapt (Kirst and Wiencke, 1995). The species probably all have the same mechanisms, which govern their success and differ from those in temperate or even tropical species. Species specific dominance in sea ice is probably related to small intraspecific differences (Huisman and Weissing, 1999) in e.g. salinity and temperature tolerance. In order to find universal mechanisms of regulation underlying these small intraspecific differences, we studied three dominant coexisting Antarctic sea ice diatoms by growing them in chemostats at −1 °C and two subsaturating light intensities. Low light acclimation is a universal physiological process, dependent on the structure and function of the photosynthetic apparatus. Photosystems and their subcomplexes, e.g. LHC (light harvesting complex), D1 (reaction center protein of photosystem II), D2 (reaction center protein of photosystem II), are anchored within the thylakoid membrane through lipids which are exclusively present in the chloroplast. This close connection between lipids and photosystem subcomplexes indicate an interdependence between both, which supports the concept of photo-

* Corresponding author. Tel.: +49-471-48-31-18-93; fax: +49-471-48-31-425.
E-mail address: tmock@awi-bremerhaven.de (T. Mock).

0031-9422/02/$ - see front matter
PII: S0031-9422(02)00215-7

Nomenclature

RC	reaction centre
PS II, I	photosystem II, I
LHC	light harvesting complex
D1/D2	PS II reaction centre proteins
Q_A	quinone A, first stable electron acceptor of PS II
Q_B	quinone B, second stable electron acceptor
F	fluorescence. Subscripts o, v, m represent the fluorescent level during light induction at the origin, variable and maximum levels, respectively
F_v/F_m	quantum yield
q	reaction centers
p	connectivity between PS II units
Φ_f	fluorescence yield
Φ_P	quantum yield
$q1$	open reaction centres
$q0$	closed reaction centres
σ	effective cross section of PS II
A	fraction of PS II characterized by a fast fluorescence decay after turnover saturation flashes at a rate of K_A
B	fraction of PS II characterized by a middle fluorescence decay after turnover saturation flashes at a rate of K_B
C	fraction of PS II characterized by a slow fluorescence decay after turnover saturation flashes at a rate of K_C
P vs I	photosynthesis (P) versus irradiance (I)
α	light limited slope of the P vs I curve/ light utilization effiziency
Ik	light level at which photosynthesis saturates
P_{max}	maximum rate of photosynthesis
K	rate constant for fluorescence decay measurements
A,B,C_{comp}	amplitudes of fluorescence decay rate constants (K)
J_{con}	connectivity between reaction centres (PS II)
FA	fatty acid
PUFA	polyunsaturated fatty acid
MGDG	monogalactosyldiacylglycerol
DGDG	digalactosyldiacylglycerol
PC	phosphatidylcholine
PG	phosphatidylglycerol
PE	phosphatidylethanolamin
PI	phosphatidylinositol
TAG	triacylglycerol
SQDG	sulfoquinovosyldiacylglycerol

synthesis regulation by changes in the thylakoid membrane structure or the entire chloroplast. Thus, lipids have to be included into our concept of light acclimation of photosynthesis. An increase in membrane fluidity at low temperatures is essential to sustain diffusivity of gases, mobile electron and proton carriers like plastoquinone (PQ) and to repair low-temperature photoinhibition damage (e.g. Russel, 1997; Saruwatari et al., 1999; Reay et al., 1999). Apart from temperature, the strong seasonality of irradiance in polar regions plays an important role in photoautotrophic life, particularly in marine habitats where water turbulence determines the supply of photons. Some investigators have observed changes in lipid or fatty acid (FA) quality during light acclimation of algae and plants in addition to quantitative changes in chloroplast lipids (Pohl and Zurheide, 1979; Harwood and Jones, 1989; Sewon et al., 1997; Klyachko-Gurvich et al., 1999). This change is more distinct in combination with low temperatures (Tasaka et al., 1996). Ice diatoms are therefore well suited to study regulation of photosynthesis on the basis of lipid metabolism which is expected to be similar for the dominant diatom species. Special attention is therefore given to lipids as structural modulators of photosystem II efficiency as well as regulators of energy flow in three Antarctic sea ice diatoms.

2. Results

2.1. Physiology

The maximum attainable algal growth rate was strongly influenced by photon flux density. At 2 μmol photons m^{-2} s^{-1} the algae grew at a rate of 0.17 day^{-1} whereas the exposure to 15 μmol photons m^{-2} s^{-1} lead to a rate of 0.55 day^{-1}. The strong light limitation at 2 μmol photons m^{-2} s^{-1} resulted in an exceptional photophysiological acclimation, which was indicated by photosystem (PS) II related parameters as well as pigment concentrations. Fluorescence measurements were based on DCMU (3-(3,4-dichlorophenyl)-1,1-dimethylurea, 20 μmol l^{-1} final concentration) induction kinetics, which reveal the potential maximum of photosynthetic performance and not the in situ kinetics. Basic analysis of PS II related parameters (Table 1) resulted in an increase in connectivity between reaction centres of ca. 50% under 2 μmol photons m^{-2} s^{-1}. Relative values for energy trapping by open reaction centres were higher under 2 μmol photons m^{-2} s^{-1} than under 15 μmol photons m^{-2} s^{-1}. Reoxidation of Q_A (primary electron acceptor) increased at 2 μmol photons m^{-2} s^{-1} for the fast (K_A), middle (K_B) and slow (K_C) component of fluorescence decay measurements after

Table 1
Fluorescence variables for growth under 15 μmol photons m^{-2} s^{-1} (0.55 day^{-1}) and 2 μmol photons m^{-2} s^{-1} (0.17 day^{-1}): connectivity (J_{con}) between reaction centres (RC), open (K_{open}) RC and quantum yield are based on DCMU induction measurements

Variable	15 μmol photons m^{-2} s^{-1}	2 μmol photons m^{-2} s^{-1}
J_{con}	0.341±0.010	0.663±0.008
K_{open}	0.408±0.0 15	0.539±0.023
Fv/Fm (yield)	0.337±0.009	0.398±0.010
K_A (ms^{-1})	11.16±1.34	23.24±1.35
K_B (ms^{-1})	0.42±0.12	0.96±0.22
K_C (ms^{-1})	0.02±0.02	0.07±0.03
r^2 ($n-5$)	0.966	0.978

Fluorescence decay rate constants for fast K_A, middle K_B and slow K_C component. Values are given as relative units; $n-5$; r^2—model fit.

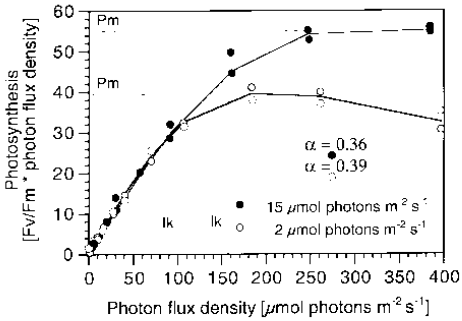

Fig. 1. Photosynthesis as F_v/F_m* photon flux density vs irradiance in ice diatoms under 15 μmol photons m^{-2} s^{-1} (μ−0.55 day^{-1}) and 2 μmol photons m^{-2} s^{-1} (μ−0.17 day^{-1}) are based on DCMU induction measurements. Photosynthetic parameters α (light utilization efficiency), Ik (quantum flux of PAR at onset of light saturation), Im (quantum flux of PAR for maximum of photosynthesis), Pm (maximum photosynthetic rate) were calculated after Eilers and Peeters (1988); $n-2$.

saturating light flashes. The fast (<10 ms) phase is attributed to electron transport from Q_A to Q_B (second electron acceptor) in PS II reaction centers that possess bound Q_B. The middle phase (10 50 ms) is thought to represent those reaction centers that had no bound Q_B before the saturating light flashes. Thus this phase may indicate the kinetics of equilibration of PQ binding to the Q_B site of D1 protein of PS II. The third, very slow component (>50 ms) seems to represent the decay of PS II centres that are unable to transmit electrons to the PQ pool. The slow Q_A reoxidation apparent from this phase is thought to result from recombination between Q_A and the water oxidation system in the S_2 state. Thus, electron transport is faster under 2 μmol photons m^{-2} s^{-1} and this is not caused by increasing amounts of Q_B bound to Q_A, which is indicated by the fluorescence amplitude of K_A (A_{comp}) the most important process for electron flow. A_{comp} remains relatively constant for both photon flux densities (0.012 and 0.011 for 15 and 2 μmol photons m^{-2} s^{-1}, respectively). Whereas B_{comp} increased under 2 μmol photons m^{-2} s^{-1} (Table 2). These amounts of bound Q_B were not influenced by dark adaptation of samples for 30 min, which revealed the comparison to measurements made only 90 s after sampling. The differences between PS II related parameters for both light intensities lead to differences in quantum yield and thus low light acclimation (Fig. 1). Maximum attainable photosynthetic rate (55 40 relative values) as well as the light level at which photosynthesis saturates (159 101 μmol photons m^{-2} s^{-1}) decreased whereas α (light utilization effiziency defined as the slope of photosynthesis vs irradiance curve; Fig. 1) increased (0.36 0.39) under 2 μmol photons m^{-2} s^{-1}. This typical photosynthetic response under low light acclimation is also supported by changes in relative pigment concentration (Fig. 2).

Pigments constituted a large proportion (±70%) of total cell carbon under 2 μmol photons m^{-2} s^{-1}, resulting in a carbon:chlorophyll (chl) *a* ratio of 3.5. However, only 30% of total algal carbon was represented by pigments in the 15 μmol photons m^{-2} s^{-1} incubation resulting in a carbon:chl *a* ratio of 7.4. No significant change in relative pigment ratios was observed compared to the major other lipids with exception of diadinoxanthin. Diadinoxanthin concentrations were reduced under 2 μmol photons m^{-2} s^{-1}, which caused a strong reduction in pigment ratios. Diadinoxanthin:chl

Table 2
Amplitudes of fluorescence decay rate constants for fast K_A (A_{comp}), middle K_B (B_{comp}) and slow K_C (C_{comp}) component for growth under 15 μmol photons m^{-2} s^{-1} (0.55 day^{-1}) and 2 μmol photons m^{-2} s^{-1} (0.17 day^{-1})

Variable	15 μmol photons m^2 s^{-1}		2 μmol photons m^2 s^{-1}	
	90 s	30 min	90 s	30 min
A_{comp}	0.011	0.012	0.016	0.011
	0.012	0.012	0.012	0.012
B_{comp}	0.006	0.004	0.017	0.018
	0.010	0.006	0.017	0.013
C_{comp}	0.001	0.001	0.004	0.001
	0.001	0.001	0.006	0.001

They were determined 90 s and 30 min after sampling; $n-2$.

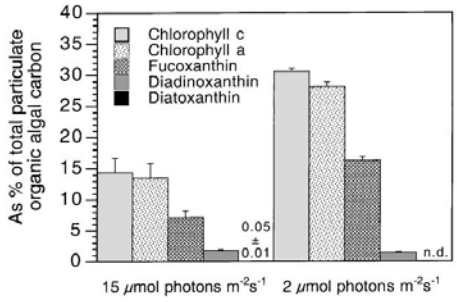

Fig. 2. Pigment composition of sea ice diatoms as % at total particulate organic algal carbon under 15 and 2 μmol photons m^{-2} s^{-1} with corresponding growth rates of 0.55 and 0.17 day^{-1}, respectively. Carotene was always below detection limit. Error bars denote standard deviations; n.d. = not detectable; $n = 3$.

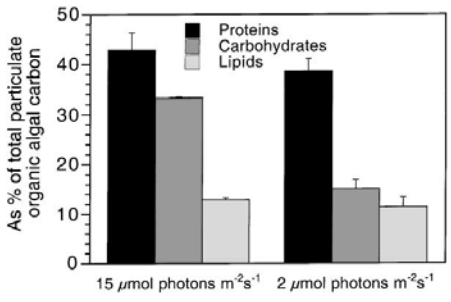

Fig. 3. Macromolecular composition of sea ice diatoms as % of total particulate organic algal carbon under 15 and 2 μmol photons m^{-2} s^{-1} with corresponding growth rates of 0.55 and 0.17 day^{-1}, respectively. Error bars denote standard deviations; $n = 3$.

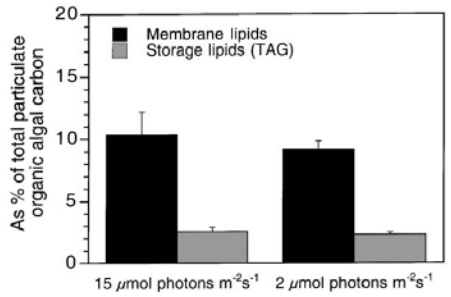

Fig. 4. Polar membrane lipids and storage lipids (triacylglycerol TAG) as % of total particulate organic algal carbon under 15 and 2 μmol photons m^{-2} s^{-1} with corresponding growth rates of 0.55 and 0.17 day^{-1}, respectively. Error bars denote standard deviations; $n = 3$.

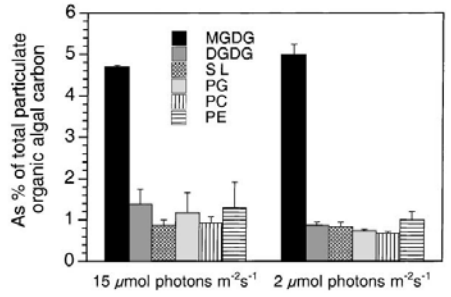

Fig. 5. Glyco- and phospholipid classes of sea ice diatoms as % of total particulate organic algal carbon under 15 and 2 μmol photons m^{-2} s^{-1} with corresponding growth rates of 0.55 and 0.17 day^{-1}, respectively. Error bars denote standard deviations; $n = 3$.

a ratio was 0.14 at 15 μmol photons m^{-2} s^{-1} and 0.04 at 2 μmol photons m^{-2} s^{-1}. Diatoxanthin as well as β-carotene represented less than 0.5% of total algal carbon.

2.2. Biochemistry

Macromolecular composition of diatoms was influenced by the availability of light (Fig. 3). Carbohydrates, as primary assimilates were reduced at 2 μmol photons m^{-2} s^{-1} whereas proteins and lipids remained unaffected under both applied photon flux densities. This is also the case for the membrane lipid fraction as well as for storage lipids of which the latter only represented a small proportion of total algal lipids (17%) (Fig. 4). The dominant membrane lipid class of ice diatoms under light limitation was MGDG, which is exclusively present in chloroplasts, particularly in thylakoid membranes (Fig. 5). DGDG as well as SQDG are also restricted to chloroplasts, whereas phospholipids also occur in non-chloroplast membranes.

The dominance of MGDG indicates that chloroplast membranes were the most abundant membranes in the cell. The most obvious effect of the reduction in irradiance on membrane lipid composition was an increase in MGDG:DGDG ratio to the unexpectedly high ratio of 5.6 at 2 μmol photons m^{-2} s^{-1} (Fig. 6). Fatty acid composition of the different membrane lipid classes as well as storage lipids was influenced by photon flux density. The proportion of polyunsaturated fatty acids (PA) (PUFA) at 2 μmol photons m^{-2} s^{-1} increased for all lipid classes with a concominant decrease of monounsaturated FA (MUFA) and saturated FA (SAFA), except for DGDG. Here, the fatty acid composition remained unchanged for both photon flux densities (Fig. 7). The strongest reduction of saturated FAs in all lipid classes except DGDG could be observed for 14:0 and 16:0 FAs at 2 μmol photons m^{-2} s^{-1}. The PUFA 20:5 increased by at least 38% in phosphatidylcholine (PC), phosphatidylglycerol (PG), sulfoquinovosyldiacylglycerol (SQDG), MGDG and triacylglycerol (TAG) at the same photon flux density. The relative proportion in phosphatidylethanolamin (PE) and DGDG remained more or less constant (Table 3).

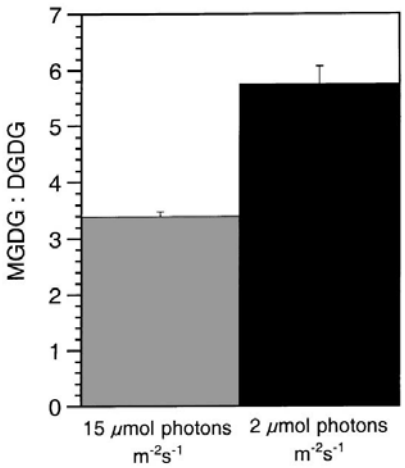

Fig. 6. Ratio of monogalactosyldiacylglycerol (MGDG) to digalactosydiacylglycerol (DGDG) under 15 and 2 μmol photons m^{-2} s^{-1} with corresponding growth rates of 0.55 and 0.17 day^{-1}, respectively. Error bars denote standard deviations; $n = 3$.

3. Discussion

Low photosynthetic active irradiance is one of the strongest determinants in the development and growth of ice algae. The efficiency of light utilization is expressed by high chl *a* content, more so under 2 μmol photons m^{-2} s^{-1} than under 15 μmol photons m^{-2} s^{-1} (e.g. Falkowski and Owens, 1980). At 2 μmol photons m^{-2} s^{-1} almost all carbon and organic nitrogen produced in the cell is converted into pigments and proteins for photosynthesis (Geider et al., 1996, 1998). Thus the flux of excitation energy into carbohydrates is strongly reduced under extreme low light conditions (Fig. 3). However, the pool of lipids, particularly the storage lipid triacylglycerol remained constant. This may be due to a minimum requirement for these lipids. The increase in cell chl *a* under 2 μmol photons m^{-2} s^{-1} was related to changes in photophysiology of PS II. α increased whereas photosynthesis was saturated at 102 μmol photons m^{-2} s^{-1} in contrast to 158 μmol photons m^{-2} s^{-1} at 15 μmol photons m^{-2} s^{-1}. Consequently, maximum attainable photosynthetic rate was reduced under 2 μmol photons m^{-2} s^{-1} (Fig. 1).

The increase in photon trapping and generation of electrons at PS II under 2 μmol photons m^{-2} s^{-1} was regulated by an increase in connectivity (J_{con}) between reaction centres. The number of PS II and/or the LHC cross section probably increased in conjunction with an increase in chl *a*. One consequence, is a stronger probability of exciton capture by the reaction centres and thus a more efficient generation of electrons. Furthermore, the electron transport from reaction centres through the plastoquinone pool is faster under 2 μmol photons m^{-2} s^{-1} which is indicated by rate constants K_A, K_B, K_C and their amplitudes. The fluorescence amplitude for A_{comp} remained relatively constant under both photon flux densities indicating a similar amount of Q_B bound to D1, but the rate constants at 2 μmol photons m^{-2} s^{-1} increased by about 50% compared to 15 μmol photons m^{-2} s^{-1}. Such an increase in electron transport velocity between bound Q_A and Q_B can be explained by increasing FA desaturation of typical chloroplast FAs (MGDG, SQDG, PG), particular by increasing 20:5 *n*-3 of MGDG and SQDG. These fatty acids support the Q_A and Q_B interactions and thus the velocity of electron flow (Horvath et al., 1987). In contrast, amplitudes for the B_{comp} increased at 2 μmol photons m^{-2} s^{-1} which is revealed by a larger amount of bound Q_B and consequently a faster electron transport. Nevertheless, the major FA 20:5 *n*-3 of the chloroplast lipid class MGDG increased by ca. 50% in total fatty acids under 2 μmol photons m^{-2} s^{-1} (Table 3) as well as pigments like chl *a*/*c* (Fig. 2). This also supports the argument that chlorophyll molecules are associated with PUFA (Kates and Volcani, 1966; Cohen et al., 1988; Thompson et al., 1990). We suggest that diatoms use pairs of 20:5 to accommodate the phytol side chain of chl *a*. The desaturation of MGDG-FAs to 20:5 *n*-3 was correlated with a shift to low photon flux densities and the activity of PS I. This adaptive response which provides alterations to lipid protein interactions in the membrane may be important for the self-assembly of active chlorophyll protein complexes for photosynthetic apparatus of PS I (Klyachko-Gurvich et al., 1999) and perhaps also for PS II.

Not only the presence of PUFAs in thylakoid membranes is important for structure and function of PS I and II, but the composition of lipid classes also significantly influences membrane structure (Block et al., 1983). Under 2 μmol photons m^{-2} s^{-1}, the concentration of non-bilayer forming MGDG increased in relation to other bilayer forming lipids, especially DGDG (Fig. 5). The ratio of 5.8 between both glycolipid classes is much higher than the critical ratio of 2.5, above which transition to non-bilayer structures begins in MGD/DGD mixtures (Sprague and Staehelin, 1984). We assume that the existence of thylakoid bilayers is required in sea ice diatoms just like in all other photosynthetic organisms. The existence of bilayers with such high proportions of non-bilayer-forming lipids is only possible when sufficient thylakoid pigment protein complexes are present (Webb and Green, 1991). If more thylakoid pigment protein complexes are present in the membranes, as found under light limitation, less bilayer-forming lipids such as DGDG are required to stabilize the bilayer structure. Differences in protein content between both photon flux densities could be neglected due to insignificant changes in protein concentrations

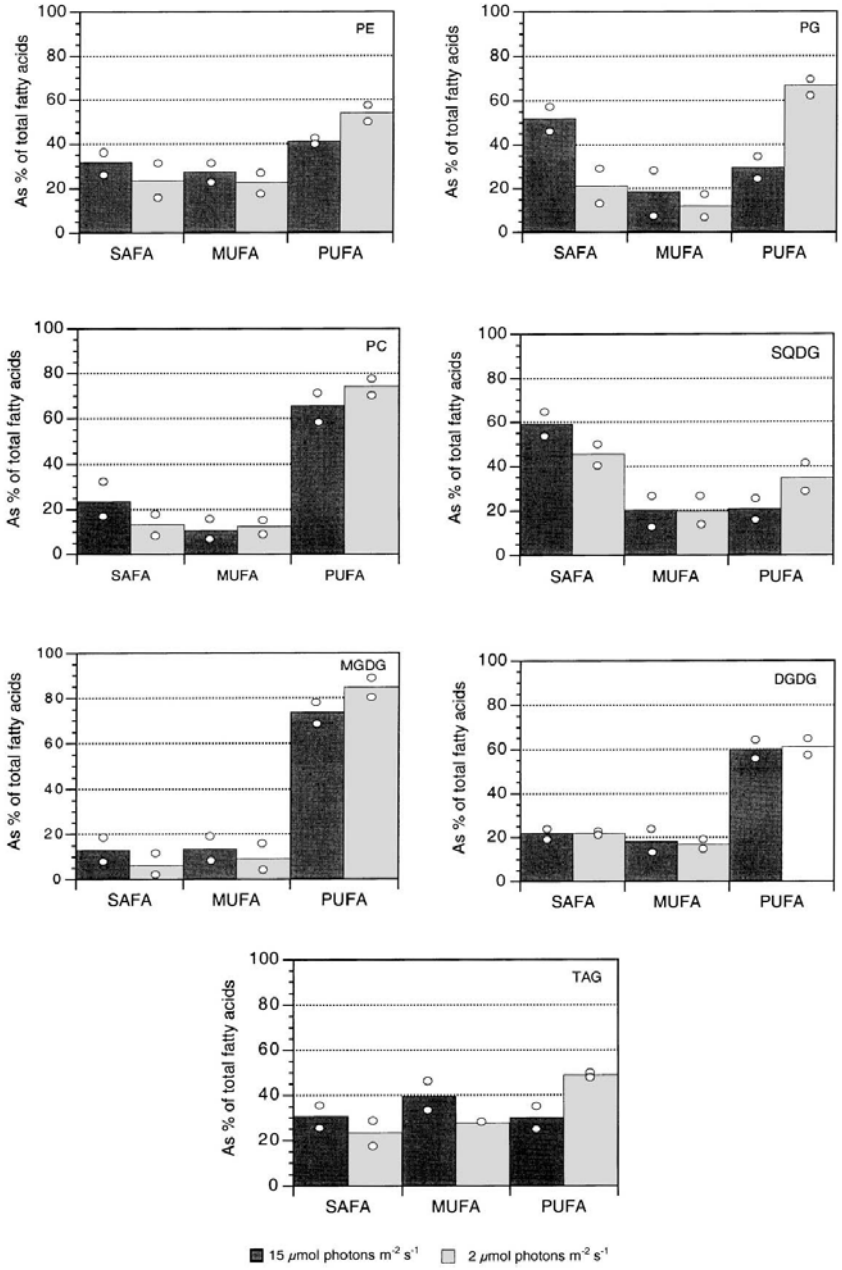

Fig. 7. Distribution of saturated (SAFA), monounsaturated (MUFA) and polyunsaturated fatty acids (PUFA) in lipid classes of sea ice diatoms as % of total particulate organic algal carbon under 15 and 2 μmol photons m^2 s^{-1} with corresponding growth rates of 0.55 and 0.17 day^{-1}, respectively; $n=2$.

Table 3
Fatty acid composition in lipid classes of sea ice diatoms at 15 μmol photons m^{-2} s^{-1} (growth rate 0.55 day^{-1}) and at 2 μmol photons m^{-2} s^{-1} (growth rate 0.17 day^{-1})

Fatty acid	PC		PE		PG		SQDG		DGDG		MGDG		TAG	
	15 μmol photons m^{-2} s^{-1}	2 μmol photons m^{-2} s^{-1}	15 μmol photons m^{-2} s^{-1}	2 μmol photons m^{-2} s^{-1}	15 μmol photons m^{-2} s^{-1}	2 μmol photons m^{-2} s^{-1}	15 μmol photons m^{-2} s^{-1}	2 μmol photons m^{-2} s^{-1}	15 μmol photons m^{-2} s^{-1}	2 μmol photons m^{-2} s^{-1}	15 μmol photons m^{-2} s^{-1}	2 μmol photons m^{-2} s^{-1}	15 μmol photons m^{-2} s^{-1}	2 μmol photons m^{-2} s^{-1}
14:0	7.46	3.44	8.40	11.65	21.37	2.43	22.80	8.87	8.17	13.48	4.66	3.07	9.65	11.00
15:0		0.27	1.24	0.58						0.34	3.32	0.95	0.43	4.10
16:0	14.12	8.95	21.02	10.81	30.60	16.94	28.58	15.84	10.81	7.63	3.50	1.70	19.34	7.10
18:0	2.04	0.54	0.95	0.48		1.77	7.67	20.92	2.89	0.52	1.37	0.33	1.11	1.30
16:1*n*-7	7.30	8.69	23.53	20.11	11.88	6.31	20.21	19.74	8.45	13.30	8.72	6.23	36.02	24.76
18:1*n*-9	1.66	1.52				0.95			6.37	1.65	0.96	0.43	3.02	2.96
18:1*n*-7	1.82	1.92	3.77	2.50	6.60	4.95				1.08	0.83	0.73		
20:1*n*-9		0.52							3.30	0.92	2.96	1.89	0.50	
16:2*n*-?	2.87	0.40		1.00		0.85			10.59	3.11	2.48	1.03	1.69	
16:3*n*-?		0.40		1.00						2.17	8.45	4.87	1.12	
16:4*n*-1		0.50				0.52	9.46	12.63	4.45	9.10	35.41	33.84	1.57	2.08
18:2*n*-6	5.55	4.53	0.80	1.21		1.03				1.27	1.84	1.03	2.18	3.24
18:3*n*-3	2.98	0.63								0.60	2.38		0.91	
18:4*n*-3	7.6	1.94			6.65				11.81	8.72		0.73	6.38	2.3
20:2*n*-?			13.36	18.48									1.47	
20:4*n*-6		3.58		0.55		9.72				1.01		1.95		
20:4*n*-3	1.62	1.08	3.20	11.12		1.18				2.81			1.08	2.27
20:5*n*-3	37.16	51.16	20.56	18.91	22.91	50.68	11.28	22.00	33.19	30.96	23.10	40.71	12.49	33.56
22:6*n*-6	7.82	9.92	3.15	1.62		2.66				1.31		0.79	1.04	5.38

Results are reported as % of total fatty acids. PC − phosphatidylcholine; PE − phosphatidylethanolamin; PG − phosphatidylglycerol; SQDG − sulfoquinovosyldiacylglycerol; DGDG − digalactosyldiacylglycerol; MGDG − monogalactosyldiacylglycerol; TAG − triacylglycerol. Not detected; $n-2$.

(Fig. 3). Pigment contents which nearly doubled under 2 μmol photons m^{-2} s^{-1} must therefore be responsible for an increase in the MGDG:DGDG ratio.

Consequently, photon flux density as an important determinant for growth in polar diatoms, influences the amount of chl *a* in the choloroplast, leading to biochemical changes of the chloroplast membranes in order to sustain intact bilayers and thus photosynthesis. Besides this influence of light on structural regulation of thylakoid membranes, light also regulates the fluidity of the thylakoid membrane.

4. Experimental

Material and methods which were applied in this investigation are identical to those in part I, described in: Photosynthetic energy conversion under extreme conditions: I. Important role of lipids as structural modulators and energy sink under *N*-limited growth in Antarctic sea ice diatoms (Mock and Kroon, 2002). Only the basic experimental conditions were changed as follows: two different photon flux densities were adjusted within continuous cultures: a total of 15.0±5.0 μmol photons m^{-2} s^{-1} resulted in a growth rate of 0.55 day^{-1} with a optical density (OD) of 0.11±0.01. A photon flux density of 2.0±1.0 μmol photons m^{-2} s^{-1} lead to an algal growth rate of 0.17 day^{-1} with an OD of 0.037±0.006. The algal composition in the first culture was 66±11% of *Navicula gelida* var. *antarctica*, 20±7% of *Fragilariopsis curta* and 14±9% of *Nitzschia medioconstricta* after ca. one week under steady state growth. At 2 μmol photons m^{-2} s^{-1} and a growth rate of 0.17 day^{-1} *Navicula gelida* var. *antarctica* constituted 65±6%, *Fragilariopsis curta* 15±6% and *Nitzschia medioconstricta* 20±7% to the total community.

Acknowledgements

We are grateful to the crew of the RV *Polarstern* for their assistance during the expedition. We thank Gerhard Kattner and Martin Graeve for valuable discussions and for kind assistance with the lipids. Gerhard Dieckmann is thanked for reviewing an earlier version of the manuscript, and making suggestions for its improvement.

References

Block, M.A., Dorne, A.J., Joyard, J., Douch, R., 1983. Preparation and characterization of membrane fractions enriched in outer and inner envelope membranes from spinach chloroplasts. II Biochemical characterization. J. Biol. Chem. 258, 13281 13286.

Cohen, Z., Vonshak, A., Richmond, A., 1988. Effect of environmental conditions on fatty acid composition of the red alga *Porphyridium cruetum*: correlation to growth rate. J. Phycol. 24, 328–332.

Eilers, P.H., Peters, J.C.H., 1988. A model for the relationship between light intensity and the rate of photosynthesis in phytoplankton. Ecol. Model. 42, 199–215.

Falkowski, P.G., Owens, T.G., 1980. Light shade adaptation: two strategies in marine phytoplankton. Plant Physiol. 66, 632–635.

Geider, R.J., MacIntyre, H.L., Kana, T.M., 1996. A dynamic model of photoadaptation in phytoplankton. Limnol. Oceanogr. 41, 1–15.

Geider, R.J., MacIntyre, H.L., Kana, T.M., 1998. Dynamic model of phytoplankton growth and acclimation: responses of the balanced growth rate and the chlorophyll a: carbon ratio to light, nutrient-limitation and temperature. Limnol. Oceanogr. 43 (4), 679–694.

Harwood, J.L., Jones, A.L., 1989. Lipid metabolism in algae. Adv. Bot. Res. 16, 1–53.

Horvárth, G., Melis, A., Hideg, E., Droppa, M., Vigh, L., 1987. Role of lipids in the organization and function of photosystem II studied by homogeneous catalytic hydrogenation of thylakoid membranes in situ. Biochim. Biophys. Acta 891, 68–74.

Huisman, J., Weissing, F.J., 1999. Biodiversity of plankton by species oscillations and chaos. Nature 402, 407–410.

Kates, M., Volcani, B.E., 1966. Lipid components of diatoms. Biochim. Biophys. Acta 116, 264–278.

Kirst, G.O., Wiencke, C., 1995. Ecophysiology of polar algae. J. Phycol. 31, 181–199.

Klyachko-Gurvich, G.L., Tsoglin, L.N., Doucha, J., Kopetskii, J., Ryabykh, I.B.S., Semenenko, V.E., 1999. Desaturation of fatty acids as an adaptive response to shifts in light intensity. Phys. Plant. 107, 240–249.

Krembs, C., Gradinger, R., Spindler, M., 2000. Implications of brine channel geometry and surface area for the interaction of sympagic organisms in Arctic sea ice. J. Exp. Mar. Biol. Ecol. 243, 55–80.

Mock, T, Kroon, B. M., 2002. Photosynthetic energy conversion under extreme conditions: I. Important role of lipids as structural modulators and energy sink under N-limited growth in Antarctic sea ice diatoms. Phytochemistry 61.

Pohl, F., Zurheide, 1979. Fatty acids and lipids of marine algae and the control of their biosynthesis by environmental factors. In: Hoppe, H.A., Levring, T., Tanaka, Y. (Eds.), Marine Algae in Pharmaceutical Science. Walter de Gruyter, Berlin, pp. 473–523.

Reay, D.S., Nedwell, D.B., Priddle, J., Ellis-Evans, C., 1999. Temperature dependence of inorganic nitrogen uptake: reduced affinity for nitrate at suboptimal temperatures in both algae and bacteria. Appl. Environ. Microbiol. 65, 2577–2584.

Russell, N.J., 1997. Psychrophilic bacteria-molecular adaptations of membrane lipids. Comp. Biochem. Physiol. 118A (3), 489–493.

Saruwatari, M., Takio, S., Ono, K., 1999. Low temperature-induced accumulation of eicosapentaenoic acids in *Marchantia polymorpha* cells. Phytochemistry 52, 367–372.

Sewon, P., Mikola, H., Lehtinen, T., Kallio, P., 1997. Polar lipids and net photosynthesis potential of subarctic *Diapensia lapponica*. Phytochemistry 46, 1339–1347.

Sprague, S.G., Staehelin, L.A., 1984. Effects of reconstitution method on the structural organization of isolated chloroplast membrane lipids. Biochim. Biophys. Acta 777, 306–433.

Tasaka, Y., Gombos, Z., Nishiyama, Y., Mohanty, P., Ohba, T., Ohki, K., Murata, N., 1996. Target mutagenesis of acyl-lipid desaturases in synechocystis: evidence for the important roles of polyunsaturated membrane lipids in growth, respiration and photosynthesis. EMBO J. 15, 6416–6425.

Thompson, P.A., Harrison, P.J., Whyte, J.N.C., 1990. Influence of irradiance on the fatty acid composition of phytoplankton. J. Phycol. 26, 278–288.

Webb, M.S., Green, B.R., 1991. Biochemical and biophysical properties of thylakoid acyl lipids. Biochim. Biophys. Acta 1060, 133–158.

EST analysis of freezing tolerance in the Antarctic diatom *Fragilariopsis cylindrus*: Detection of numerous cold acclimation-related genes and a gene transfer event

Thomas Mock[1,*] and Klaus Valentin[1]

[1]Alfred Wegener Institute for Polar and Marine Research, Am Handelshafen 12, 27570 Bremerhaven, GERMANY

*corresponding author E-mail: tmock@awi-bremerhaven.de

Tel. Nr.: 0049(0)471 4831 1893

Fax Nr.: 0049(0)471 4831 1425

Running head:

Cold acclimation-related genes in *Fragilariopsis cylindrus*

Keywords

Antarctica, Arctica, cold acclimation, diatom

EST, *Fragilariopsis cylindrus*, gene expression, sea ice

ABSTRACT

Fragilariopsis cylindrus is dominant in polar sea ice and open oceans. It is special with respect to its ability to survive extreme temperatures (8 to -20°C), salinities (0 – 150 PSU) and pH values (7 – 11). Here we describe an approach to isolate genes involved in cold tolerance using random sequencing of genes expressed (= expressed sequence tags – EST) under freeezing temperature conditions. Cells were grown at optimal conditions (+5°C, 35 µmol photons $m^{-2}s^{-1}$) and then transferred to –2°C simulating freezing into sea ice. After 5 days mRNA was isolated and the complementary DNA was cloned, which resulted in a cDNA-Library of 1.5 Mio recombinant clones per ml. Sixhundred clones where analysed for insert sizes and those between 564 and 2500 bp were chosen for partial sequencing producing 260 interpretable sequences. These represented 186 contigs of an average size of 539 base pairs. 40% of the contigs could be identified by gene bank comparison. Among these we detected 10 genes (5%) potentially involved in psychrophily or acclimation to cold conditions. Among genes identified there were at least one of possible red algal origin indicating secondary gene transfer. Interestingly the most abundant ESTs could not be identified indicating the presence of yet unknown cold tolerance genes.

INTRODUCTION

Polar oceans are most important for global climate and primary production (e.g. Legendre et al., 1992; Arrigo et al., 1997). Sea ice is an important component of the polar oceans in structuring the entire ecosystem (Eicken, 1992). At its maximum, it covers 13 % of the Earth´s surface. The largest expanse of sea ice occurs in the Southern Ocean where, during winter, 20 million square kilometers are covered by ice of approximately 1m thickness. Sea ice, in contrast to fresh water ice, is not solid but comprises a system of brine channels that provide a habitate characterized by low temperatures (-2° to – 15°C), high salinity (35 – 150 PSU), high pH (up to 11) and low irradiances (0.3 – 100 µmol photons $m^{-2}s^{-1}$; Eicken, 1992; Gleitz et al., 1995; Mock and Gradinger, 1999; McMinn et al., 2000; Trenerry et al., 2002). Despite these extreme condition the brine channels can be heavily populated by diatoms (Thomas and Dieckmann, 2002). Among these *Fragilariopsis cylindrus* is perhaps the most successful species (Kang and Fryxell, 1992; Quillfeld, 1997; Gleitz et al, 1998) and a key paleo-oceanographic species (Leventer, 1998). It is obligately adapted to these growth conditions, i.e. not able to survive temperatures above +8°C (Fiala and Oriol, 1990). High

concentrations of polyunsaturated fatty acids (PUFAs) and especial sterols indicate sophisticated membrane adaptations to low temperatures and low irradiances in sea ice (Nichols et al., 1986; Mock and Kroon, 2002). However, *F. cylindrus* is not restricted to sea ice but is also among the most successful species in open arctic oceans making it a key algae in the polar environment.

Organisms, especially photosynthetic ones, living at extremely low temperatures are interesting from several points of view. Protein biochemists are interested in the molecular basis of psychrophilic enzymes. In most cases, the adaptation is archieved through a reduction in the activation energy, leading to a high catalytic efficiency, which possibly originates from an increased flexibility of either a selected area or the overall protein structure (Zecchinon et al., 2001). Lipid biochemists want to understand how membrane fluidity is maintained at temperatures well below zero. Physiologists focus on the general adaptation mechanisms enabling organisms to survive in extreme niches. Ecologists attempt to quantify the primary production of polar autotrophic organisms (Mock, 2002) of which marine micro-algae are the most important carbon fixers and thus the food source for the entire polar marine ecosystem. In recent years, the ice-covered seas of Jupiter´s moon Europa and Ganymede attracted Astrobiologists by their possibility to harbour psychrophilic microorganisms such as those in sea ice on our earth (Thomas and Dieckmann, 2002). Finally the economical value of proteins and lipids from psychrophile cells may be high. They usually contain substantial amounts of PUFAs essential for human nutrition. Enzymes from psychrophiles are likely active at low temperatures which makes them candidates for industrial processes at such temperatures. Despite this only little is known about the molecular basis of cold adaptation in organisms living in the coldest environments on earth, especially photosynthetic eucaryotes. Most data available were gained in bacterial systems (e.g. Russel, 1998, Zecchinon et al., 2001). For plants systematical experiments were done mainly with *Arabidopsis thaliana* (e.g. Thomashow, 1998, 2001; Allen and Ort, 2001; Seki et al., 2001; Stitt and Hurry, 2002). However, this species is adapted to temperate regions and is only distantly related to the dominating taxa in the ocean, i.e. diatoms and other heterkont algae.

The aim of this study therefore was to establish a primary molecular database regarding extreme cold adaptation in an important polar diatom. *Fragilariosis cylindrus* was chosen because it is one of the most successful species in this area. We used an EST approach to identify genes expressed under extreme cold conditions. This method allows to identify

potentially interesting genes among hundreds of others. It also provides sequence information and clones for subsequent expression analysis. Here we present an initial dataset of partial EST gene sequences among which 40 % could be identified by gene bank comparison, and at least 10 (= 5%) are potentially involved in cold adaptation.

RESULTS

Determination of the appropriate sampling time

Optimal growth conditions for *F. cylindrus* were found to be + 5°C, 34 PSU and 35 µmol photons $m^{-2}s^{-1}$with a light-dark cycle of 16 : 8 h. Under these conditions algae had a maximum quantum yield of PS II of 0.605 Fv/Fm and a division rate of 0.7 day^{-1}. Chilling to -2 °C caused an instant decrease of Fv/Fm and a subsequent recovery. Initial values of Fv/Fm were attained 5 days later (Fig. 1). Thus, physiological acclimation with a potential steady state expression of cold acclimation related genes were established after this time period. Consequently algae were harvested and mRNA was islolated five days after chilling.

The EST library

A phage cDNA library was established consisting of approximately 1.5 Mio recombinant clones per ml thus probably covering the expressed genome at this time point. Sixhundred recombinant plaques were analysed by PCR and 564 of these contained an insert (94%). The sizes of the inserts were in the range of ca. 400 to 2500 base pairs and 63% were larger than 564 bp (Fig. 2) 350 clones with inserts larger than 564 bp were chosen for partial sequencing from the 5'-end. This size restriction was made because it was found that in chromophytic genes the size of the region between the stop codon and the polyA tail may be rather large (Moulin et al., 1999; Crepineau et al., 2000). Several clones (24) were sequenced from both ends. 260 Sequences obtained were compared to each other in order to identify overlapping clones and/or duplicates, resulting in 186 contigs. Only 10% of the contigs were represented by more than one clone. The most abundant EST contig was represented by 12 clones (6%), another by 7 clones (4%), 6 ESTs by 3-4 clones, and 10 ESTs by 2 clones, i.e. 168 out of 186 EST contigs (90 %) were unique clones.

41 out of the 186 contigs contained a poly A tail. For at 8 of these we could localise the gene end relative to the poly A tail. The average length of the eight 3' untranslated regions (UTR) was 160 bp (100 – 260 bp), significantly shorter than in *Laminaria digitata* (Crepineau et al. 2000). However, we do not regard our sample size as sufficient to draw any final conclusion concerning the size of UTRs in *F. cylindrus*. In fact, most ESTs (33 out of 41, up to 1123 bp long) that contained a poly A signal were not identifiable by BLAST searches. It is possible that in some of these cases only 3' UTRs were blasted, indicating that 3' UTRs actually may be much longer. The GC content of ESTs clearly identified as nuclear genes were in the range of 48 – 38 % (average ca. 43%) which is slightly lower than in *P. tricornutum* (49%, Scala et al., 2002).

EST identification and identities

The 186 contigs identified were compared to data banks by BLAST searches and BLAST results were carefully analysed (Fig. 3). As a first approximation clones producing matches of more than 30% in an overlap of more than 80 aa were regarded as significant. In some cases only the end of a gene was located on the clones resulting in shorter overlaps (e.g. hsp70, a putative NADPH flavin oxidoreductase, desA) which were also regarded as significant. Degrees of similarity below 30% were accepted in case of large overlaps or proteins known to be only weakly conserved (e.g. a putative calcium protein kinase, homoserine dehydrogenase, phosphodiesterase). For many BLAST results the area of a BLAST hit that matched a *F. cylindrus* EST was again blasted against Genbank. We than compared these matches with the *F. cylindrus* match and in case they were much higher the *F. cylindrus* match was rejected. Additionally we compared the size of the EST clone with the expected size of the matching protein and its relative location on the EST. These approaches in some cases could confirm or reject, respectively, the BLAST hit.

Of the 186 EST contigs 72 (40%) showed homology to known proteins or hypothetical conserved open reading frames (A detailed summary (Table 2) is available under http://www.awi-bremerhaven/XXX). This value is comparable to data from other chromophytic algae (e.g. *Laminaria digitata* 39 – 48%, Crepineau et al., 2000; *Phaeodactylum tricornutum* < 40 %, Scala et al., 2002; *Chrysochromulina polylepis* 43%, Uwe John, pers. communication), but is higher than in a Dinophyte (*Alexandrium ostenfeldii* 22%, John pers. comm.). The most abundant identifiable *F. cylindrus* genes were the fcp

genes (4 sequences = 3 contigs, indicating the presence of a multi gene family), two probable mitochondrial contigs (a hypothetical protein - 3 sequences in one contig and two ribosomal proteins [rpl2 and rps19] – 3 sequences in one contig), and a Zn binding protein (3 sequences in one contig). These results are in good agreement with those from other chromophytic algae (Crepineau et al., 2000; Scala et al., 2002).

Most identifiable genes showed the highest degree of similarity to eukaryotic counterparts from the plant, animal or fungal kingdom. In no case, however, an *F. cylindrus* EST was more similar to a one of these than any other of the eucaryotic sequences. A number of ESTs are likely of organellar origin (e.g. tufA, ftsH, mitochondrial rpl2 and rps 19, Acetyl-CoA-carboxylase, a homologue to ORF 148 from the diatom *Odontella sinensis* plastom). Two genes were detected that may originate from a former red algal nucleus, i.e. psbU and the cell cycle protein 48, which are both most similar to red algal or cryptophyte counterparts. This was most obvious for psbU, which is 51% similar to the *C. caldarium* (red alga) homologue and only 39-45% similar to cyanobacterial counterparts.

A surprising finding was that all but 4 (see above) of the 18 EST represented by more than one sequence did not produce any hit in gene bank comparisons, even when a yet unpublished data bank for a fully sequenced diatom, *Thalassiosira pseudonana*, was included. This implies that the most important transcripts under freezing conditions in *F. cylindrus* are completely unknown.

Potentially cold-acclimation related genes

Among the 72 ESTs producing significant hits in BLAST searches 10 (= 13 % of the known genes, 5 % of all contigs) are potentially involved in cold stress acclimation (Table 1; Fig. 3). This number much higher than in other chromophytic EST libraries. All of these 10 EST were represented by a single sequence. We assume that among the unknown, especially among the highly expressed genes (see above), there are more cold-adaptation genes to be identified.

DISCUSSION

We have established the first EST dataset for a polar, psychrophilic alga, which represents an ecological relevant species for both Arctic and Antarctic oceans and sea ice (Kang and Fryxell, 1992; Quillfeld, 1997; Gleitz et al., 1998). The amount of identifiable genes in our library is (Fig. 3) comparable to the numbers seen in two other chromophytes, but it is, for example, much higher than in a dinoflagellate. This indicates that the genetic complexity in *F. cylindrus* is comparable to other chromophytes and not significantly higher as may be expected due to its unusual life conditions. However, *F. cylindrus* under freezing condition strongly expresses several genes that could not be identfified by gene bank comparisons. It is likely that at least a proportion of these genes are involved in cold acclimation indicating that this alga posesses new and strongly expressed cold acclimation proteins. Actually, our efforts to isolate genes possibly involved in cold-acclimation resulted in the detection of a high proportion in the cold-acclimated EST library: 5% of the ESTs encode for such genes. Most cold acclimated genes in *F. cylindrus* are related to protein synthesis, folding and membrane desaturation and stabilisation (Table 1). This number is much higher than in other chromophytes (Crepineau et al., 2000; Scala et al., 2002) and demonstrates that one strategy of *F. cylindrus* to survive at low temperatures is to express a variaty of cold stress-related genes, some of them potentially at a high level.

Most identifiable genes were similar to eukaryotic counterparts from the plant, animal or fungal kingdom. However, no statement is possible as to whether the majority of *F. cylindrus* genes are of animal, plant or fungal origin, respectively. Sometimes of course the "best match" was exclusively against on of these but more careful analyses revealed that this was rather artificial. In all cases where we found a clear best match against an eukaryotic crown group (either animal, plant or fungus) we tested the significance by blasting the proportion of the gene that matched against the databanks. It always turned out that animal, fungal, or plant genes were more similar to each other than either was to the *F. cylindrus* gene. This indicates that the evolutionary lineage leading to the diatoms separated from the "crown group lineage" before this one branched into plant, animal and fungal kingdoms.

A number of ESTs seems to be of organellar origin. Either this is the result of mispriming of the primers for cDNA first strand synthesis or, more likely, these genes are nuclear-encoded in *F. cylindrus*. The latter case would imply gene transfer events from the diatom plastid

genome (= former red algal plastid genome, Valentin et al., 1992) to the host cell nucleus (see below).

Three ESTs showed similarity only to bacterial sequences, i.e. an efflux transporter, a homoserine dehydrogenase, and an aconitate hydratase. These genes may have entered the *F. cylindrus* genome via an organellar genome or by lateral gene transfer, or they have been lost in those higher eucaryotes yet completely sequenced. Of particular interest is the aconitate hydratase because it is a known cold shock protein in bacteria (Lottering and Streips, 1995).

The fact that diatoms are the result of a secondary endosymbiosis (Valentin et al., 1992) makes them interesting candidates to study gene transfer events. Such studies have yet been focussed on green plants where a large number of potential plastid genes have been detected in the nuclear genome (Martin et al., 2002). The situation in Diatoms is more complicated and gene transfer events can be expected not only from the plastid to the nucleus but also from the former nucleus of the endosymbiont to the host cell nucleus (Deane et al., 2000). We found for the first time direct evidence for a gene transfer from the former red algal nucleus to the diatom host cell nucleus. The psbU gene, not known from green plants, but present in cyanobacteria (Nishiyama et al., 1999) and in the red algal nucleus (Ohta et al., 1999) resides in the nuclear genome in *F. cylindrus*. This suggests an early secondary gene transfer from the nucleus of the endosymbiotic red alga to the diatom host cell nucleus, already before a nucleomorph-phase of the red algal nucleus as indicated by the absence of psbU in the nucleomorph genome (Douglas et al., 2001).

In summary, *F. cylindrus* is an excellent model organism to further develop the molecular basis of psychrophilic live in polar oceans and sea ice. It is worthwhile to expand the EST analysis and we are therefore currently establishing a much larger databbase of cold-induced ESTs. Such information adds to recently established EST databanks from chromophytic algae and higher plants, which were however organisms from temperate regions. Research on psychrophiles will not only unravel their special mechanisms of adaptation but will also further our understanding of molecular evolution of species. Knowledge of the molecular basis of freezing tolerance and cold adaptation will probably elucidate the development of new strategies essential for living in the cold and thus selecting these adapted species. Determining such strategies in psychrophiles is not only of basic scientific interest, but also

has potential practical applications to improve plant freezing tolerance for increased plant productivity and expanded areas of agricultural production (Thomashow, 1998).

MATERIALS AND METHODS

Growth and photosystem II quantum yield of algae

Fragilariopsis cylindrus was isolated from Antarctic sea ice during a "Polarstern" expedition (ANT XVI/3) in the eastern Weddell Sea. For the cold shock experiment algae were grown at +5°C in a 10L batch culture under 35 µmol photons $m^{-2}s^{-1}$ (16h light, 8h dark) in double f/2 medium (Guillard and Ryther, 1962). Bubbling with air (150 ml/min) ensured sufficient CO_2 supply and contineous mixing. The culture was chilled to –2°C in the middle of the exponential growth phase (ca. 1.5 Mio cells ml^{-1}). Quantum yield of photosystem II (PS II) was determined daily in the middle of the light phase with a Xenon-PAM (Puls-Amplitude-Modulated) Fluorometer (Walz GmbH, Germany). Five parallels were measured after a dark incubation for 15 min under temperature-controlled conditions. Samples for mRNA extraction were taken 5 days after chilling.

Isolation of mRNA

Total RNA was isolated with a RNeasy Plant Mini Kit (Qiagen). The mRNA was isolated from ca. 100 µg total RNA with an Oligotex mRNA Midi-Kit (Qiagen). Approximately 800 ng poly A^+ mRNA were used for first-strand cDNA synthesis.

cDNA library construction

The cDNA library was synthesised with a SMART™ cDNA Library Construction Kit (Clontech). Total poly A^+ mRNA was used for first-strand synthesis with SMART IV™ oligonucleotides and CDS III/3´PCR primer. Double-strand cDNA synthesis was done by LD PCR with an Eppendorf Thermocycler using the following program: 95°C for 5 min denaturation and subsequent 20 cycles at 95°C (2min) and 68°C (6min). After SfiI digestion the cDNA was fractionated with CHROMA Spin™ - 400 columns in order to ligate only cDNAs above 400bp. These cDNAs were ligated at 16°C overnight into pTriplEX2 vectors. A separate λ-phage packaging reaction (Promega) was used to obtain an amplified library with a titer of $2.7x10^9$ pfu/ml. A blue/white screening with IPTG and X-gal revealed a recombination efficiency of ca. 70%. White plaques were used for large scale PCR analysis

(fig. 1) with 5´and 3´ λTripEx LD-Insert Screening Amplimers. Approximately 350 clones larger than 564bp were chosen for sequencing analysis.

Sequence analysis

Inserts were sequenced from the 5' end with λTripEx2 Sequencing Primer. On average 500 bp were determined. Sequences were compared to each other in order to detect overlapping clones. All contigs were compared to GENBANK by BLAST searches using the BLASTX option, i.e. we compared the translated sequences (all possible reading frames) against protein databanks and translated DNA databanks. All results were checked by eye and those searches producing unclear results were further analysed. Tentatively matches were checked producing similarities below 30% and overlaps of less than 80 aa. In general those clones producing a match on the non-coding strand were sorted out. The size of the matching protein and the localization of the match on our clone were compared to the size of the clone. In the case of weak similarities we determined the degree of conservation within that matching gene and other homologues, and compared it to the degree of conservation between our clones and the match. In some cases we could reject possible matches. For instance HSP70 is certainly a match despite a score of only 34 because the match was restricted to the last 20 aa of the protein.

ACKNOWLEDGMENTS

We wish to thank Linda Medlin for providing lab space and generous support, Gernot Glöckner for help with the contig establishment, and Uwe John for his helpful collaboration in the lab.

LITERATURE CITED

Allen DJ, Ort DR (2001) Impacts of chilling temperatures on photosynthesis in warm-climate plants. Trends Plant Sci **6**(1): 36-42

Arrigo KR, Worthen DL, Lizotte MP, Dixon P, Dieckmann G (1997) Primary production in Antarctic sea ice. Science **276**: 394-397

Crepineau F, Roscoe T, Kaas R, Kloareg B, Boyne C (2000) Characterisation of complementary DNAs from the express sequence tag analysis of life cycle stages of *Laminaria digitata* (Phaeophyceae). Plant Mol Biol **43**: 503-513

Deane JA, Fraunholz M, Su V, Maier UG, Martin W, Durnford DG, McFadden G (2000) Evidence for nucleomorph to host nucleus gene transfer: Light harvesting complex proteins from cryptomonads and chlorarachniophytes. Protist **151**: 239-252

Douglas S, Zauner S, Fraunholz M, Beaton M, Penny S, Deng LT, Wu X, Reith M, Cavalier-Smith T, Maier UG (2001) The highly reduced genome of an enslaved nucleus. Nature **410** (6832): 1091-1096

Eicken H (1992) The role of sea ice in structuring Antarctic ecosystems. Polar Biol **12**: 3-13

Fiala M, Oriol L (1990) Light-temperature interactions on the growth of Antarctic diatoms. Polar Biol **10**: 629-636

Gleitz M, Vonderloeff MR, Thomas DN, Dieckmann GS, Millero FJ (1995) Comparison of summer and winter inorganic carbon, oxygen and nutrient concentrations in Antarctic sea ice brine. Mar Chem **51**(2): 81-91

Gleitz M, Bartsch A, Dieckmann GS, Eicken H (1998) Composition and succession of sea ice diatom assemblages in the eastern and southern WeddellSea, Antarctica. *In:* MP Lizotte, KR Arrigo, eds, Antarctic sea ice, biological processes, interactions and variability. Antarctic Research Series, Vol. 73, American Geophysical Union, Washington, DC, USA, pp 107-120

Guillard RR, Ryther JH (1962) Studies of marine plankton diatoms. I. Cyclotella nana (Husted) and Detonula confervacea (Cleve). Can J Microbiol **8**: 229-239

Hon WC, Griffith M, Mlynarz A, Kwok YC, Yang DS (1995) Antifreeze proteins in winter rye are similar to pathogenesis-related proteins. Plant Physiol 109(3): 879-889

Kang SH, Fryxell GA (1992) *Fragilariopsis cylindrus* (Grunow) Krieger: The most abundant diatom in water column assemblages of Antarctic marginal ice-edge zones. Polar Biol **12**: 609-627

Kaye C, Neven L, Hofig A, Li QB, Haskell D, Guy C (1998) Characterization of a gene for spinach CAP160 and expression of two spinach cold-acclimation proteins in tabacco. Plant Physiol **116**: 1367-1377

Legendre L, Ackley SF, Dieckmann GS, Gulliksen B, Horner R, Hoshiai T, Melnikov IA, Reeburgh WS, Spindler M, Sullivan CW (1992) Ecology of sea ice biota 2. Global significance. Polar Biol **12**: 429-444

Leventer A (1998) The fate of Antarctic "sea ice diatoms" and their use as paleoenvironmental indicators. *In:* MP Lizotte, KR Arrigo, eds, Antarctic sea ice, biological processes, interactions and variability. Antarctic Research Series, Vol. 73, American Geophysical Union, Washington, DC, USA, pp 121-137

Lottering EA, Streips UN (1995) Induction of cold shock proteins in *Bacillus subtilis*. Curr Microbiol **30**: 193-199

Martin W, Rujan T, Richley E, Hanson A, Cornelsen S, Lins T, Leister D, Stoebe B, Hasegawa M, Penny D (2002) Evolutionary analysis of *Arabidopsis*, cyanobacterial and chloroplast genomes reveals plastid phylogeny and thousands of cyanobacterial genes in the nucleus. Proc Natl Acad Sci USA **99**: 12246-12251

McMinn A, Ashworth C, Ryan KG (2000) In situ net primary productivity of an Antarctic fast ice bottom algal community. Aquat Microb Ecol **21**: 177-185

Mizoguchi T, Irie K, Hirayama T, Hayashida N, Yamaguchi-Shinozaki K, Matsumoto K, Shinozaki K (1996) A gene encoding a mitogen-activated protein kinase is induced simultaneously with genes for a mitogen-activated protein kinase and an S6 ribosomal protein kinase by touch, cold, and water stress in Arabidopsis thaliana. Proc Natl Acad Sci **93**: 765-769

Mock T, Gradinger R (1999) Determination of Arctic ice algal production with a new *in situ* incubation technique. Mar Ecol Prog Ser **177**: 15-26

Mock T, Kroon BMA (2002) Photosynthetic energy conversion under extreme conditions-II: the significance of lipids under light limited growth in Antarctic sea ice diatoms. Phytochem **61**: 53-60

Mock T (2002) *In situ* primary production in young Antarctic sea ice. Hydrobiol **470**: 127-132

Moulin P, Crepineau F, Kloareg B, Boyen C (1999) Isolation and characterisation of six cDNAs involved in carbon metabolism in *Laminaria digitata* (Phaeophyta). J Phycol **35**: 1237-1245

Nichols PD, Palmisano AC, Smith GA, White DC (1986) Lipids of the Antarctic sea ice diatom Nitzschia cylindrus. Phytochem **25**(7): 1649-1653

Nishiyama Y, Los DA, Murata N (1999) PsbU, a protein associated with photosystem II, is required for the acquisition of cellular thermotolerance in Synechococcus species PCC 7002. Plant Physiol **120**: 301-308

Ohta H, Okumura A, Okuyama S, Akiyama A, Iwai M, Yoshihara S, Shen JR, Kamo M, Enami I (1999) Cloning, expression of the *psbU* gene, and functional studies of the recombinant 12-kDa protein of photosystem II from a red alga *Cyanidium caldarium*. Biochem Biophys Res Commun **260**(1): 245-250

Quillfeld CHv (1997) Distribution of diatoms in the Northeast Water Polynia, Greenland. J Mar Syst **10**: 211-240

Russel NJ (1998) Molecular adaptations in psychropilic bacteria: potential for biotechnological applications. Adv Biochem Eng Biotechnol **61**: 1-21

Sabehat A, Weiss D, Lurie S (1996) The correlation between heat-shock protein accumulation and persistence and chilling tolerance in tomato fruit. Plant Physiol **110**(2): 531-537

Sakamoto T, Shen G, Higashi S, Murata N, Bryant DA (1998) Alteration of low-temperature susceptibility of the cyanobacterium Synechococcus sp. PCC 7002 by genetic manipulation of membrane lipid unsaturation. Arch Microbiol **169**(1): 20-28

Scala S, Carels N, Falciatore A, Chiusano ML, Bowler C (2002) Genome properties of the diatom *Phaeodactylum tricornutum*. Plant Physiol **129**: 993-1002

Seki M, Narusaka M, Abe H, Kasuga M, Yamaguchi-Shinozaki K, Carninci P, Hayashizaki Y, Shinozaki K (2001) Monitoring the expression pattern of 1300 Arabidopsis genes under drought and cold stresses by using a full-length cDNA microarray. Plant Cell **13**: 61-72

Stitt M, Hurry V (2002) A plant for all seasons: alterations in photosynthetic carbon metabolism during cold acclimation in *Arabidopsis*. Curr Opin Plant Biol **5**: 199-206

Tahitiharju S, Palva T (2001) Antisense inhibition of protein phosphatase 2C accelerates cold acclimation in Arabidopsis thaliana. Plant J **26**(4): 461-470

Trenerry LJ, McMinn A, Ryan KG (2002) In situ oxygen microelectrode measurements of the bottom-ice algal production in McMurdo Sound, Antarctica. Polar Biol **25**: 72-80

Thomas DN, Dieckmann GS (2002) Antarctic Sea ice – a habitat for extremophiles. Science **295**: 641-644

Thomas T, Cavicchioli R (2002) Cold adaptation of archaeal elongation factor 2 (EF-2) proteins. Curr Protein Pept Sci **3**(2): 223-230

Thomashow MF (1998) Role of cold-responsive genes in plant freezing tolerance. Plant Physiol **118**: 1-7

Thomashow MF (2001) So what´s new in the field of plant cold acclimation? Lots! Plant Physiol **125**: 89-93

Valentin K, Cattolico RA, Zetsche K (1992) Phylogenetic origin of the plastids. *In*: RA Lewin, ed, Origins of plastids, Chapman Hall, New York, pp 193-222

Zecchinon L, Claverie P, Collins T, D´Amico G, Delille D, Feller G, Georlette D, Gratia Emmanuelle, Hoyoux A, Meuwis MA, Sonan G, Gerday C (2001) Did psychrophilic enzymes really win the challenge? Extremophiles **5**: 313-321

FIGURES AND TABLE

Table I. *Cold acclimation related proteins in F. cylindurs*

Protein	Function	Reference for cold acclimation
aconitase	catalyses the stereo-specific isomerisation of citrate to isocitrate via aconitate in the TCA-cycle	Lottering & Streips 1995
cold acclimation protein (CAP 160)	stabilisation of supramolecular structures such as membranes, ribosomes or cytoskeletal elements	Kaye et al. 1998
HSP70	molecular chaperon	Sabehat et al. 1996
delta-12-desaturase	desaturation of membrane lipids	Sakamoto et al. 1998
elongation factor TS (no.1)	protein translation at the ribosomes	Thomas & Cavicchioli 2002
elongation factor TS (no.2)		
receptor protein kinase	signal transduction	Mizoguchi et al. 1996
phosphoprotein phosphatase	phosphorylation of proteins	Tahtiharju & Palva 2001
disease resistant protein (no.1)	pathogen defence related proteins	Hon et al. 1995
disease resistant protein (no.2)		

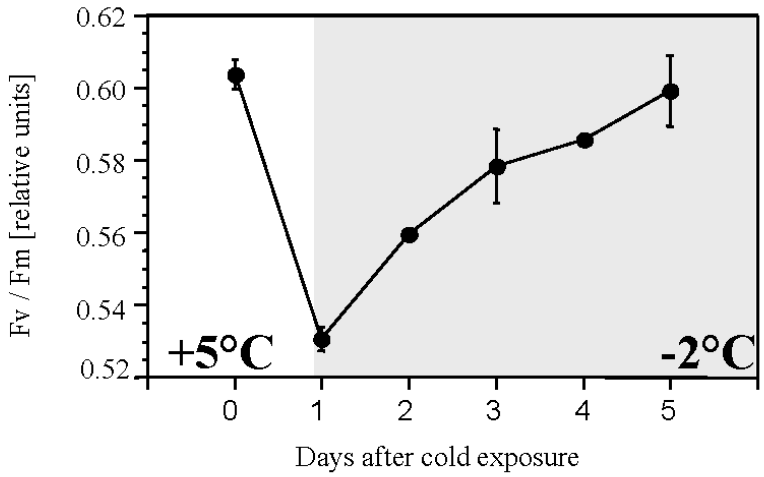

Fig. 1 Temporal development of quantum yield (Fm/Fm) after cold exposure to -2°C at day 0. Measurements were conducted once a day in the middle of the light phase (8h after switch on the light); n = 5; Error bars denote standard deviations

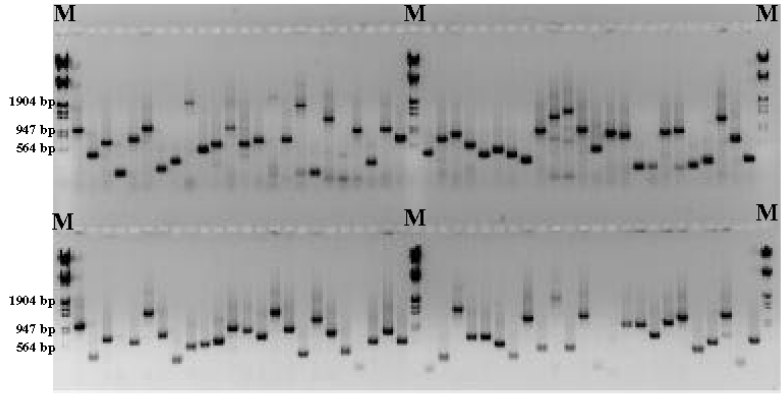

Fig. 2. PCR-screening of 96 recombinant EST clones. Insert sizes ranged from 400 to more than 1900 bp. Inserts larger than 564 bp were used for sequencing. M = Marker (base pairs)

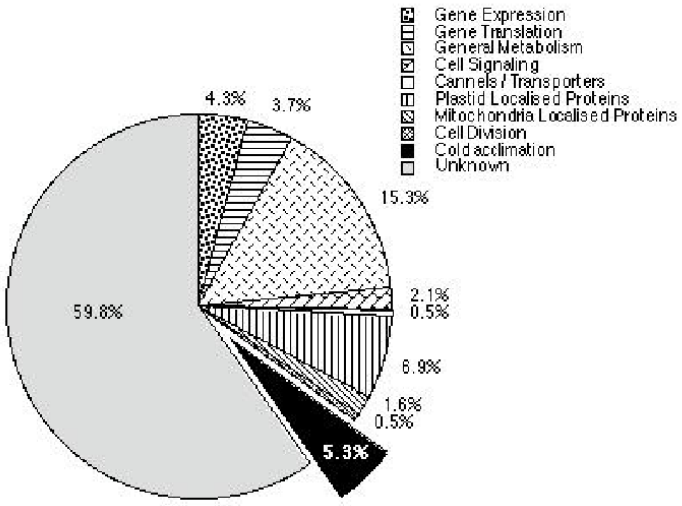

Fig. 3 Functional classification of derived coding sequences from *F. cylindrus* (ESTs in %). The nonredundant BLASTX contigs shown in Table II (Supplementary Information at http://www.awi-bremerhaven./XXX) were classified manually into different functional groups shown.

Table II Supplementary Information: BLASTX contigs

Nr	internal name	size/bp	redundancy	polyA	gene end	best hit	score	comments
1	2f fw	316	1	X		none		seq too short?
2	B2 fw	272	1	X		none		seq too short?
3	A12 fw	77	1	X		none		seq too short?
4	A5 fw	237	1	X		none		seq too short?
5	A11rev	392	2	X		none		seq too short?
6	Cox3-2 up	260	1		Y	lactam utilization protein	45/84	
7	Cox3-11up	206	1			cox1		
xxx	Cox3-9up	282	1			none		not from library, not counted
9	L4rp	464	4			none		
xxx	8t	922	24	X		18s rDNA		contamination - not counted for library
11	29	316	2	X		none		seq too short?
12	9p2	423	2	X		none		
13	L1up	450	4			none		
14	L5 up	469	3			none		
15	L8 up	449	3			none		
16	1g fw	778	12	X		none		
17	1d fw	424	3	X		Zn binding protein gene end	43/41	
18	2d fw	513	1	X		none		
19	3b fw	491	1	X		none		
20	4v fw	619	4	X		none		
21	4l fw	589	2	X		fcp		
22	5a fw	808	1	X		none		
23	5h fw	490	2			none		
24	5w fw	735	1	X		Vitellogenin precursor, egg protein	145	unlikely
25	A10up	1123	2	X		none		
26	A3rp	738	4			psbA	1251	
27	A7 up	884	1	X		none		
28	B1 fw	887	1	X	Y	U6 snRNA-associated Sm-like protein LSm3	59/88	full gene
29	Cox3-8 up	447	1			none		
30	5l rev	466	2	X		none		
31	EST6	552	1	X		Peptidyl-prolyl cis-trans isomerase C2		
32	D56	694	3	(X)	Y	hypothetical alpha purple protein	139	mt protein?
33	7a	549	1			fcp		
34	7c	550	1			none		
35	7e	550	1			none		
36	7f	457	1	X		SAM1, S-adenosylmethiionin synthetase	33/135	gene end
37	7j	550	1			putative mitochondrial matrix protein	44/103	
38	8a	576	1			none		
39	8alpha	549	1			Receptor kinase/disease res. Protein	36/152	cold acclimation
40	8b	550	1			hypoth. Prot. Plasm. Yoellii	76/74	frame shift
41	8d	548	1			ypothetical protein C0415c P. falc.	38/84	
42	8e	456	1	X		Omega 6 desturase	50/73	cold acclimation
43	8i	549	1			putative calcium protein kinase	26/130	
44	8m	547	1			none		
45	8p	747	2			none		
46	8w	549	1		Y	IMP-GMP specific 5'-nucleotidase	33/160	purine nucleotide degradation
47	8z5	548	1			none		
48	10	538	1			none		
49	12	544	1			none		
50	13	538	1			none		
51	1	475	2	X		Membrane subunit of LPS efflux transporter	66/233	only bacterial hits
52	22	388	1	X		none		
53	23	540	1			none		
54	27	527	1	X		none		

Nr	internal name	size/bp	redundancy	polyA	gene end	best hit	score	comments
55	28	294	1	X		fcp, gene end	75/44	
56	33	542	1		Y	Translation elongation factor 3A	47/122	cold acclimation, protein translation
57	37	538	1			putative cell adhesion protein Sym32	32/106	
58	41	548	1			Cold induced protein 160 spinach	32/89	cold acclimation
59	5	519	1	X		none		
60	6	535	1		Y	ADP ribosylation factor	75/80	elicitor response in rice
61	7	367	1	X		none		
62	9f	720	3	X	Y	rpl2 bacterial & rps19	44/139	mitochondrial DNA piece
63	9h	397	1	X		none		seq too short?
64	9m	471	1	X		none		
65	9p1	539	1			hypothetical yeast protein SPBC16D10.01C	26/171	
66	9T	525	1			possible isocitrate dehydrogenase	36/49	mt protein
67	9v	517	1			none		
68	9w	493	1			none		
69	D10	420	1	X		none		
70	D16	450	1			ORF148 o.sin pt	44/79	plastid DNA?
71	D1	342	1			none		
72	D21	451	1	X		Adenylosuccinat sythetase	46/86	de novo adenylat synthesis
73	D25	542	1			none		
74	4f rev	386	1	X		none		
75	D31	518	1	X		none		
76	D33	512	1	X		putative NADPH-flavin oxidoreductase	30/75	gene end
77	D34	511	1			7alpha-cephem-methyloxidase	42/136	best hit to bacteria
78	D39	542	1			none		
79	D42	495	1	X		none		
80	D43	541	1			none		
81	D48	546	1			none		
82	D4	539	1			Homoserine dehydrogenase	27/116	bacterial hits
83	D52	538	1		Y	Dead/deah helicase	46/151	
84	D54	542	1			peroxysomal protein	35/116	stress induced in yeast
85	D55	475	1	X		none		
86	D58	466	1	X		none		
87	D70	544	1			none		
88	D71	544	1	Y		Homeobox protein	44/170	
89	D73	547	1			rpl13a, cytosolic	55/94	
90	D74	548	1			none		
91	D79	459	1			none		
92	D88	544	1	X		none		
93	D8	550	1			none		
94	D93	543	1			none		
95	D95	543	1			Vacuolar sorting receptor	36/131	prot transp from golgi to vacuole
96	D9	544	1		Y	Calpain protease	32/173	
97	8R	310	1	X		none		
98	L11 rp	451	0.5			rbcL	100%	plastid DNA
99	L11 up	471	0.5			rbcl	100%	plastid DNA
xxx	Cox2-8 up	309	1			none		not from library, not counted
101	Cox3-10 up	362	1			cox1	74/119	
102	cox3-12 up	542	1			none		
103	empty							not counted
104	4q fw	551	0.5	4qr	Y	Beta glucan binding, elicitor	35/167	
105	4q rev	463	0.5	X	Y	none		
106	5p fw	513	0.5			S1 RNA bd domain	27/111	
107	5p rev	462	0.5	X		none		
108	5v fw	525	1			none		
109	6a	445	1	X		none		
110	6e	648	1			Pumilio RNA bd protein	44/196	
111	6g	406	1	X		potentially hsp70, gene end	44/38	cold acclimation
112	A6up	356	1	X		none		
113	Do2	459	1			Succinate dehydrogenase	75/81	prob. mitochondrial gene
114	EST 10	550	1			Glycoprotein, ATP bd domain	41/117	
115	EST 11	544	1			none		
116	EST 13	550	1			none		

Nr	internal name	size/bp	redundancy	polyA	gene end	best hit	score	comments
117	EST 14	550	1		Y	rps3 cytoplasm.	73/126	
118	Est 15	550	1			none		
119	Est 16	550	1			Hypothetical A. thal protein	33/112	
120	EST 17	550	1			none		
121	Est 18	547	1			none		
122	Est 19	550	1			none		
123	EST 1	524	1			none		
124	Est 20	550	1			gapC1	91/174	plastid protein
125	Est 22	550	1			rpl10 cytoplasmatic	56/113	
126	Est 23	550	1			none		
127	Est 24	550	1			none		
128	Est 25	550	1			none		
129	EST 26	550	1			possible cytosin 5 methyltransferase	30/82	generally weakly conserved
130	EST 27	550	1			none		
131	Est 28	550	1			nuclear GTPase	35/142	
132	Est 29	550	1			none		
133	EST 30	550	1			Acetyl CoA carbocylase, nu gene, pt protein	68/73	probable plastid protein
134	Est 31	550	1			none		
135	EST 32	550	1			none		
136	EST 33	550	1			CDK5 activator protein, kinase	58/166	
137	Est 34	550	1			UDP galactose transporter, euc.	47/140	protein galactosylation in the golgi?
138	Est 37	550	1			none		
139	EST 38	550	1		Y	Phosphoribosylpyrophosphate synthetase	48/143	nucleotid sythsesis
140	EST 39	550	1			none		
141	Est 40	550	1			none		
142	Est 43	550	1			none		
143	EST45	550	1			Translation elongation factor 3e, eucaryotic	42/107	cold acclimation protein translation
144	EST 46	550	1			none		
145	EST 48	550	1			tufA, gene start, short overlap	67/28	pt encoded in non green algae
146	Est 49	550	1		Y	Neuroglobin, bacterial hemoglobin	33/101	Oxygen metabolisms
147	Est 4	550	1			none		
148	Est 50	550	1			none		
149	Est 51	550	1			Lectin domain???	30/86	
150	EST 52	650	1		Y	phosphoglycerate kinase	75/201	organellar gene (plastid?)
151	EST 53	638	1			none		
152	Est 54	651	1			none		
153	Est 55	649	1			Ubiquitin-activating enzyme E1	50/161	eucaryotic
154	Est 56	649	1			similar to histon H1 and other K-rich prot.	33/107	Lysin rich
155	Est 57	595	1	X		none		
156	Est 58	594	1			none		
157	Est 59	650	1			none		
158	Est 5	550	1			none		
159	EST 60	650	1			ftsH, plastid protein	60/155	should be pt-encoded
160	Est 61	650	1			nonclathrin coat protein zeta2-COP	33/113	
161	Est 62	650	1			none		
162	Est 63	594	1			none		
163	Est 65	650	1			cell division cycle protein 48	36/166	most similar to G.theta nucleomorph
164	EST 66	650	1			none		
165	EST 67	650	1			none		
166	EST 68	650	1			none		
167	EST 69	219	1			none		
168	Est 70	650	1			hypersensitive-induced response protein	64/78	plant (64%) and bacterial (57%) hits
169	Est 71	615	1	X		none		
170	Est 72	637	1			formate dehydrogenase	34/96	growth on formate
171	Est 73	650	1			none		
172	EST 74	650	1			rps2, cytoplasmatic	73/130	
173	EST 76	560	1			none		
174	Est 77	650	1			Adenylsulfate reductase, pt protein	33/109	plastid protein
175	Est 78	650	1			prolyl tRNA synthetase	35/174	gene end
176	Est 79	650	1			possible phophodiesterase	27/150	
177	EST 7	550	1			none		

Nr	internal name	size/bp	redundancy	polyA	gene end	best hit	score	comments
178	EST 80	650	1			none		
179	Est 82	650	1			putative aldo/keto reductase	51/68	gene end
180	EST 83	650	1			none		
181	Est 84	650	1			disease resistance protein	39/167	only plant hits, cold acclimation
182	EST 86	650	1			none		
183	Est 87	477	1			phosphoprotein phosphatase	34/59	cold stress gene
184	Est 88	503	1			aconitate hydratase 2	70/123	cold stress gene, only bact. Hits
185	EST 89	607	1			none		
186	EST 8	527	1			none		
187	EST 90	650	1			none		
188	Est 91	650	1			none		
189	EST 92	650	1			none		
190	EST 93	356	1			psbU	51/120	red algal - gene transfer

Molecular cold acclimation in the polar diatom *Fragilariopsis cylindrus* - requirement for low light at low temperatures

Thomas Mock[1]*, Klaus Valentin[1]

[1]Alfred-Wegener-Institute for Polar and Marine Research, Am Handelshafen 12, 27570 Bremerhaven, Germany, [1]*email: tmock@awi-bremerhaven.de

Fragilariopsis cylindrus (Bacillariophyceae) is an important primary producer in Arctic and Antarctic sea ice. We used this diatom as a model organism to study cold acclimation during cooling from +5°C to the freezing point of sea water (ca. -1.8°C) at two different light intensities (35 and 3 µmol photons $m^{-2}s^{-1}$). At -1.8°C and 35 µmol photons $m^{-2}s^{-1}$, growth ceased and cold shock photoinhibition was induced. Rapid increase in expression of a RNA-helicase indicated changes in RNA structure and subsequent expression of elongation factors was necessary for enhanced protein translation. Protein synthesis resulted in an increased demand of chaperons as HSP 70 was strongly up-regulated. Induction of a chloroplast protease (FtsH) indicated enhanced protein turnover in the plastids. New proteins are apparently used to replace photo damaged thylakoid proteins in order to recover photosynthesis. In contrast, cold exposure at 3µmol photons $m^{-2}s^{-1}$ induced low light acclimation without expression of chaperons and genes involved in protein synthesis. The proportion of absorbed energy utilised for growth is therefore higher under extreme low light because there is neither photo damage nor cold shock. Consequently, at freezing temperatures maximum photosynthesis in *F. cylindrus* is reduced by photo damage of proteins already at moderate light intensities.

It is still unknown how polar diatoms regulate their growth on a molecular level. Hence, there is a need to understand how these diatoms survive in the most climate-sensitive ecosystems on earth and how they react to changes in environmental conditions. We selected *Fragilariopsis cylindrus* isolated from Antarctic sea ice as a model organism to study the molecular basis for cold acclimation, because this diatom is a bipolar species and lives in both open waters and sea ice with a preference for the latter (*1,2*). Paleooceanographers, therefore, have used *F. cylindrus* and its sediment record to evaluate glacial / interglacial developed through the Neogene but also past climate changes in general (*3*). Its maximum temperature for survival is +8°C, making this diatom an obligate psychrophilic photoautotroph (*4*). Optimal growth is at +5°C, 35 µmol photons $m^{-2}s^{-1}$ and a light-dark cycle of 16:8h, respectively. Its growth rate under these conditions is 0.72 divisions per day, which is never attained in its natural habitat where temperatures are lower. When transferred from optimal growth temperatures to the freezing point of sea water (approx. -1.8°C at 34 PSU) *F. cylindrus* expresses a comparably high number of potential cold stress-related genes as shown by an EST analysis (*5*). We used a subset of genes from the EST analysis and cloned additional relevant genes to study the molecular acclimation of *F. cylindrus* to simulated freezing at unchanged light intensity (35 µmol photons $m^{-2}s^{-1}$), and extreme low light intensity (3 µmol photons $m^{-2}s^{-1}$) and compared the results to optimal growth conditions (35 µmol photons $m^{-2}s^{-1}$ at +5°C) using macro-array technology (*6*). Gene expression studies were paralleled by biophysical and biochemical investigations relevant for photosynthesis (*7*).

At 35 µmol photons $m^{-2}s^{-1}$ temperature reduction to -1.8°C halted growth (fig. 1) by cold shock photoinhibition during the first hours after cold exposure (fig. 2). A reduction in efficiency of energy transfer at this rather moderate light intensity from the light-harvesting complex to PS II reaction center was indicated by decreasing Fv/Fm and connectivity between PS II reaction centres. Electron transport rates between primary (Q_A) and secondary electron acceptor (Q_B) were simultaneously reduced during the first hours after cold exposure (fig. 2).

Temperature reduction in combination with decreasing light intensity (3 µmol photons $m^{-2}s^{-1}$) did not initiate cold shock photoinhibition, but rather low light acclimation with increased fucoxanthin synthesis. Therefore improved connectivity between PS II reaction centers was obtained as compared to cold exposure under unchanged light intensities (35 µmol photons m^{-}

$^{2}s^{-1}$). Electron transport rates at 3µmol photons $m^{-2}s^{-1}$ between Q_A and Q_B were faster during the first hours after cold exposure (fig.2), whereas Fv/Fm remained similar to the control.

The first molecular response in *F. cylindrus* was most marked under unchanged light intensity (35 µmol photons $m^{-2}s^{-1}$) and was characterised by transient strong changes in gene expression of which the most pronounced were related to chaperon gene expression and dynamic photoinhibition of photosystem II (PSII) (fig. 3). This was partly because the lowering of temperature generally reduces reaction rates ("Q10 rule") and can therefore limit the sinks for the absorbed excitation energy, in particular CO_2 fixation (*8*). Smaller sinks for the absorbed excitation energy increase the redox state of PS II and thus oxidative damage, notably to the D1 component at the core of PS II (*9*). Steady state mRNA levels of psbA, psbU, the light harvesting complex (LHC) genes, psbC, and the fucoxanthin/chlorophyll a binding proteins (fcp) decreased in *F. cylindrus* during cold shock, indicating a transcriptional down-regulation of PS II reaction centre and light harvesting (fig. 4). Thus down-regulation of photosynthesis seems to be a mechanism of photoprotection in *F. cylindrus*. Increasing concentrations of the pigment diatoxanthin (fig 2) may further increase the energy dissipation as heat and fluorescence (*10*). CO_2 - fixation was possibly reduced during cold shock, revealed by down-regulation of RUBISCO large subunit (rbcL) under constant light and reduced light intensity. Down-regulation of psbA and psbC was also observed at reduced light intensities indicating that the effect on these genes was mainly triggered by temperature. In contrast, fcp and psbU were transiently up-regulated at low light intensities probably in order to improve light harvesting and probably to stabilise the water splitting complex at PS II (*11*).

Cold shock photoinhibition in *F. cylindrus,* initiated at 35 µmol photons $m^{-2}s^{-1}$ and the freezing point of sea water, was also accompanied by changes in protein metabolism, indicated by transient up-regulation of genes responsible for transcription, translation, and amino acid- and protein synthesis and folding, as well as for protein transport and storage. Therefore, enhanced protein turnover and changes in protein conformation seems to be the molecular consequence of cold shock photoinhibition in *F. cylindrus*. The first response after cold exposure was an up-regulation of the DEAD/DEAH box RNA helicase, elongation factor TS and a GTPase (fig. 4). RNA helicases catalyse the unwinding of RNA duplexes in an ATP-dependent manner. They are implicated in reorganisation of RNA structure, such as transcription, mRNA splicing and translation initiation (*12*). Translation requires binding of mRNA and ribosomal subunits to a complex of a specific tRNA-Initiation factor (IF 1- 3).

Other aminoacyl-tRNAs (aa-tRNA) are bound to the ribosome by elongation factors (EF-Tu, Ts). They are central in the process of protein biosynthesis (*13*). The programmed ribosome stimulates GTP hydrolysis, and the complex EF-Tu-GDP leaves the ribosome. The elongation-factor Ts (EF-Ts) catalyses the exchange of GTP for GDP. The GTPase activity of some, but not all, members of the GTPase superfamily can be enhanced by GTPase activating enzymes, one of which was transiently expressed after cold shock in *F. cylindrus*. Enhanced reorganisation of mRNAs by DEAD/DEAH box RNA helicases, of which some also have chaperon functions (*14*), possibly were used to translate new proteins as a first response after cold exposure in *F. cylindrus*.

The second molecular response after translation initiation was the up-regulation of genes responsible for synthesis of amino acids (fig. 4). An example is phosphoribosyl-pyrophosphatase, known as a stress response gene in yeast (*15*). In bacteria and lower eukaryotes this enzyme hydrolyses 5-phosphoribosyl 1-pyrophosphate (PRPP), a precursor for histidine and tryptophan biosynthesis (*16*). Also the chaperon HSP 70 was transiently up-regulated 5-fold only under unchanged light intensity with a delay of a few hours after cold exposure, again indicating enhanced synthesis of proteins. One reason for this could have been an increased protein turnover within the chloroplast (e.g. repair damaged thylakoid proteins). The chloroplast FtsH protease for instance, known to degrade photo-damaged PS II reaction centre D1 protein (*17*), remained strongly up-regulated after cold exposure at 35 µmol photons $m^{-2}s^{-1}$. In summary enhanced transcription of genes involved in protein synthesis obviously resulted in reconstitution of thylakoid proteins. Quantum yield and electron transport recovered as a result of these processes (fig. 2).

At the end of acclimation, the mRNA of a vacuolar-sorting receptor is 4-fold up-regulated under both light intensities (fig. 4). Vacuolar-sorting-receptors select proteins at the Golgi-apparatus for sorting to clathrin-coated vesicles and delivery to the vacuole (*18*). Protein synthesis in *F. cylindrus* was thus possibly accompanied by a selection of specific proteins and their storage or at least transport to prevacuoles before increasing growth under new acclimated conditions. These proteins seem to have a function for cold acclimation, e.g., for osmoregulation. Osmoregulatory substances are often stored in vacuoles to avoid dehydration caused by increasing salinities in brine during freezing of sea water (*19*). Diatoms have a large central vacuole where it is likely that the osmoregulatory substances could be stored.

This process in *F. cylindrus* seems to be light independent because vacuolar-sorting receptors were expressed at the same level under both light intensities.

Reconstituted growth after acclimation, i.e. long-term acclimation, at the freezing point of sea water and 35 µmol photons $m^{-2}s^{-1}$ seems to require additional continuous synthesis of diatoxanthin, a pigment for excitation energy dissipation (*7*) and up-regulation of the PS II gene psbU, which stabilises the water splitting complex. PsbU is only known from cyanobacteria, red algae, and diatoms (*8*).

No obvious effect was observed for respiration regulation as cytochrome oxidase I (COXI) gene was generally expressed at a low level, and no further reduction of expression could be detected by temperature decrease to the freezing point of sea water under both light intensities. Mitochondrial respiration has been proposed to be reduced in cold living algae by low temperatures through the Q10 rule, increasing the proportion of anabolic processes and thus energy utilisation for growth (*20*).

Our study reveals that low temperatures in combination with low incident irradiances, such as 3 µmol photons $m^{-2}s^{-1}$, prevented photoinhibition but a cold shock response was not completely suppressed (fig. 4). The up-regulation of the DEAD/DEAH box RNA helicase was in the same order of magnitude under extreme low light intensity as under 35µmol photons $m^{-2}s^{-1}$. An elongation factor TS and a GTPase were rapidly up-regulated but back on control level after 9 h. A reorganisation of mRNAs seemingly was used to translate new proteins as a first response regardless of light intensities. In addition to this basic cold shock response, protein synthesis was of increasing importance whenever light intensity increased and temperature remained constantly low. The permanent up-regulation of two elongation-factors (TS) provided unequivocal evidence of enhanced translation at - 1.8°C and 35 µmol photons $m^{-2}s^{-1}$ compared to -1.8°C and 3 µmol photons $m^{-2}s^{-1}$. Light stress conditions (even at 35 µmol photons $m^{-2}s^{-1}$) at the freezing point of sea water, require differentiated repair mechanisms in *F. cylindrus*, which are costly. The higher the light intensity the lower the proportion of energy that can be utilised for growth. Maximum photosynthesis (Pmax) is therefore reduced by photo damage at sub-optimal growth temperatures and probably also by reduced CO_2-fixation.

References and Notes

1. sS.H. Kang, G.A. Fryxell, *Polar Biol.* **12**, 609 (1992)
2. C.H.v. Quillfeld, *J. Mar. Syst.* **10**, 211 (1997)
3. A. Leventer, in Antarctic Sea Ice, Biological Processes, Interactions and Variability, M.P. Lizotte, K.R. Arrigo, Eds. (American Geophysical Union, Washington DC, USA, 1998), pp. 121-137
4. M. Fiala, L. Oriol, *Polar. Biol.* **10**, 629 (1990)
5. T. Mock, K. Valentin, submitted
6. Total RNA was isolated using the RNAqueous Kit according to the manufacturers instructions (Ambion) and used for the labeling reaction. Radioactive labeled cDNA probes were prepared from the total RNA pool by direct incorporation of $dCTP^{32}$ during the first-strand reverse transcriptase reaction using the EndoFree RT Kit (Ambion). Reverse transcription was performed at 42°C for 1h using anchord oligo dT and random decamer primers (Ambion). Unincorporated radioactive nucleotides were removed using 200bp spin columns (Amersham). Macro-arrays were composed of 44 genes. Gene specific oligonucleotides (50mer) were obtained by Operon Inc. and spotted (one spot for each gene) with a slot-blot-spotting-device (Biorad) on nylon-membranes (Amersham). Hybridisation was conducted with ULTRAarray hybridisation buffer according to the manufacturers instruction (Ambion) as well as washing of membranes. At least 3 replicate hybridisations were performed for each macro-array. The arrays were scanned with a FujiFilm Fluorescent Image Analyzer FLA-3000. Data analyses were performed using Aida software. The raw data were normalised to the average intensity of ribosomal genes 30S and 40S. Negative control and array background was substracted.
7. In vivo quantum yield (Fv/Fm) was determined using a Xenon-Pam Fluorometer (Walz) equipped with a stirrer and a cooling device whereas DCMU and reoxidation measurements were performed with a Dual-Modulation LED Kinetic Fluorometer. Connectivity between PS II reaction centers and electron transport rates were calculated according to T. Mock, B.M.A. Kroon, *Phytochem.*, **61**, 41 (2002) as well as the determination of pigment composition.
8. N.P.A. Huner, G. Öquist, F. Sarhan, *Trends Plant Sci.*, **3**, 224 (1998)
9. E.M. Aro, I. Virgin, B. Andresson, *Biochim. Biophys. Acta*, **1143**, 113 (1993)
10. J. Lavaud, B. Rousseau, H.J. van Gorkom, A-L Etienne, *Plant Physiol.*, **129**, 3, 1398 (2002)
11. Y. Nishiyama, D.A. Los, N. Murata, *Plant Physiol.*, **120**, 301 (1999)
12. J. de la Cruz, D. Kressler, P. Linder, *Trends Biochem. Sci.*, **24**, 192 (1999)
13. J. Nyborg, M. Kjeldgaard, *Curr. Opin. Biotechnol.*, **7**, 369 (1996)
14. S. Mohr, J.M. Stryker, A.M. Lambowitz, *Cell*, **109**, 769 (2002)
15. E. Dubois, B. Scherens, F. Vierendeels, M.M. Ho, F. Messenguy, S.B. Shears, *J. Biol. Chem.*, **277**, 23755 (2002)
16. K. Fujimori, O. Daisaku, *Plant Physiol.*, **118**, 275 (1998)
17. Z. Adam, A.K. Clarke, *Trends Plant Sci.*, **7**, 10, 451 (2002)
18. T. Kirsch, N. Paris, J.M. Butler, L. Beevers, J.C. Rogers, *Proc. Natl. Acad. Sci.*, **91**, 8, 3403 (1994)
19. L. Xiong, J.K. Zhu, *Plant Cell Environm.*, **25**, 131 (2002)
20. J.A. Raven, A.M. Johnston, J.E. Kubler, R. Korb, S.G. McInroy, L.L. Handley, C.M. Scrimgeour, D.I. Walker, J. Beardall, M.N. Clayton, M. Vanderklift, S. Fredriksen, K.H. Dunton, *Ann. Bot.*, **90**, 525 (2002)

21. We wish to thank Linda Medlin for providing lab space and generous support, Niko Hoch, Andreas Krell, Erika Allhusen and Gerhard Dieckmann for their helpful collaboration in the lab. We thank V. Smetacek for his advice.

Figures

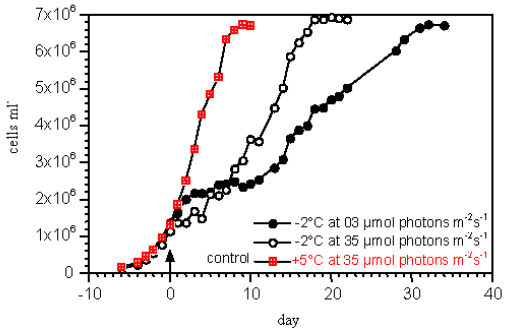

Fig. 1. Temporal development of *Fragilariopsis cylindus* cell concentrations in 3 aerated batch cultures at +5°C and 35 µmol photons $m^{-2}s^{-1}$ under a light-dark cycle of 18:6h. Two cultures were chilled at day 0 (end of dark period - arrow) to -2°C under either unchanged irradiance level or reduced light intensity at 3 µmol photons $m^{-2}s^{-1}$. Mid exponential growth phase samples of the untreated culture (+5°C and 35 µmol photons m^{-2} s^{-1}) from day 0 to 2 were used (control) for comparison with treated cultures; n = 2

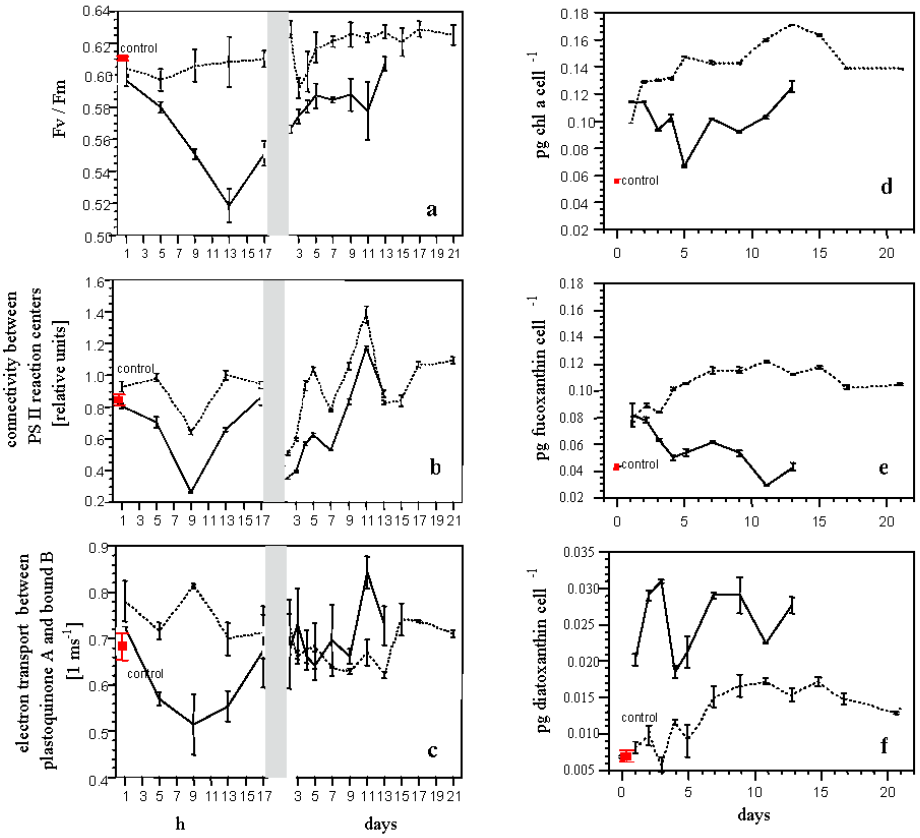

Fig. 2. Data are based on fluorescence induction (**a-c**) and on HPLC analyses (**d, e**). Temporal development of photosynthesis and pigment composition was measured during the light period (18h) from the first hour after cold exposure, during the acclimation phase and till the new acclimated growth (mid-exponential growth phase: day 13 for 35 µmol photons $m^{-2}s^{-1}$, day 21 for 3 µmol photons $m^{-2}s^{-1}$). Measurements at day 1 were conducted on a hourly basis, whereas measurements only once a day (mid-light period -9h light) were used at all subsequent days. Solid line represents -2°C and 35 µmol photons $m^{-2}s^{-1}$, dotted line -2°C and 3 µmol photons $m^{-2}s^{-1}$. The control (red) represents data, which were obtained from pooled measurements of the untreated culture (+5°C and 35 µmol photons $m^{-2}s^{-1}$) during the exponential growth. (**a**) Temporal development of quantum yield (Fv/Fm), (**b**) connectivity between PS II reaction center, (**c**) electron transport between first stable electron acceptor (plastoquinone A) and bound plastoquinone B (second stable electron acceptor), (**d**) pg chlorophyll *a* $cell^{-1}$,(**e**) pg fucoxanthin $cell^{-1}$, (**f**) pg diatoxanthin $cell^{-1}$; n = min. 5; error bars = ± SD

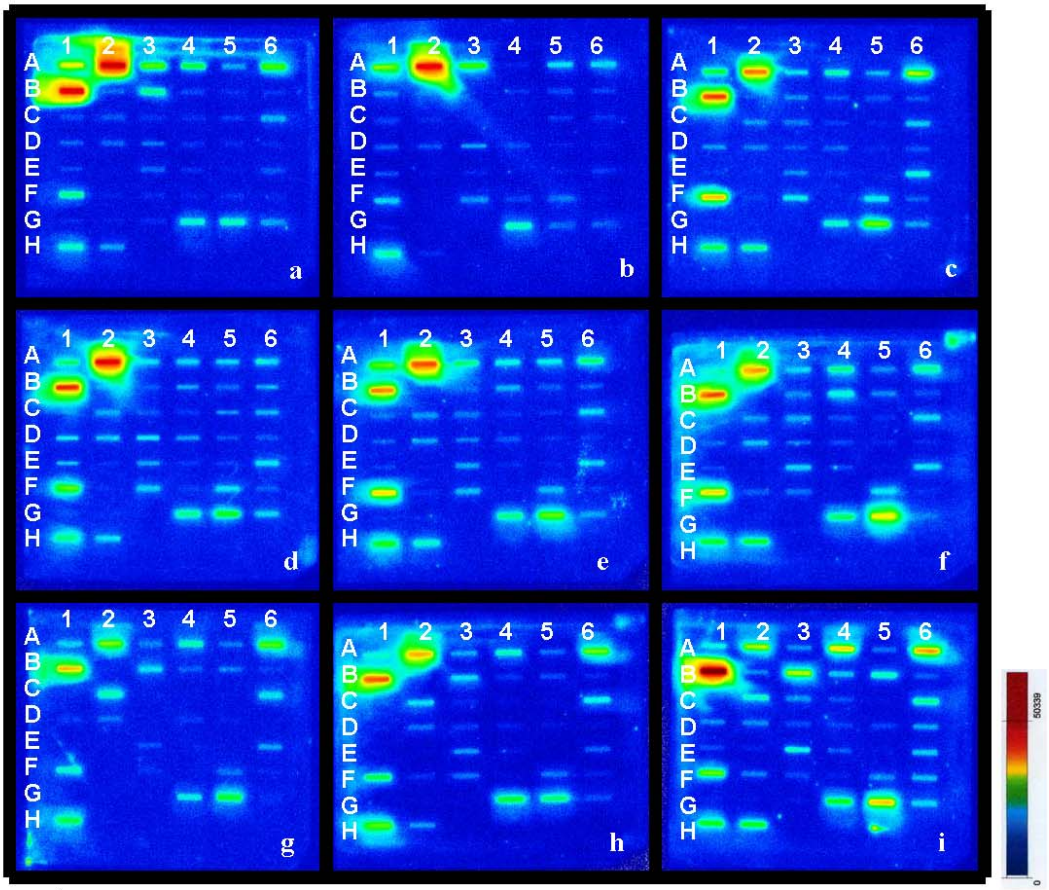

#

Fig. 3. Macroarrays (**a-i**) of which each is composed of 44 genes (A1-H2) spotted as oligonucleotides (50mer) in horizontal lines. Arrays were hybridised with $dCTP^{32}$-labeld cDNA and analysed with a FujiFilm Fluorescent Image Analyzer FLA-3000. (**a**) macro-array of the untreated culture (pooled samples from day 0 to 2; mid-light period -9h light; +5°C; 35 µmol photons $m^{-2}s^{-1}$) and (**b - i**) macro-arrays after cold exposure (end of dark period at day 0) to -2°C under unchanged light intensities: (b) 1 hour, (c) 9 hours and (d) 17 hours after cold exposure at day 1. (**e**) day 2, (**f**) day 3, (**g**) day 5, (**h**) day 7 and (**i**) day 13 during the mid-light period - 9h light.

Spotted Oligonucleotides:

A	1	rbcL	
	2	psbA	
	3	psbC	
	4	plastid orf 148	
	5	GAPDH	
B	1	fcp no. 1	
	2	fcp no. 2	
	3	fcp no. 3	
	4	vacuolar sorting rezeptor	
	5	FtsH protease	
	6	NADPH flavin oxidoreductase	
C	1	cytochrom-oxidase I (COX I)	
	2	cell division cycle protein	
	3	mitochondrial matrix protein precursor	
	4	UDP-galactose translocase	
	5	acetyl-coA-carboxylase	
	6	adenosylsulfatereductase	
D	1	delta 12 desaturase	
	2	phosphoglyceratkinase	
	3	disease resistant protein no. 1	
	4	DEAD/DEAH box RNA helicase	
	5	CAP 160	
	6	disease resistant protein no. 2	
E	1	Ca^{2+}-dependent protein kinase	
	2	hypersensitive induced protein	
	3	aconitat hydratase	
	4	phosphoproteinphosphatase	
	5	phosphodiesterase	
	6	phosphoribosylpyrophosphatase	
F	1	hsp70	
	2	pumilio MPT5	
	3	GTPase	
	4	oxidoreductase	
	5	elongation factor no. 1	
	6	elongation factor no. 2	
G	1	calpain protease	
	2	ubiquitin activating enzyme	
	3	ATP-binding protein	
	4	ribosomal protein 30 S	positive control
	5	ribosomal protein L 10	
	6	ribosomal protein 3 S	
H	1	ribosomal protein 40 S	positive control
	2	ribosomal protein L 20	
	3	*Escherichia coli* RNA	negative control

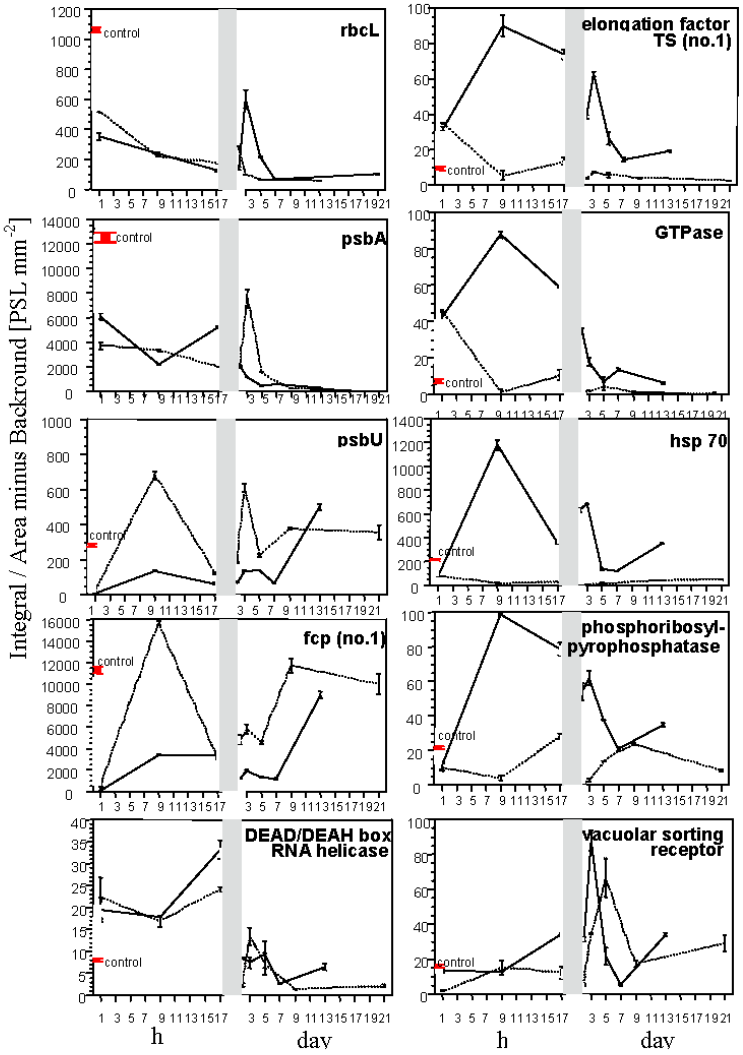

Fig. 4. Temporal development of steady state mRNA levels of selected genes from the macro-array analysis during the light period (18h) from the first hour after cold exposure (end of dark period at day 0), during the acclimation phase and till the new acclimated growth (mid-exponential growth phase: day 13 for 35 µmol photons $m^{-2}s^{-1}$, day 21 for 3 µmol photons $m^{-2}s^{-1}$). Measurements at day 1 were conducted on a hourly basis, whereas measurements only once a day (mid-light period -9h light) were used at all subsequent days. Solid line represents -2°C and 35 µmol photons $m^{-2}s^{-1}$, dotted line -2°C and 3 µmol photons $m^{-2}s^{-1}$. At least 3 replicates were conducted for each array, whereas data were normalised to averaged 30S and 40S ribosomal genes. Negative control on the array as well as array background was substracted. The control (red) represents data, which were obtained from pooled measurements of the untreated culture (+5°C and 35 µmol photons $m^{-2}s^{-1}$) during the exponential growth; n = 3; error bars = ± SD

4 DISCUSSION

Photosynthesis in Antarctic sea ice diatoms is probably not fundamentally different from that in temperate or even tropical autotrophic organisms. Basic molecular processes of light harvesting, electron generation and carbon fixation are highly conserved in all photoautotrophic organisms, despite extremely variable environmental conditions. Interestingly, also physiological responses such as cold shock photoinhibition, observed in temperate cyanobacteria and warm climate plants have been detected in obligate psychrophillic Antarctic diatoms (publication **7**). The requirement to cope with freezing temperatures evolved late in the evolution of photosynthesis. Photosynthesis originated by 2.500 Ma in cyanobacteria (Raymond et al. 2002) and first evidence of glaciation was 1000 Ma later during the Archaen. Thereafter several glaciations occurred in the Late-Proterozoic, Late-Ordovician, Permo-Carboniferous and the Cenozoic. Diatoms first appear in very small numbers in the Triassic (ca. 250 Ma before present) where no glaciation occurred (Holba et al. 1998, Medlin et al. 2000). Earliest evidence of the return to massive sea ice development was ca. 50 Ma before present (Cenozoic). Fifty Ma of cold exposure in diatom evolution versus 2.500 Ma of photosynthesis in cyanobacteria is a short time span for adaptation to low temperature conditions.

Mechanisms to cope with light stress developed earlier during the evolution of photosynthesis than mechanisms to cope with low temperatures. New models based on molecular data reveal that the original function of light harvesting complexes was not to collect light and to transfer the energy to the reaction centres but to disperse the absorbed light energy in the form of heat or fluorescence (Montane & Kloppstech 2000). These energy-dispersing proteins are believed to have originated in cyanobacteria. Early light-inducible and high light inducible proteins (ELIPs and HLIPs respectively) of phycobilisomes are the ancestors of light-harvesting complexes of higher plants. ELIPs first arose with a primary function in energy dispersion to protect photosynthetic pigments against photo-oxidation. Dissipation of light would have been the first constraint of photosynthetic ancestor cells, whereas the function as a tool for collecting light (LHC I and II families) was developed later in evolution. Causes may include decreasing light intensity by a denser atmosphere and clouds, changes in scalar irradiance or shading due to a denser plant vegetation (Rhynia). Effective light harvesting is

important particular in sea ice where the ice surface reflects more than 70 % of the incoming irradiance (Eicken 1992). However, for diatoms which evolved under warmer conditions, temperatures below the optimum for growth such as in sea ice mimics high light conditions again (publication **7**). Hence, dissipation of excess excitation energy seems to be as relevant under recent polar conditions as it was for the early ancestor growing under higher temperatures and higher irradiance. Mechanisms of excitation energy dissipation were developed during the evolution of light harvesting complexes. Examples are the xanthophyll cycle in algae (e.g. Lohr & Wilhelm 1999, Elrad et al. 2002) or state transitions in higher plants (Allen & Forsberg 2001). These mechanisms efficiently dissipate excitation energy under excessive light conditions. Formation of reactive oxygen species (ROS) caused by excessive light is reduced by the production of antioxidative enzymes (e.g. catalase) and during photorespiration (e.g. Aro et al. 1993, Schriek 2000, Padmasree et al. 2002). Catalases of low-temperatures intolerant plants are often light sensitive and photosynthesis in such plants is completely suppressed under low temperatures (e.g. Streb et al. 1999). The Antarctic ice diatom *Entomoneis kufferatii* in contrast shows high catalase activity under temperatures below 0°C and high light intensity. This indicates a cold-adapted and high light insensitive enzyme (Schriek 2000). Light insensitive repair mechanisms are also important in alpine plants, where strongly fluctuating light conditions are combined with low temperatures. Translational control mechanisms ensure that rates of repair can be rapidly adjusted to fluctuating light conditions (e.g. Streb et al. 1998).

Polar phytoplankton and especial sea ice algae in contrast are often subjected to temperatures below the freezing point of sea water regardless of light intensity (e.g. Kirst & Wiencke 1995, Boyd 2002). Strong scalar irradiance often occurs in the surface polar ocean and in the upper parts of sea ice during spring and summer. Thus, although scalar irradiance rises, temperatures remain constantly low in these polar aquatic habitats. Continuos synthesis of chaperons (e.g. HSP70) as observed in *Fragilariopsis cylindrus* (publication **7**) seems one important mechanism by which it cope their growth under such conditions. Expression of chaperons increased in *F. cylindrus* due to the decrease of temperature. Most extreme are the conditions existing in the upper parts of sea ice where the lowest temperatures occur in combination with high salinities and strong fluctuating scalar irradiance (e.g. Bartsch 1989, Stöcker et al.

2000, Thomas & Dieckmann 2002). Dinophytes are known to develop cysts under such conditions in order to avoid the stress conditions (Stöcker et al. 2000) However, metabolically active algae require catalase activity to detoxify ROS, which is produced under excessive light and low temperatures (Schriek 2000).

Molecular oxygen is often concentrated in gas bubbles in and under sea ice (e.g Tsurikov 1979). Optode measurements in undisturbed small brine channels or even pockets in upper layers of sea ice revealed a strong out-gasing of dissolved oxygen due to oversaturation (publication **2**). This is partly caused by diatom photosynthesis and physical entrapment of oxygen between the ice crystals during its formation. Photosynthesis measurements in newly formed Antarctic sea ice showed that algae still actively assimilate CO_2 with increasing chl *a* specific assimilation rate from bottom to top of the ice (publication **1**). Under this assumption growth should therefore be higher near the top of the ice (e.g. Geider et al. 1998). However, biomass in terms of chl *a* and cell counts revealed the opposite. Enhanced inorganic carbon assimilation in the top layers of sea ice was therefore possibly used for osmoregulation (e.g. proline and dimethylsulfoniopropionate (DMSP) synthesis) or ROS detoxification (catalase synthesis) and repair of damaged chloroplast proteins in order to sustain thylakoid structures (e.g. Davidson 1991, Xiong & Zhu 2002). Almost all of the incoming scalar energy is apparently used to overcome the damaging effect of cold shock photoinhibition, which is probably enhanced by increasing salinities (e.g. Bates & Cota 1986). Also excitation energy dissipation as heat possibly is a positive feedback mechanism by which the algae create "warm islands" to improve enzymatic reactions and thus repair (Zeebe et al. 1996).

Growth is possible even under higher light intensities and low temperatures (e.g. Fiala & Oriol 1990, Davidson 1991) when sufficient nutrients, particularly dissolved nitrogen and iron, are available in order to compensate the higher demand for protein synthesis. Such environmental conditions are seen at the ice edges of the Ross Sea and the Weddell Sea, where large surface water blooms of diatoms occur. Iron input from the continent is presumably the factor inducing these blooms. Infiltration layers in Antarctic sea ice represent another high light environment, where sufficient supply of new nutrients from surrounding sea water is used to acclimate to strong scalar irradiance (Kritiansen et al. 1998). Nitrogen limitation and limitation of essential trace elements such as iron have a

strong impact on algal growth by restricting the synthesis of proteins and pigments responsible for acclimation to high light intensities (e.g. Falkowski et al. 1989). Nitrogen is a key component of proteins and amino acids and iron is often part of the functional groups in chloroplast enzymes. Therefore nutrient limitation causes photoinhibition by reducing excitation energy dissipation as well as the turnover of chloroplast proteins and the production of chaperons. Dynamic photoinhibition under cold exposure and nutrient replete conditions will change to chronic photoinhibition under nutrient limitation, because damage exceeds repair (publication **4**). Under these conditions cells therefore route their energy into the synthesis of triacylglyerols (neutral lipids not containing N and Fe). Many studies have reported on high lipid contents of polar diatoms, especially at the end of blooms under nutrient depleted conditions (e.g. Smith & Morris 1980, Palmisano & Sullivan 1985, Mock & Gradinger 2000). Carbohydrates, found to be the primary energy sink under excess light in diatoms from temperate and tropical habitats, are less important in polar diatoms (publication **4**). Carbohydrate metabolism in higher plants has a greater instantaneous low temperature sensitivity than other components of photosynthesis (e.g. Leegood & Edwards 1996) and this probably also is the case in diatoms. The lipid pathway thus becomes increasingly important under polar conditions, not only concerning storage of superfluous energy but also for temperature adaptation (e.g. Nishida & Murata 1996) and for structural modulation under stress (publication **4**, **5**). Decreasing temperature generally causes a reduction in membrane fluidity (e.g. Lyons 1973), essential passive or active transport processes are negatively effected. The reduced fluidity of membranes acts as a temperature sensor. Membrane bound enzymes are activated, triggering a signal cascade in order to express genes which encode enzymes to increase the fluidity (ω3-desaturases; e.g. Suzuki et al. 2000, Brows & Xin 2001, McKemy et al. 2002). Thylakoid membranes in chloroplasts of polar diatoms consist of high amounts of 20 : 5 poly-unsaturated-fatty-acids (PUFAs) in each chloroplast lipid class. They regulate the connectivity between light harvesting protein complexes (LHC) and pigments, are also responsible for D1 replacement, and ensure plastoquinone diffusion for efficient electron transport (e.g. Gombos et al. 1994, Siegenthaler & Murata 1998, Morgan-Kiss et al. 2002). Regulation of membrane structure is also implemented by changes in lipid class composition (publication **4**, **5**). Repair under light and nutrient stress in polar diatoms is therefore not only related to

chaperon synthesis and replacement of damaged chloroplast proteins but also to changes in fatty acid and lipid class composition in chloroplasts.

Light stress conditions (even at 35 µmol photons $m^{-2}s^{-1}$) at the freezing point of sea water require differentiated repair mechanisms, which are costly. The higher the light intensity and the degree of nutrient limitation, the lower is the amount of energy which can be utilised for growth. Maximum photosynthesis (Pmax) is therefore reduced by photo damage at low temperatures and probably by reduced CO_2-fixation. Living as a diatom in polar aquatic ecosystems therefore requires appropriate repair mechanisms, which are insensitive to low temperatures and high light intensities. Under low light conditions a greater proportion of incoming radiation can be used for growth. Deep-water chl *a* maxima in waters of the Southern Ocean and dense accumulations of diatoms under thick sea ice reveal such acclimation to growth under lower light intensities (e.g. Rysgaard et al. 2001, Kühl et al. 2001, Boyd 2002). Physiological investigations confirm the ability of these diatoms to use light in a highly efficient manner (e.g. Kirst & Wiencke 1995, Robinson et al. 1995, Cota 1985). One mechanism underlying this unique low light adaptation is a strongly increased synthesis of the pigment fucoxanthin. Low ratios of chl *a* : chl *c* (< 2) compared to temperate diatoms (> 2) were additionally measured (Boczar & Palmisano 1990). Fucoxanthin and chl *c* have an absorption maximum at ca. 440nm, which is part of blue-green wavelength spectrum reaching clear polar deep water layers and under thick sea ice (e.g. Palmisano et al. 1987, Jeffrey et al. 1997). Chlorophyll-protein complexes are assumed to have a different molecular structure in polar diatoms caused by unusually high amounts of fucoxanthin and chl *c* (Boczar & Palmisano 1990). Hence, the energy absorbed under low light, which is not directly used for growth, is used to synthesise LHC-complexes and chaperons essential for living in the cold (publication **7**). This growth is thermodynamically more efficient than investing most of the energy in the repair of damaged cellular structures under light stress conditions at 35 µmol photons $m^{-2}s^{-1}$). This strategy of stress avoidance is also realised by aquatic animals (Abele 2002). They are mostly stressed by ROS, which damages proteins and membranes of mitochondria. Particularly the evolutionary older oxygen-conforming animals prefer sub-oxic zones and colder water to reduce their metabolism and thus ROS formation.

The capacity of low light adaptation is probably most important in polar

ecosystems with strong seasonal light fluctuations including a period of darkness. Diatoms probably remain in an active state during winter by uptake of dissolved organic carbon (Thomas & Dieckmann 2002). When light conditions improve in spring, photosynthesis and growth can respond rapidly. Tolerance against low temperatures combined with high quantum yields under low irradiance are key features for the success of diatoms in polar oceans, whereas especially in sea ice the tolerance against increasing salinities is also of importance. Prymnesiophytes, with the major polar species *Phaeocystis antarctica,* seem also to be well adapted to low temperatures as revealed by the development of large blooms in open polar waters and even in sea ice. Unfortunately no detailed molecular studies are available on mechanisms of temperature adaptation in *P. antarctica*. Physiological investigations under nutrient replete conditions indicate a better acclimation under higher irradiances and low temperatures in *P. antarctica* than in diatoms (Moisan et al. 1998, Hegarty & Villareal 1998, Moisan & Mitchell 1999). It is therefore likely that *P. antarctica* has improved physiological mechanisms to increase energy excitation dissipation via the diadino-/ diatoxanthin cycle and to repair photodamaged proteins at low temperatures and high light intensities. An efficient detoxification of ROS may also contribute to the improved high light acclimation in contrast to diatoms. *P. antarctica* harvests light less efficiently under extreme low light conditions which is probably caused by different pigment composition and structural organisation of the chlorophyll-protein complexes. *P. antarctica* is therefore not able to occupy extreme low light environments such as under thick pack ice as successfully as diatoms.

The EST-library of *Fragilariopsis cylindrus* enabled us to discover cellular mechanisms of cold adaptation and photosynthesis on a broader genomic scale by using the macro-array technology. This approach should also be extended to test molecular acclimation on higher salinities, different CO_2 concentrations and nutrient limitations, which are important parameters influencing growth of sea ice diatoms and psychrophilic diatoms in general. These data would then provide the basis for further investigations of how changes in environmental conditions effects diatom growth in polar ecosystems as soon as more sequence data will be available by continuation of the EST-project and for instance by sequencing of the plastid genome, micro-arrays can be used to investigate the expression of thousands of genes simultaneously.

5 SUMMARY

This thesis was conducted to apply new techniques for measuring photosynthesis in Antarctic sea ice diatoms. A systematic approach of investigations was applied to obtain precise measurements of photosynthesis under natural conditions in the field from which questions were derived for further analysis in the laboratory. *In situ* measurements with the tracer ^{14}C through the entire thickness of a young sea ice floe revealed that algae are able to actively assimilate dissolved inorganic carbon under extreme conditions (e.g. -7°C, < 10 µmol photons m^{-2}) after inclusion into newly formed sea ice. These measurements were conducted with ice slices suspended in a new incubator. Unfortunately such bulk measurements did not provide encompass photosynthesis prevailing in the network of brine channels, pockets or bubbles. New sensors (oxygen micro-optodes) were therefore introduced into sea ice research which withstand freezing without damage, an important prerequisite to measuring oxygen dynamics directly within brine channels or brine pockets without disturbing the ice texture or brine chemistry. A new laboratory sea ice microcosm was developed to simulate natural conditions of sea ice and to cultivating a sea-ice diatom (*Fragilariopsis cylindrus*) directly within brine channels. Hence, changes of environmental conditions (e.g. melting, freezing, nutrient and light limitation) can now be simulated in the laboratory and effects on diatom photosynthesis can be investigated with the optodes without disturbing the habitat. However, how changes of environmental conditions influence photosynthesis and how these diatoms are generally adapted to their habitat still remained unresolved. Consequently, the first molecular data base of an obligate psychrophilic diatom (*Fragilariopis cylindrus*) was conducted using an EST (expressed sequence tag) approach under freezing conditions. This preliminary EST-library consists of 189 unique sequences. More than half (59%) of these sequences could not be identified by GenBank comparison, indicating the existence of many unknown genes. A subset of identified genes and additional genes responsible for photosynthesis, respiration and cold adaptation were cloned and arranged on a macro-array to investigate gene expression under freezing conditions. These molecular measurements were paralleled by biophysical and biochemical investigations. Experimental results revealed that acclimation of diatom photosynthesis under freezing temperatures of sea water and different resource limitations (light, nutrients) requires chaperons and repair mechanisms in order to sustain chloroplast membranes and proteins which are responsible for energy generation and carbon dioxide fixation.

6 ZUSAMMENFASSUNG

Diese Arbeit befaßte sich mit der Entwicklung und dem Einsatz neuer Techniken für die Messung der Photosynthese in antarktischen Meereisdiatomeen. *In situ* Messungen der Kohlenstoffassimilation in einer jungen Meereisscholle konnten erstmals für die Antarktis nachweisen, daß die Mikroalgen über die gesamte Eisdicke aktive Photosynthese betrieben. Der dafür neu entwickelte Inkubator ermöglichte es, Messungen mit dem Radiotracer ^{14}C in 1 cm dicken Eisscheiben über die gesamte Eisdicke durchzuführen. Diese Messungen waren jedoch nicht hochauflösend genug, um die Variabilität der Photosynthese direkt in den Solekanälen des Meereises erfassen zu können. Aus diesem Grund wurden neue widerstandsfähige Sauerstoffsensoren, die Mikrooptoden, während der Eisbildung in einem Mesokosmos in das Eis eingefroren. Diese Untersuchungen konnten zeigen, wie jeder einzelne Sensor in einem Solekanal die Sauerstoffentwicklung der Algen mißt. Für Untersuchungen im kleineren Maßstab und unter kontrollierteren Bedingungen wurde ein Mikrokosmos entwickelt, in dem die bipolare Diatomee *Fragilariopsis cylindrus* dauerhaft direkt im Meereis kultiviert wurde. Mit Sauerstoff-Mikrooptoden konnte hier die Netto-Photosynthese in den Solekanälen der Meereis-Wasser-Grenzfläche untersucht werden. Wie die Diatomeen jedoch an diese extremen Bedingungen überhaupt angepaßt sind und dadurch Photosynthese betreiben können, blieb bisher relativ unbekannt. Aus diesem Grund wurde bei *F. cylindrus* begonnen, das Genom aufzuklären. Die erste EST-Bank (expressed sequence tag) einer psychrophilen Diatomee besteht bisher aus 189 unterschiedlichen Sequenzen, von denen mehr als die Hälfte (59%) nicht über einen Datenbankvergleich aufgeklärt werden konnte, was auf einen hohen Anteil unbekannter Gene schließen läßt. Ein Teil der identifizierten Sequenzen aus der EST-Bank und zusätzlich klonierte Gene für die Photosynthese, Kälteanpassung und Respiration wurden zu einem Macroarray zusammengestellt, um die Genexpression dieser Diatomee am Gefrierpunkt von Meerwasser zu untersuchen. Diese molekularbiologischen Untersuchungen wurden durch biophysikalische und biochemische Experimente in Chemostaten ergänzt. Ergebnisse aus diesen Untersuchungen deuten darauf hin, daß die Photosynthese unter Temperaturlimitation und bei Nitratlimitation schon durch relativ geringen Lichtintensitäten geschädigt wird. Nur durch effiziente Reparaturmechanismen und Hilfsproteine (Chaperons, wie z.B. HSP70) ist es *F. cylindrus* vermutlich möglich, im Meereis zu überleben.

7 REFERENCES

Abele D (2002) Toxic oxygen: the radical livegiver. Nature 420:27

Allen JF, Forsberg J (2001) Molecular recognition in thylakoid structure and function. Trends Plant Sci 6(7):317-326

Allen DJ, Ort DR (2001) Impacts of chilling temperatures on photosynthesis in warm-climate plants. Trends Plant Sci 6(1):36-42

Aletsee L, Jahnke J (1992) Growth and productivity of the psychrophilic marine diatoms *Thalassiosira antarctica* Comber and *Nitzschia frigida* Grunow in batch cultures at temperatures below the freezing point of sea water. Polar Biol 11:643-647

Aro EM, Virgin I, Andersson B (1993) Photoinhibition of photosystem II. Inactivation, protein damage and turnover. Biochim Biophys Acta 1143(2):113-134

Bates SS, Cota GF (1986) Fluorescence induction and photosynthetic responseof Arctic ice algae to sample treatment and salinity. J Phycol 22:421-429

Bartsch A (1989) Die Eisalgenflora des Weddellmeeres (Antarktis): Arten-zusammensetztung und Biomasse sowie Ökophysiologie ausgewählter Arten. Ber Polarforschung 63:1-110

Boczar BA, Palmisano AC (1990) Photosynthetic pigments and pigment-proteins in natural populations of Antarctic sea ice diatoms. Phycologia 29(4):470-477

Boyed PW (2002) Environmental factors controlling phytoplankton processes in the southern ocean. J Phycol 38:844-861

Browse J, Xin Z (2001) Temperature sensing and cold acclimation. Curr Opin Plant Biol 4:241-246

Cota GF (1985) Photoadaptation of high Arctic ice algae. Nature 315:219-222

Cota GF, Sullivan CW (1990) Photoadaptation, growth and production of bottom ice algae in the Antarctic. J Phycol 26:399-411

Davidson IR (1991) Environmental effects on algal photosynthesis: temperature. J Phycol 27:2-8

Dubinsky Z, Falkowski PG, Wyman K (1986) Light harvesting and utilization in phytoplankton. Plant Cell Physiol 27:1335-1349

Eicken H (1992) The role of sea ice in structuring Antarctic ecosystems. Polar Biol 12:3-13

Elrad D, Niyogi KK, Grossman AR (2002) A major light-harvesting polypeptide of photosystem II functions in thermal dissipation. Plant Cell 14:1801-1816

Falkowski PG (1980) Light-shade adaptation in marine phytoplankton. In: Primary productivity in the sea. Falkowski PG (ed), Plenum Press, New York, pp 99-119

Falkowski PG, Sukinek A, Herzig R (1989) Nitrogen limitation in Isochrysis galbana (Haptophyceae). II. Relative abundance of chloroplast proteins. J Phycol 25:471-478

Falkowski PG, LaRoche J (1991) Adaptation to spectral irradiance in unicellular algae. J Phycol 27:8-14

Falkowski PG, Raven JA (1995) Aquatic photosynthesis. Blackwell Scientific Publishers, Oxford

Fiala M, Oriol L (1990) Light-temperature intercations on the growth of Antarctic diatoms. Polar Biol 10:629-636

Geider RJ, MacIntyre HL, Kana TM (1998) A dynamic regulatory model of phytoplanktonic acclimation to light, nutrients, and temperature. Mar Ecol Prog Ser 148:187-200

Girija C, Smith BN, Swamy PM (2002) Interactive effects of sodium chloride and calcium chloride on the accumulation of proline and glycinebetaine in peanut. Environ Exp Bot 47:1-10

Gleitz M, Rutgers vdLoeff M, Thomas DN, Dieckmann GS, Millero FJ (1995) Comparison of summer and winter inorganic carbon, oxygen and nutrient concentrations in Antarctic sea ice brine. Mar Chem 51:81-91

Gleitz M, Kukert H, Riebesell U, Dieckmann GS (1996) Carbon acquisition and growth of Antarctic sea ice diatoms in closed botle incubations. Mar Ecol Prog Ser 135:169-177

Gombos Z, Wada H, Murata N (1994) The recovery of photosynthesis from low-temperature photoinhibition is accelerated by the unsaturation of membrane lipids: a mechanism of chilling tolerance. Proc Natl Acad Sci 91:8787-8791

Hambrey MJ, Harland WB (1981) Earth´s pre-Pleistocene glacial record. Cambridge University Press, Cambridge, UK

Hegarty SG, Villareal TA (1998) Effects of light level and N:P supply ratio on the competition between Phaeocystis cf. pouchetii (Hariot) Lagerheim (Prymnesiophyceae) and five diatom species. J Exp Mar Biol Ecol 226(2):241-258

Hibbert JM, Quick WP (2002) Characteristics of C_4 photosynthesis in stems and petioles of C_3 flowering plants. Nature 415:451-454

Holba AG, Tegelaar EW, Huizinga BJ, Moldowan JM, Singletary MS, McCaffrey MA, Dzou LIP (1998) 24-norcholestanes as age-sensitive molecular fossils. Geology 26(9):783-786

Jeffrey SW, Mantoura RFC, Wright SW (1997) Phytoplankton pigments in oceanography, UNESCO, Paris, France

Jeong SW, Choi SM, Lee DS, Ahn SN, Hur Y, Chow WS, Park Y (2002) Differential susceptibility of photosynthesis to light-chilling stress in rice (*Oryza sativa l.*) depends on the capacity for photochemical dissipation of light. Molecules Cells 13(3):419-428

Kühl M, Glud RN, Borum J, Roberts R, Rysgaard S (2002) Photosynthetic performance of surface associated algae below sea ice as measured with a pulse amplitude modulated (PAM) fluorometer and O_2 microsensors. Mar Ecol Prog Ser 223:1-4

Kaplan A, Reinhold L (1999) CO_2 concentrating mechanisms in photosynthetic microorganisms. Annu Rev Plant Physiol 50:539-570

Kirst GO, Wiencke C (1995) Ecophysiology of polar algae. J Phycol 31:181-199

Kristiansen S, Farbrot T, Kuosa H, Myklestad S, Quillfeld CHv (1998) Nitrogen uptake in the infiltration community, an ice algal community in Antarctic pack-ice. Polar Biol 19:307-315

Leegood RC, Edwards GE (1996) Carbon metabolism and photorespiration: temperature dependence in relation to other environmental factors. In: Photosynthesis and the Environment. Baker NR (ed), Kluwer Academic, Amsterdam, Netherlands

Lyons JM (1973) Chilling injury in plants. Ann Rev Plant Physiol 24:445-466

Lohr M, Wilhelm C (1999) Algae displaying the diadinoxanthin cycle also possess the violaxanthin cycle. Proc Natl Acad Sci 96:8784-8789

Lomas MW, Glibert PM (1999) Temperature regulation of nitrate uptake: a novel hypothesis about nitrate uptake and reduction in cool-water diatoms. Limnol Oceanogr 44(3):556-572

Maestrini SY, Rochet M, Legendre L, Demers S (1986) Nutrient limitation of the bottom-ice microalgae biomass (southern Hudson Bay, Canadian Arctic). Limnol Oceanogr 31(5):969-982

Maxwell DP, Falk S, Trick CG, Huner NPA (1994) Growth at low temperature mimics high-light acclimation in *Chlorella vulgaris*. Plant Physiol 105(2):535-543

McMinn A, Skerratt J, Trull T, Ashworth C, Lizotte M (1999) Nutrient stress gradient in the bottom 5 cm of fast ice, McMurdo Sound, Antarctica. Polar Biol 21:220-227

McMinn A, Ashworth C, Ryan KG (2000) *In situ* net primary productivity of an Antarctic fast ice bottom algal community. Aquat Microb Ecol 21:177-185

McKemy DD, Neuhausser WM, Julius D (2002) Identification of a cold receptor reveals a general role for TRP channels in thermosensation. Nature 416:52-58

Medlin LK, Lange M, Barker GLA, Hayes PK (1995) Can molecular techniques change our ideas about the species concept? In: Joint I (ed) Molecular ecology of aquatic microbes. Springer-Verlag Berlin, Heidelberg

Medlin LK, Kooistra WCHF, Schmid AMM (2000) A review of the evolution of the diatoms-a total approach using molecules, morphology and ecology. In: Witkowski A, Sieminska J (eds) The origin and early evolution of the diatoms: fossile, molecular and biogeographical approaches. W Szafer Institute of Botany, Polish Academy of Sciences, Cracow

Michel CL, Beardall J (1996) Inorganic carbon uptake by an Antarctic sea-ice diatom, *Nitzschia frigida*. Polar Biol 16:95-99

Moisan TA, Mitchell BG (1999) Photophysiological acclimation of Phaeocystis antarctica Karsten under light limitation. Limnol Oceanogr 44(2):247-258

MontaneMH, Kloppstech K (2000) The family of light-harvesting-related proteins (LHCs, ELIPs, HLIPs): was the harvesting of lighttheir primary function? Gene 258:1-8

Mock T, Gradinger R (1999) Determination of Arctic ice algal production with a new in situ incubation technique. Mar Ecol Prog Ser 177:15-26

Mock T, Gradinger R (2000) Changes in photosynthetic carbon allocation in algal assemblages of Arctic sea ice with decreasing nutrient concentrations and irradiance. Mar Ecol Prog Ser 202:1-11

Morgan-Kiss R, Ivanov AG, Williams J, Khan M, Huner NPA (2002) Differential thermal effects on the energy distribution between photosystem II and photosystem I in thylakoid membranes of a psychrophilic and a mesophilic alga. Biochim Biophys Acta 1561:251-265

Moisan TA, Olaizola M, Mitchell BG (1998) Xanthophyll cycling in *Phaeocystis antarctica*: changes in cellular fluorescence. Mar Ecol Prog Ser 169:113-121

Nishida I, Murata N (1996) Chilling sensitivity in plants and cyanobacteria: the crucial contribution of membrane lipids. Annu Rev Plant Physiol Plant Mol Biol 47:541-568

Padmasree K, Padmavathi L, Raghavendra AS (2002) Essentiality of mitochondrial oxidative metabolism for photosynthesis: optimization of carbon assimilation and protection against photoinhibition. Crit Rev Biochem Mol Biol 37(2):71-119

Palmisano AC, Sullivan CW (1985) Pathways of photosynthetic carbon assimilation in sea-ice microalgae from McMurdo Sound, Antarctica. Limnol Oceanogr 30:674-678

Palmisano AC, Beeler SooHoo J, Sullivan CW (1987) Effects of four environmental variables on photosynthesis-irradiance relationships in Antarctic sea-ice microalgae. Mar Biol 94:299-306

Raven JA, Geider RJ (1988). Temperature and algal growth. New Phytol 110: 441-461

Raymond J, Zhaxybayeva O, Gogarten JP, Gerdes SY, Blankenship RE (2002) Whole-genome

analysis of photosynthetic prokaryotes. Science 298:1616-1619

Reay DS, Nedwell DB, Priddle J, Ellis-Evans JC (1999) Temperature dependence of inorganic nitrogen uptake: reduced affinity for nitrate at suboptimal temperatures in both algae and bacteria. Appl Envir Microbiol 65:2577-2584

Richardson K, Beardall J, Raven JA (1983) Adaptation of unicellular algae to irradiance: an analysis of strategies. New Phytol 93:157-191

Robinson DH, Arrigo KR, Iturriaga R, Sullivan CW (1995) Microalgal light-harvesting in extreme low-light environments in McMurdo Sound, Antarctica. J Phycol 31:508-520

Robinson DH, Kolber Z, Sullivan CW (1997) Photophysiology and photoacclimation in surface sea ice algae from McMurdo Sound, Antarctica. Mar Ecol Prog Ser 147:243-256

Rysgaard S, Kühl M, Glud RN, Hansen JW (2001) Biomass, production and horizontal patchiness of sea ice algae in a high-Arctic fjord (Young Sound, NE-Greenland). Mar Ecol Prog Ser 223:15-26

Sage RF (2001) Environmental and evolutionary preconditions for the origin and diversification of the C_4 photosynthetic syndrome. Plant Biol 3:202-213

Sairam RK, Srivastava GC (2002) Changes in antioxidant activity in sub-cellular fractions of tolerant and susceptible wheat genotypes in response to long term salt stress. Plant Sci 162(6):897-904

Schrieck R (2000) Effects of light and temperature on the enzymatic antioxidative defense systems in the Antarctic ice diatom *Entomoneis kufferathii* (Manguin). Reports on Polar Research 349, pp 130

Siegenthaler PA, Murata N (1998) Lipids in Photosynthesis: structure, function and genetics. In: Advances in Photosynthesis Vol 6. Govindjee (ed), Kluwer Academic, Amsterdam, Netherlands

Smith AE, Morris I (1980) Synthesis of lipid during photosynthesis by phytoplankton of the Southern Ocean. Science 207:197-199

Streb P, Shang W, Feierabend J, Bligny R (1998) Divergent strategies of photoprotection in high-mountain plants. Planta 207(2):313-324

Streb P, Shang W, Feierabend J (1999) Resistance of cold-hardened winter rye leaves (Secale cereale L.) to photo-oxidative stress. Plant Cell Envir 22(10):1211-1224

Stitt M, Vaughan H (2002) A plant for all seasons: alterations in photosynthetic carbon metabolism during cold acclimation in *Arabidopsis*. Curr Opin Plant Biol 5(3):199-206

Stoecker DK, Gustafson DE, Baier CT, Black MMD (2000) Primary production in the upper sea ice. Aquat Microb Ecol

Suzuki I, Los DA, Kanesaki Y, Mikami K, Murata N (2000) The pathway for perception and transduction of low-temperature signals in *Synechocystis*. EMBO J 19(6):1327-1334

Thomas DN, Dieckmann GS (2002) Antarctic sea ice- a habitat for extremophiles. Science 295:641-644

Thomashow MF (2001) So whats new in the field of plant cold acclimation? Lots! Plant Physiol 125:89-93

Thoms S, Pahlow M, Wolf-Gladrow DA (2001) Model of the carbon concentrating mechanism in chloroplasts of eukaryotic algae. J Theor Biol 208:295-313

Tsurikov VL (1979) The formation and composition of the gas content of sea ice. J Glaciol 22:67-81

Xiong L, Zhu JK (2002) Molecular and genetic aspects of plant responses to osmotic stress. Plant Cell Envir 25:131-139

Zeebe RE, Eicken H, Robinson DH, Wolf-Gladrow D, Dieckmann GS (1996) Modeling the heating and melting of sea ice through light absorption by microalgae. J Geophys Res 101(C1):1163-1181

8 ACKNOWLEDGEMENTS

- Mein herzlicher Dank gilt Herrn Prof. Victor Smetacek, der es mir ermöglicht hat meine Promotion am Alfred-Wegener-Institut für Polar- und Meeresforschung in Bremerhaven durchzuführen und die sehr guten Arbeitsbedingungen in seinem Fachbereich.
- Mein besonderer Dank gilt Dr. Gerhard Dieckmann und Dr. Klaus Valentin. Gerhard hat mich in allen Zeiten immer in dem unterstützt was ich getan habe. Nur in Freiheit kann gute Wissenschaft gedeihen – danke Gerhard! Klaus, mein Betreuer in allen Sachfragen der Molekularbiologie und KFZ-Reparatur, brachte mir nicht nur bei, daß die Kunst der molekularbiologischen Arbeitsweise im genauen Hinsehen und Überprüfen liegt, sondern, daß man genau durch eben diese Arbeitsweise auch feststellen kann warum mein Diesel so schwer anspringt. Klaus, ohne all deine selbstlose, unermüdlichen Hilfe und deine kreativen Ideen, wäre ich an der Molekularbiologie vielleicht gescheitert – Danke! Ich hoffe unser Zusammenarbeit bleibt weiterhin so fruchtbar.
- Dr. Bernd Kroon danke ich für viele sehr anregenden Gespräche nicht nur über die Wissenschaft. Bernd, du hast mir beigebracht die Photosynthese besser zu verstehen und mit Algen so umzugehen, daß man sich auch im Labor an ihnen erfreuen kann. Außerdem hatte ich bei deinen zahlreichen Umzügen die Gelegenheit meine Muskeln zu stählen. Vielen Dank für deine Unterstützung, deinen Humor und deine positive Art.
- Ein großer Dank gilt Prof. Uli Bathmann, Dr. Gerhard Kattner, Dr. Linda Medlin und Dr. Klaus Valentin, die sich engagiert für eine Vertragsverlängerung eingesetzt haben, nachdem abzusehen war, daß meine Promotion wegen der Schwerpunktverlagerung in der offiziellen Zeit nicht abzuschließen war.
- I wish to thank Linda Medlin for her warm reception as an associated scientsist in her AG and for providing lab space and generous support – thanks a lot, Linda !
- Allen Kollegen und Freunden aus der AG Medlin möchte für die immer große Unterstützung bei meinen Arbeiten danken. Besonders die freundliche und lockere Atmosphäre in dieser Arbeitgruppe ist mir in guter Erinnerung geblieben und hat über so manche Enttäuschung bei der Arbeit hinweggeholfen! Mein besonderer Dank gilt hier Dr. Uwe John. Uwe hat mir bei den ersten Schritten in dem für mich noch relativ neuem Gebiet der Molekularbiologie sehr geholfen und ich hoffe, Uwe, ich konnte dir bei deinen ersten Schritten zum Marathon auch ein paar Tips mit auf den Weg geben.
- Liebe Erika Allhusen, dir danke ich besonders für die praktische Unterstützung bei vielen Laborarbeiten und bei der Pflege der Kulturen. Besonders aber für die vielen leckeren Kuchen, die du mitgebracht hast. Noch nie habe ich eine so engagierte TA getroffen – danke Erika und weiterhin auf gute Zusammenarbeit und viel Spaß miteinander.
- Dr. Gerhard Kattner und Dr. Martin Graeve danke ich besonders für die zeitweise Bereitstellung eines Arbeitsplatzes in ihrer Arbeitgruppe und für die Hilfe bei Arbeiten im Lipidlabor.
- Für die Bereitstellung eines Arbeitsplatzes im Isotopenlabor und die immer gute Zusammenarbeit möchte ich ganz herzlich Dr. Elisabeth Helmke danken.
- Andreas Krell und Niko Hoch danke ich besonders für die Hilfe bei einem aufwendigen Experiment im letzten Jahr meiner Dissertation. Danke, daß du auch die Nächte durchgehalten hast, Niko! Hierbei möchte ich auch Dr. Magnus Lucassen danken, der mir einen Phospho-Imager zur Verfügung gestellt hat, um Makroarrays aus diesem Experiment bestmöglich auszuwerten.
- Allen Mitarbeitern aus der Sektion Biologische Ozeanographie und dem Fachbereich Pelagische Ökosysteme, sowie der Besatzung und den Wissenschaftlern an Bord von „Polarstern“ möchte ich danken, die mich im Laufe der gesamten Promotionszeit unterstützt haben und dadurch auch einen wichtigen Anteil an dieser Promotion haben. Jede noch so kleine Hilfe kann für die Arbeit von großer Bedeutung sein. Allen möchte ich hier auch für das freundliche Arbeitsklima danken und die immer weit geöffneten Türen. Ich habe mich bei euch sehr wohl gefühlt. Besonders sei hier Fr. Helga Schwarz gedankt, die mich von Anfang an begleitet hat und in der Sektion den Zusammenhalt und die gegenseitige Aufmerksamkeit zwischen den Kollegen fördert – vielen Dank dafür Fr. Schwarz.
- Ein ganz liebes Dankeschön geht an meine Freundin und Frau Claudia für ihre vielfältige Unterstützung und ihr Verständnis für diese Arbeit.